High-precision microholes are widely used, for example, in the automobile and consumer electronics industries. The helical drilling technology using ultrashort pulsed lasers can generate higher precision in the hole geometry: through the layer-by-layer ablation strategy thanks to the helical movement of the laser pulses. Moreover, it is easier to control and more flexible in fabricating microholes with adjustable diameters, greater conicity and higher complexity.

This work aims to investigate and clarify the behavior and influence of laser energy deposition on the fabrication of microholes with the ultrashort-pulsed-laser helical-drilling process. In order to quantify the laser energy deposition in the helical drilling process, the superposed laser intensity on the helical path is investigated. These paths are visualized by means of numeric simulation and camera-based experimental acquisition. The three-dimensional helical path is rotationally symmetric and determined by the parameter setting of the helical optics – the parallel offset and the tilt angle of the focused laser beam. A classic and dynamic helical process can be defined depending on the dimension of the helical path.

For classic helical drilling, the influence of the parameters like laser pulses and helical optics, as well as the process ambient conditions on the morphological and metallurgic properties of the boreholes are investigated. With the specified laser beam sources, a maximum hole aspect ratio of 10:1 in 1 mm thick stainless steel plate can be achieved. A dynamic helical drilling process can be performed when the helical path is changed during the drilling process. With this change, the hole entrance can be shaped to a designated profile and, thus, the complexity of hole geometry enhanced. Indeed, the maximum hole aspect ratio can be increased to 50:1. In addition to that, a reduced model for dynamic helical ablation was built by investigating the development of ablation depth at varied processing parameters over the whole helical diameter. The drilling results with adapted laser energy deposition on the helical path agree well with the simulation by the reduced model. Moreover, thanks to the advantages of the dynamic helical drilling process with adapted energy deposition, the performance of the helical optics can be enhanced, with respect to drilling precision, complexity and productivity.

ISBN 978-3-86359-916-4

LASERTECHNIK

High-precision and Complex Geometry Helical Drilling by Adapted Energy Deposition

Chao He



Chao He

High-precision and Complex Geometry Helical Drilling by Adapted Energy Deposition

Edition Wissenschaft Apprimus

Lehrstuhl für Lasertechnik LLT | RWTH AACHEN UNIVERSITY | Fraunhofer ILT

High-precision and Complex Geometry Helical Drilling by Adapted Energy Deposition

Hochpräzisions-Wendelbohren komplexer Geometrien mittels angepasster Energiedeposition

Von der Fakultät für Maschinenwesen
der Rheinisch-Westfälischen Technischen Hochschule Aachen
zur Erlangung des akademischen Grades eines
Doktors der Ingenieurwissenschaften
genehmigte Dissertation

vorgelegt von

Chao He

Berichter:

Univ.-Prof. Dr. rer. nat. Reinhart Poprawe
Univ.-Prof. Dr.-Ing. Thomas Bergs

Tag der mündlichen Prüfung: 22. September 2020

Diese Dissertation ist auf den Internetseiten der Universitätsbibliothek online verfügbar.

ERGEBNISSE AUS DER LASERTECHNIK

Chao He

High-precision and Complex Geometry Helical Drilling by Adapted Energy Deposition

Bibliografische Information der Deutschen Nationalbibliothek
Die Deutsche Nationalbibliothek verzeichnet diese Publikation in der Deutschen Nationalbibliografie; detaillierte bibliografische Daten sind im Internet über https://portal.dnb.de abrufbar.

Chao He:

High-precision and Complex Geometry Helical Drilling by Adapted Energy Deposition

1. Auflage, 2020

Gedruckt auf holz- und säurefreiem Papier, 100% chlorfrei gebleicht.

Apprimus Verlag, Aachen, 2020
Wissenschaftsverlag des Instituts für Industriekommunikation und Fachmedien
an der RWTH Aachen
Steinbachstr. 25, 52074 Aachen
Internet: www.apprimus-verlag.de, E-Mail: info@apprimus-verlag.de

Printed in Germany

ISBN 978-3-86359-916-4

D 82 (Diss. RWTH Aachen University, 2020)

Acknowledgements

I wrote the present doctoral thesis while I worked as a scientific assistant at the Chair for Laser Technology at the RWTH Aachen University and Fraunhofer Institute for Laser Technology ILT. At this point I would like to thank all those who accompanied me during my doctoral studies and have supported the success of this work.

First of all, I would like to thank the German Academic Exchange Service (DAAD) for the financial support for the first three and half years of my PhD study. With this support, I could successfully begin studying, researching and living in Germany.

I would like to express my sincere gratitude to my supervisor, Univ.-Prof. Dr. rer. nat. Reinhart Poprawe, for supporting this work and the discussions on its content, as well as the interesting talks during the business trips together in China.

I also would like to thank Prof. Dr.-Ing. Thomas Bergs for his kind agreement on being my second referee of this thesis. In addition, I would like to thank Univ.-Prof. Ph. D. Marek Behr for taking over the role of the chair of the dissertation committee.

I am grateful to Dr. -Ing. Arnold Gillner for supervising the content of my dissertation, for regularly discussing of interim results and making valuable scientific suggestions. He kept me on the right track throughout my research work and meanwhile gave me with considerable freedom for developing my ideas about the helical drilling technology.

Many thanks to my colleagues for the openness, the creative and constructive thoughts and ideas in many discussions. In particular I would like to thank Dr. Frank Zibner, Dr. Stefan Janssen, Dr. Jens Holtkamp, Dr. Chen Hong, Dr. Michael Steger, Dr. Christian Fornaroli and Dr. Claudia Riester. Furthermore, I would like to thank my student assistant Jannik Bühring, Malte Weber, Jan Christoph Müller and graduate student Dominik Esch for their special contribution to the success of this work. I would also like to thank Bruce Carnevale for his very helpful commitment as proofreader. Thanks a lot to Dr. Keming Du from EdgeWave GmbH for kindly providing the high-pulse-energy picosecond laser source for exploring some of the interesting issues in the helical drilling process.

My special thanks go to my wife Mi, in particular, for her patience and affectionate support during the entire promotion phase. She has shown me a

great deal of understanding when I had to work overtime and was still able to motivate me. Finally, I thank my parents for the unflagging support they provided me in every situation of my life.

Aachen, October 2020 Chao He

Abstract

High-precision microholes are widely used as, for example, nozzles and venting holes in the automobile and consumer electronics industries. Owing to the development of modern devices and applications, the requirements on such holes have increased, not only in terms of geometric complexity but also of high precision. The helical drilling technology using ultrashort pulsed lasers is able to meet such requirements since it can generate higher precision in the hole geometry: through the layer-by-layer ablation strategy thanks to the helical movement of the laser pulses. Moreover, it is easier to control and more flexible in fabricating microholes with adjustable diameters, greater conicity and higher complexity.

This work aims to investigate and clarify the behavior and influence of laser energy deposition on the fabrication of microholes with the ultrashort-pulsed-laser helical-drilling process. In order to quantify the laser energy deposition in the helical drilling process, I investigated the superposed laser intensity on the helical path. These paths are illustrated and visualized by means of numeric simulation and camera-based experimental acquisition. The three-dimensional helical path is rotationally symmetric and determined by the parameter setting of the helical optics – the parallel offset and the tilt angle of the focused laser beam. A classic and dynamic helical process can be defined depending on the dimension of the helical path.

For classic helical drilling, I have investigated how the parameters of laser pulses and helical optics, as well as the process ambient conditions influence the morphological and metallurgic properties of the boreholes. With the specified laser beam sources, a maximum hole aspect ratio of 10:1 in 1 mm thick stainless steel plate can be achieved. A dynamic helical drilling process can be performed when the helical path is changed during the drilling process. With this change, the hole entrance can be shaped to a designated profile and, thus, the complexity of hole geometry enhanced. Indeed, the maximum hole aspect ratio can be increased to 50:1. In addition to that, a reduced model for dynamic helical ablation was built by investigating the development of ablation depth at varied processing parameters over the whole helical diameter. The drilling results with adapted laser energy deposition on the helical path agree well with the simulation by the reduced model. Moreover, thanks to the advantages of the dynamic helical drilling process with adapted energy deposition, the performance of the helical optics can be enhanced, with respect to drilling precision, complexity and productivity.

Kurzfassung

Hochpräzise Mikrobohrungen sind industriell in der Fertigung weit verbreitet, z.B. als Düsen- und Entlüftungsbohrungen. Durch die Entwicklung moderner Geräte im Bereich der Mikroelektronik (MEMs) und hochpräzisen Anwendungen sind die Anforderungen an solche Bohrungen in Bezug auf die geometrische Komplexität und die Präzision gestiegen. Der Prozess des Wendelbohrens mit ultrakurz gepulsten Lasern ermöglicht eine sehr hohe Präzision in der Bohrungsgeometrie durch die spiralförmige Bewegung der Laserpulse entlang einer Kreisbahn und der verdampfungsdominierte Abtragsprozess trägt das Material schichtweise für die höchst mögliche Qualität ab. Die Wendelbohroptik verfügt über hohe Beherrschbarkeit und Flexibilität bei der Herstellung von Mikrolöchern mit einstellbarem Durchmesser, definierbarer Konizität und geometrischer Komplexität.

Die vorliegende Arbeit beschäftigt sich mit Untersuchungen und Charakterisierung des Verhaltens und des Einflusses der Laserenergiedeposition auf die Herstellung von Mikrolöchern im Wendelbohrprozesses. Zur Quantifizierung der Laserenergiedeposition s wird die überlagerte Laserintensität auf der Wendelbahn untersucht. Die Wendelbahn wird durch die Einstellung des Parallelversatzes und des Einfallswinkels des fokussierten Laserstrahls beschrieben. Diese rotationssymmetrische Wendelbahn wird mittels numerischer Simulation und kamerabasierter Erfassung dargestellt und visualisiert. Ein klassischer und dynamischer Wendelprozess kann in Abhängigkeit von der Dimension der Wendelbahn definiert werden.

Für das klassische Wendelbohren werden untersucht, wie die Parameter der Laserpulse und der Wendeloptik sowie die Prozessumgebungsbedingungen die morphologischen und metallurgischen Eigenschaften der Bohrungen beeinflussen. Ein dynamischer Wendelbohrprozess kann durchgeführt werden, wenn die Wendelbahn während des Bohrprozesses geändert wird. Dadurch kann der Bohrungseintritt zu einem definierten Profil geformt und somit die Komplexität der Bohrungsgeometrie erhöht werden. Das maximale Bohrungsquerschnittsverhältnis kann von 10:1 in 1 mm dickem Edelstahlblech auf 50:1 in 3 mm erhöht werden. Ein reduziertes Modell für die dynamische Wendelablation zeigt die Entwicklung der Abtragstiefe bei unterschiedlichen Prozessparametern über den gesamten Wendeldurchmesser. Die Bohrergebnisse mit angepasster Laserenergiedeposition auf der Wendelbahn bestätigen das Modell. Die Leistung der Wendeloptik in Bezug auf Bohrpräzision, Komplexität und Produktivität kann durch dynamische Anpassung der Energiedeposition im Wendelbohrprozess signifikant gesteigert werden.

Index

List of abbreviations		**III**
Symbols		**IV**
1	**Introduction and objective**	**1**
1.1	Motivation	1
1.2	Objectives and methodology	4
2	**The state of the art**	**7**
2.1	Laser-beam micro drilling	7
2.1.1	Influential factors in laser-beam micro drilling	8
2.1.2	Laser drilling strategies	10
2.1.3	Definition of hole geometry and its complexity	12
2.1.4	Multidimensional laser-beam micro drilling	14
2.2	Ultrashort pulsed laser material processing	15
2.2.1	Ultrashort pulsed laser ablation	15
2.2.2	Thermal effects during ultrashort pulsed laser processing	17
2.3	Laser-beam helical drilling technology	20
2.3.1	Systems engineering for laser-beam helical drilling	20
2.3.2	Helical drilling of complex microholes	24
3	**Experimental setup and instruments for characterization**	**27**
3.1	Helical drilling systems and process	27
3.1.1	Laser beam sources	27
3.1.2	Helical drilling optics	28
3.2	Materials and analysis methods	30
4	**Helical path in helical drilling processes**	**31**
4.1	Helical path	31
4.1.1	Two-dimensional helical path	32
4.1.2	Three-dimensional helical path	34
4.2	Visualization of helical path	35
4.3	Laser intensity distribution on helical path	39
4.3.1	Pulse distribution on helical path-pulse overlap	39
4.3.2	Superposed laser intensity distribution	41
4.4	Summary	46

5	**Classical helical drilling process and influential factors**	**47**
5.1	Laser parameters	47
5.1.1	Single pulse energy	47
5.1.2	Pulse repetition rate	51
5.1.3	Drilling duration	53
5.2	Helical optical parameters	55
5.2.1	Tilted angle of incident laser beam to Dove prism	56
5.2.2	Parallel offset of incident laser beam to Dove prism	57
5.2.3	Focal position of the laser beam	58
5.2.4	Rotational speed of the Dove prism	61
5.3	Process ambient conditions	63
5.3.1	Type of process gas	64
5.3.2	Pressure of process gas	65
5.4	Hole geometry and surface morphology of classic helical drilling	66
5.5	Summary	69
6	**Adaption of energy deposition and its applications**	**71**
6.1	Adaption of energy deposition in classic helical drilling	71
6.1.1	Multiple-step strategy	72
6.1.2	Dynamic adaption of focus position	75
6.2	Dynamic helical drilling process	77
6.2.1	Ablation behavior in dynamic helical drilling process	77
6.2.2	Influential factors in dynamic helical drilling	79
6.3	Adaption of energy deposition in dynamic helical drilling	87
6.3.1	Adaption of single pulse energy	88
6.3.2	Adaption of drilling duration	89
6.3.3	Adaption of pulse repetition rate	90
6.4	Application examples of energy-deposition-adapted dynamic helical drilling	92
6.5	Summary	101
7	**Conclusion and outlook**	**103**
Bibliography		**109**
Appendix		**117**

List of abbreviations

Abbreviation	Definition
(µ)EDM	(Micro) Electrical Discharge Machining
µs	Microsecond(10^{-6} s)
3D	Three-Dimensional
CAD	Computer Aided Design
CMOS	Complementary Metal-Oxide-Semiconductor
CNC	Computerized Numerical Control
DOE	Diffractive Optical Element
fs	Femtosecond(10^{-15} s)
HAZ	Heat Affected Zone
kHz	Kilohertz=10^3 Hz
KP	Wedge Prism Position
LBO	Lithium triborate (LiB_3O_5)
LIPSS	Laser Induced Periodic Surface Structures
LSM	Laser Scanning Microscope
MHz	Megahertz=10^6 Hz
ms	Millisecond(10^{-3} s)
ns	Nanosecond(10^{-9} s)
OT	Optical Table Positions
ps	Picosecond(10^{-12} s)
QCW	Quasi-Continuous Wavelength
RMS	Root-Mean-Squared
RPM	Revolutions Per Minute
rps	Revolutions Per second
SEM	Scanning Electron Microscope
SHG	Second Harmonic Generation
TBC	Thermal Barrier Coating
USP	Ultrashort Pulses

Symbols

Symbol	Name	Unit
a_{wp}	Wedge prism angle	°
A_c	Area of through microhole	µm²
A_P	Effective focal spot area	µm²
c_p	Specific heat capacity	J/(kg·K)
d_h	Helical diameter	µm
d_{raw}	Raw beam diameter	mm
D_{ab}	Ablation depth	µm
E_p	Single pulse energy	µJ
f_{REP}	Repetition rate rate	Hz
F_{th}	Fluence of threshold	J/cm²
I_a	Average absorbed laser intensity	W/cm²
I_s	Superposed laser intensity	W/cm²
k	Thermal conductivity	W/(m·K)
M^2	Beam quality factor	
N_{ppl}	Number of laser pulses per unit length	μm^{-1}
P_c	Perimeter of through microhole	µm
P_{max}	Max. average power	W
P_{peak}	Laser peak power	W
r_h	Helical radius	µm
R_0	Hole radius at the entrance	µm
Rq	Root-mean-squared surface roughness	µm
V_{wedge}	angular rotation speed of wedge prism	°/s
w_0	Beam intensity 1/e² radius of the laser spot at focus	µm
T_m	Melting temperature	K
T_v	Evaporating temperature	K
α_{Abs}	Absorption coefficient	cm^{-1}
δ	Energy penetration depth	nm
δ_h	Heat penetration depth	nm
δ_{opt}	Optical penetration depth	nm
Δa	Parallel offset of laser beam	mm
$\Delta\beta$	Tilt angle of incident laser beam	°
$\Delta T(t)$	Time-independent temperature increase	K

Symbol	Name	Unit
η_{or}	Overlap degree	
κ	Thermal diffusivity	mm²/s
λ	Wavelength	nm
ρ	Density	g/cm³
ρ_c	Circularity of microhole	
τ_p	Laser pulse duration	ps/fs
τ_p[Pa]	Modulus of elasticity	kN/mm²
χ	Conicity of microhole	
ω_b	Laser beam rotating speed	rps/RPM
ω_m	Rotating frequency of Dove prism	rps/Hz
Ω_0	effective working diameter to ablation threshold	µm

1 Introduction and objective

1.1 Motivation

The miniaturization of modern devices imposes higher requirement on manufacturing technology. After its development and exploration for more than 50 years, laser beam machining technology is considered to be one of the most effective solutions in industrial manufacturing. Due to its advantages like non-contact processing, no external mechanical stress, the application spectrum for lasers has been broadened from metallic to dielectric materials such as glass and ceramics, which cover most industrial branches. Laser drilling as one of the well-established laser processes offers a great advantage over conventional precision drilling methods such as Electrical Discharge Machining (EDM) thanks to its non-selectivity of material combined with high flexibility of the process [RRF14]. Nowadays, cylindrical microholes fabricated by laser drilling are used in many industrial products from the consumer electronic industry [Ha18a], like micro filters for electronic products, via the automotive industry [Sc18], such as injection nozzles, to the aviation industry, which used air-cooling holes for aerospace turbine blades, as three examples [MFP04] [Dü08] [As11]. All applications have high requirements on the precision and the complexity of the hole geometry, as well as the flexibility of the drilling process. The hole geometry mainly refers the hole diameter, aspect ratio, roundness of entrance and exits, conicity and profile of the cross section as well as roughness of the hole-wall. These are the most important parameters to evaluate the quality of the drilling, and furthermore the precision of the processing.

Thanks to the rapid development of innovative laser sources, laser drilling enables high precision holes with diameters ranging from less than one micrometer to several millimeters while maintaining the same drilling depths in a variety of materials. The research on laser drilling today focuses on combining enhancing productivity with the increasing demand for high quality with respect to geometrical tolerances and reduced processing side effects, mainly thermal effects [An08]. Such thermal effects include change of metallurgy and generation of recast, cracks and burr etc. which lead to a dramatic reduction of performance, reliability and lifetime of components [We14]. The requirements on decreasing thermal effect is therefore extremely crucial in the case of fabrication of cooling air holes in turbomachinery components [RV16]. By taking advantage of short laser pulses – especially ultrashort laser pulses with the laser pulse duration in the regime from tens of picoseconds down to several hundred of femtoseconds – the mechanism of material ablation is dominated by material vaporization [Da03]. Due to that, an extraordinary geometrical precision of

drilling with minimized thermal effect can be achieved in a variety of materials [RV16] [FD03].

The multidimensional microholes are characterized by a complex profile in the cross-section, which have for instance, a converging taper at the hole entrance and a diverging taper at the exit [RFR16]. The microhole has more than one degree of freedom in the variation of hole diameter along the hole depth. Due to its undercut shape, this kind of hole is usually manufactured from two sides of the workpiece including a time-consuming coaxial alignment [Be11][Lo09] [MB18]. The application of high-precision, multidimensional holes can be found in many technical applications, such as fuel injectors, de Laval nozzles or micro filters [RFR16] [Li18] [Lo09]. One of the most fascinating applications of three-dimensional shaped holes is cooling air holes in a turbine blade [KI14]. As the state-of-the-art technology, a two-step drilling process is employed to fabricate such shaped holes in turbomachinery components with optimized three-dimensional (3D) geometries [SS12] [Be11]. As the first step, a cylindrical through hole is drilled by a trepanning optic using a QCW laser with millisecond pulse duration. Following that, the hole exit is shaped by means of a short-pulsed laser ablation and scanning optics. The employment of ms-QCW laser contributes to a high productivity due to its high pulse energy from millijoule to joule. However, in turn, redundant thermal load could be introduced in materials and cause micro cracks around the drilling. This load results in delamination between thermal barrier coating (TBC) layer and base alloys and reduce the life span of the turbomachinery components [UFK16]. From the process point of view, the two-step drilling strategy with two optics and laser beam sources increases the technical complexity and the precision can be impaired by misalignment. Compared to the current state of the art, a one-sided drilling strategy has numerous advantages regarding flexibility, precision and process efficiency. Recent research work on fabricating shaped holes with high power ultrafast lasers and a galvanometer scanner has demonstrated the advantages of the ultrashort pulse duration with regard to metallurgic characteristics (e. g. heat effect zone, recast layer, etc.) and high precision. The product yield and cost-efficiency, however, need to be increased to meet the industrial requirement.

Laser drilling is also one of the few techniques for producing high aspect-ratio microholes – holes with a depth-to-diameter ratio much greater than 10:1 but a hole diameter smaller than 200 µm [Fo07]. Laser-drilled high-aspect-ratio microholes are used in many applications, including the oil gallery of some engine blocks, aerospace turbine-engine cooling holes, laser fusion components, and printed circuit board micro-vias [JKS13] [Dö13] [BWE08]. The achievable aspect ratio of a precision drill hole is, however, limited by several factors. First of all, when drilled by ultrashort pulse laser (USP) radiation, the drilling depth is restricted by the maximum single pulse energy of the laser source. The fluence for laser ablation must be greater than the ablation threshold of material even when the ablation takes place at defocused conditions. Secondly, the achievable

aspect ratio is limited by the beam propagation behavior in the drilling channel. Multiple reflections of laser beam occur in the bore channel during drilling of high aspect-ratio microholes [ON10]. The process stability regarding the hole geometry and achievable aspect ratio especially within the percussion drilling process can be strongly impaired due to the limited possibility to control the multiple reflections along the bore wall. The removal rate decreases sharply with increasing drilling depth due to the beam divergence and multiple reflections. Thirdly, the dynamic of the laser ignited plasma in the bore channel has an influence on the laser energy deposition. The plasma congestion can even shield the laser radiation and interrupt the ablation process. Therefore, producing high aspect-ratio microholes in thick material poses a major challenge to manufacturing.

The helical drilling optics that use a Dove prism as image rotator have been under development for more than a decade. In contrast to a scanner-system-based rotating system, the helical path of the laser pulses using helical drilling optics is an analog continuous circle. This is a result of a total internal reflection of the laser beam passing through the spinning Dove prism. Therefore, the circularity of the helical path using the helical drilling optics is excellent. In the helical drilling process, the incident angle and parallel offset of the laser beam relative to the sample can be adjusted. Thus, the multiple reflection behavior in the bore channel can be adapted. This makes it possible to carefully control the drilling process and fabricate deep holes with small hole diameters. In addition, the spatial helical path can be adapted for varied hole profiles by adjusting the optical parameters such as parallel shift and incident angle of laser beam. By means of that, the helical drilling optics enables the fabrication of multidimensional shaped holes within one step [HBG18].

In most of the technical literature, the helical drilling technology is addressed with respect to the principle and the drilling results of the helical optics [Go15] [Wa15] [KMG18]. The understanding of the helical path is, however, insufficient. The helical path describes the behavior of the laser pulses in the helical drilling process and is deterministic to the final hole geometry. The controllability of the helical path in the helical optics as well its precision and technical limitation have to be recognized. For this purpose, systematic and thorough investigations on the influential factors such as laser pulse energy, repetition rate etc. in the helical drilling process using ultrashort laser pulses are essential. Finally, the technical term "energy deposition" is frequently used in the laser machining technology especially in the laser ablation process [Ru98][Ha14]. This work will attempt to explain the correlation between the behavior of laser energy deposition and the drilling result.

1.2 Objectives and methodology

The objective of this work is: to identify and clarify precision influencing phenomena of laser energy deposition in ultrashort-pulsed-laser helical drilling and the influence of adapting the energy deposition on the hole morphological and metallurgic properties.

Several research questions and hypotheses are proposed in order to clarify the problems about the laser fabrication of high-precision microholes described in the introduction.

Research questions:

1. What are the influential factors in the helical drilling process?
2. How can the laser energy deposition in the helical drilling process be characterized and quantified?
3. What is the correlation of energy deposition, heat accumulation, ablation efficiency, drilling geometry, processing time and surface quality?
4. How can the laser energy deposition be adapted to enhance the precision, productivity and complexity of helical-drilled microholes?

Research hypotheses

The distribution of laser pulses and the energy deposition play a vital role in the laser ablation process. The helical drilling optics enable a circular movement of laser pulses relative to the workpiece, while the revolution of the laser pulses modulates the spatial energy deposition by offsetting the consecutive pulses on the helical path. On the other hand, the ultrashort pules lasers emits the single pulse with a pulse duration of sub-picoseconds to a few picoseconds, and the temporal distance between pulses is controllable by setting the repetition rate. Thus, the overlap of pulses can be regulated by the setting of the helical-optics parameters and laser parameters.

In the classic helical drilling, the revolution diameter of the laser pulses, namely the helical diameter, is fixed. However, it can be adjusted during the drilling process. By means of that, a dynamic helical drilling process can be performed similar to the trepanning process. Besides the pulse overlap of the dynamic helical drilling process, the overlap of the helical path in the dynamic helical drilling can be adjusted.

Based on the above-mentioned characteristics of the helical drilling process, the following research hypotheses can be proposed:

1. With the available process parameters, the laser energy deposition in the classic helical drilling can be quantified and simulated.

2. By establishing the correlation of hole geometry with the energy deposition, parameters for the helical drilling process can be optimized and the fabrication quality and efficiency can be enhanced.

3. By adapting the laser energy deposition, the complexity of the microholes regarding the aspect-ratio, and the dimension of the hole profile can be increased.

Methodology for verification of the research hypotheses

The flowchart for the objectives and methodology is schematically shown in Fig. 1.

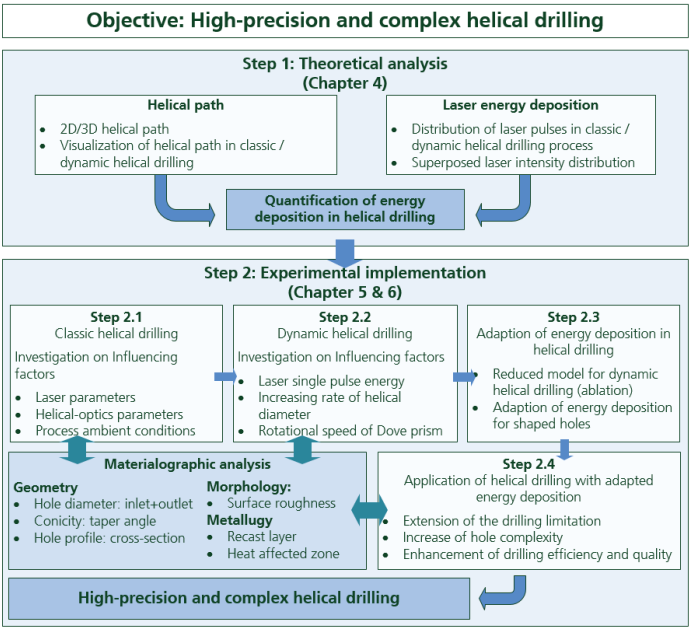


Fig. 1 Flow chart of methodology

In order to verify the research hypotheses, a two-step methodology has been adopted. In the first step theoretic analysis, the helical path and the laser energy deposition will be addressed. Following that in the second step, the experimental implementation will be discussed, including investigations on the classic helical drilling and dynamic helical drilling, as well as the adaption of the energy deposition and its applications.

Step 1: Theoretic analysis

Firstly, the helical path in the helical drilling process will be studied. The helical path on one plane and space – namely 2-dimensional and 3-dimensional helical path – will be illustrated. In order to achieve an intuitive overview of the development, the helical path is visualized by means of camera-based data acquisition. The behavior of the laser pulse distribution on the helical path is addressed; moreover, the influence of the helical diameter, the rotational speed of the Dove prism and the laser pulse repetition rate on the pulse overlap is analyzed. Furthermore, the superposed laser intensity distribution on the helical path of classic and dynamic helical drilling process is represented by the numeric simulation software Matlab. By means of that, the laser energy deposition in the helical drilling process can be quantified

Step 2: Experimental implementation

Following Step 1, the experimental investigations on a 1 mm thick stainless steel plate were carried out with both the classic and dynamic helical drilling process. The influential factors and the effects on the hole geometry were identified. The influential factors for the classic helical drilling include laser parameters (single pulse energy, pulse repetition rate and drilling time), helical–optics parameters (inclination angle and parallel offset of incident laser beam relative to Dove prism, the rotational speed of Dove prism and focal position of the laser beam in material) and process ambient conditions (type and pressure of assistance gas). For the dynamic helical drilling process, increasing rate of helical diameter, laser single pulse energy and rotational speed of the Dove prism as key factors were investigated. Based on that, a reduced model for the energy deposition in the dynamic helical drilling was set up. Furthermore, the applicability and accuracy of the reduced model for fabrication of designated hole geometry was evaluated. At the last step, the applications of helical drilling with adaption of energy deposition are represented. The results of the helical drilling with and without adaption of energy deposition have been compared in aspects of quality and productivity. For the experimental implementation, the morphologic and metallurgic properties of the boreholes with classic and dynamic helical drilling were characterized and analyzed.

2 The state of the art

2.1 Laser-beam micro drilling

Laser-beam drilling is a form of defined material removal. According to DIN 8580, this method is classified in the main group "cutting" because it eliminates the material cohesion at the processing point. In general, laser drilling offers some advantages over conventional methods such as mechanical drilling with regard to quality or material specificity [HG09] The drilling process is termed as micro drilling when the fabricated diameter of bore hole is less than 1 mm [PP18].

Laser-beam micro drilling has a wide range of industrial applications like fuel injection nozzles in the automobile industry, through vias in glass or silicon substrates for microelectronic devices. Typical examples of current industrial applications of laser-beam micro drilling are shown in Fig. 2.

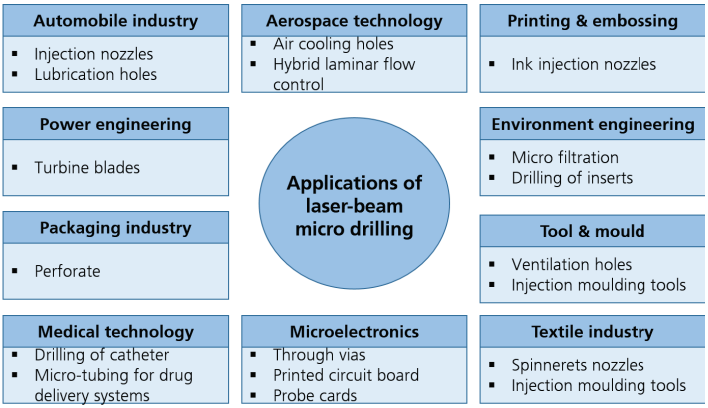


Fig. 2 Application examples of laser micro drilling in different branches

The demand for specially shaped and high-precision micro-drilling is constantly increasing in industrial applications. The requirements on the specifications of microholes and fabrication speed differ greatly in different industrial branches. For instance, for injection nozzles in the automobile industry, the accuracy and precision of hole shape and overall-quality are of high priority, whereas for microfiltration applications, the density of microholes and the productivity are the most important issue [SMP10]. Generally, when the requirements on accuracy, precision and quality are crucial, laser-beam micro drilling is

indispensable. The accuracy of drilling refers to the proximity of measurement results of hole geometry to the specified value. And the precision of drilling is the degree of the reproducibility under unchanged conditions [Jo08].

2.1.1 Influential factors in laser-beam micro drilling

As one of the most important indicators of the influencing variables in laser material processing, the absorption represents the proportion of optical energy that is converted into heat in the material and is not reflected or transmitted. The transmitted part is negligible for metals. Absorption is influenced by many factors [Po05]. According to [Ch96]. and [No97] et. al., the absorption of short laser pulses is characterized by a dominance of the electronic system of metals. How strongly a sample absorbs radiation depends on its absorption coefficient α_{abs}. However, α_{abs} is not a material constant and depends on various influences, such as refraction and wavelength.

Another important factor for the interaction between photons and matter is the optical penetration depth δ_{opt}. The optical penetration depth equals the distance inside the sample, within which the intensity of the laser beams drops down to approx. 37% of the value at the sample surface [Po11]. This can be used to describe the effect of the laser on the interaction volume. Mathematically, δ_{opt} corresponds to the reciprocal of α_{Abs}. For metals, δ_{opt} is typically about 10^{-6} to 10^{-5} cm at an incidence laser beam with wavelength in the visible and near-infrared. The resulting strongly localized absorption of energy in the surface layer leads to temperature gradients of about 10^{10} K·s^{-1} at the ablation front.

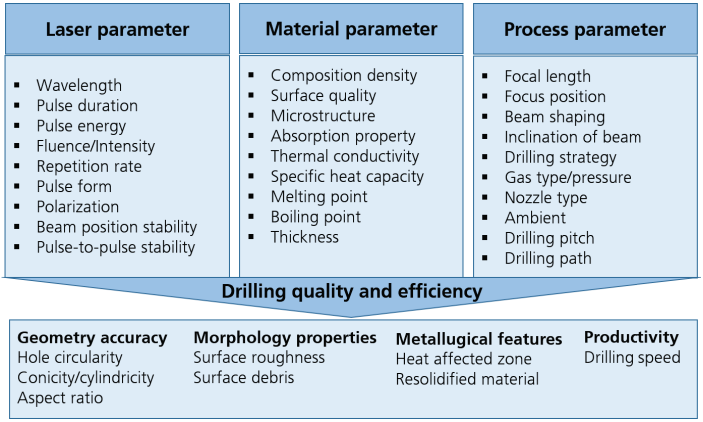


Fig. 3 Overview of the influential factors in the laser drilling process

In addition to these phenomena, other parameter fields influencing the result occur, which are clearly presented in Fig. 3. The major influencing parameters in laser-beam micro drilling can be grouped into three categories: the laser parameter, material parameter and process parameter.

As the machining tool, the laser source plays a vital role in the drilling quality and efficiency [MY15]. The laser parameters cover almost all of the specifications provided by the manufacturer, including the wavelength of laser beam [WRH16], pulse duration, available maximum single pulse energy, maximum pulse repetition rate, etc. In practice, the pulse form, beam quality (M^2), beam position stability and pulse-to-pulse stability are normally fixed and not applied as variable laser parameters. However, the influence of these parameters on the processing cannot be neglected. The polarization of the laser beam emitting from the laser source is generally linear; depending on the application, a $\lambda/4$ waveplate can be used to alter the polarization state from linear into circular where it is necessary [No99].

The material parameters describe the intrinsic properties of the objectives to be processed [PP18]. The material parameters are deterministic factors for the laser-material interaction effect. The composition and surface topography, for example, determine the absorptivity of the material to a certain laser wavelength. In addition, the thermal conductivity and vapor/liquid points are directly linked to the heat accumulation behavior during the drilling process.

Compared to the parameters of laser source and material, the parameters for the process development have greater flexibility and controllability in terms of the energy deposition of laser beam. With the same laser parameters, the focal length of the focusing optics determines the spot size, the divergence angle and Rayleigh length of the focused laser beam. The effects on achievable aspect ratios and morphologies of the microholes produced in silicon nitride substrates were investigated in [Na18] By employing lenses with shorter focal length, the achievable holes' aspect-ratio by percussion drilling can be increased and the cylindricity of borehole can be improved.

The drilling strategy in combination with the laser parameter can significantly change the behavior of laser energy deposition by means of the temporal and spatial adaption of laser pulse deposition. The classification of the laser-beam micro-drilling strategies is described in detail in subsection 2.1.2.

The quality of boreholes and the efficiency of drilling process are often used to evaluate the laser-beam micro-drilling process. Characterization and controlling of the drilling quality are important factors in fulfilling the requirements of various applications. The drilling quality can be characterized by different concrete indices such as accuracy of geometry. These indices can be divided into to three categories: geometry accuracy, morphology properties and metallurgical

features. The hole circularity, conicity/cylindricity and aspect ratio belong to the geometrical accuracy. The morphology properties refer to the surface roughness on the borehole wall and the surface debris. The metallurgical features represent the thermal effects on the borehole in terms of heat affected zone and resolidified material, especially recast layer [Du16]. In addition, the drilling efficiency is characterized by the productivity.

2.1.2 Laser drilling strategies

In order to meet the various requirements on the micro drilling, the adaption of drilling approaches is necessary to achieve an effective process. Fig. 4 shows a classification of laser drilling processes according to the relative movement between laser spot and workpiece [Wa08] [RV16] [PP18]. In addition, the drilling strategies are characterized by the drilling efficiency versus the drilling precision and hole complexity.

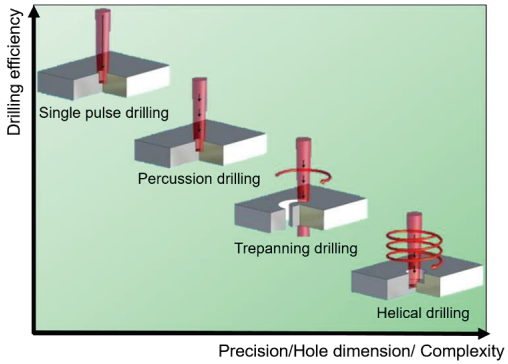


Fig. 4 Classification of laser-beam drilling strategies according to the behavior of drilling efficiency and precision/ hole complexity

Single pulse drilling and percussion drilling are static methods in which the laser beam always hits the same part of the material, while trepanning and helical drilling are dynamic processes in which the laser beam moves over the material [BMB13] [Wa08].

The single pulse drilling is the least complex drilling strategy, where merely one laser pulse hits the target. It is the most efficient drilling process and mostly performed with laser pulses with long pulse duration, usually in range of several hundreds of µs and with a high pulse energy as shown in Fig. 5 [Tr04]. As a result of the long pulse duration, the mechanism of material removal is based on expulsion of melt, i.e a melting-dominated drilling process. The material expulsion takes place largely in the form of melt and reduces the achievable

quality. With the development of ultrashort pulsed lasers, the single pulse drilling has been widely applied in drilling of thin foils [Ch09].

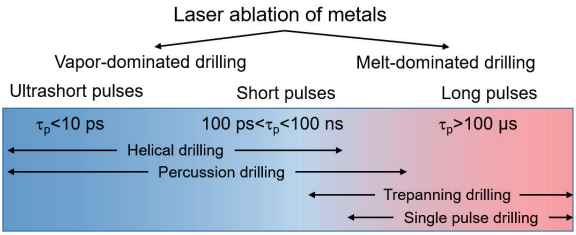


Fig. 5 Categoriation of drilling with pulsed lasers [Tr04]

The percussion drilling delivers a successive number of laser pulses in the same position to produce holes. Due to the time-divided deposition of the energy, the workpiece is locally less thermally stressed, and the proportion of sublimated material increases compared to single pulse drilling. Thus, the accuracy of the drill holes can be increased by percussion drilling process. Another advantage of percussion drilling is not only the increase of hole depth, but also the controllability in defining it [Ha18b]. Microholes with high aspect ratio of more than 30:1 can be achieved by the percussion drilling process [Ya12] [Fö18]. As laser drilling strategies without relative movement between laser spot and workpiece, single pulse drilling and percussion drilling have less flexibility in tuning the hole diameter and taper angle. Laser pulse energy, spot size, pulse repetition rate, exposure time and focus position are the most frequently employed variables to control the drilling geometry [An09][GSL16]. Owing to the short processing time, the microholes can be fabricated by "on-the-fly" drilling, which describes a drilling technique with fast movement of laser spots over the workpiece and nonstop at the hole location. This process is often performed in combination with a galvanometer scanner.

Trepanning drilling is characterized by a process with two phases: first, a starting through hole is drilled using percussion drilling. This is followed by a cutting movement along a closed path which creates the contour of a bigger hole through to the final geometry. Through the use of protective or process gases, the melt produced during cutting is expelled downwards through the starting hole. By means of that, the quality of boreholes in terms of the volume of recast can be enhanced. The relative movement between laser spot and workpiece is mostly achieved by two approaches: the CNC programs of motion axes and galvanometer scanner. Similar to laser single pulse drilling, trepanning drilling is often performed with long pulsed lasers. The hole diameter can be controlled by setting the diameter of cutting movement.

Helical drilling describes a drilling process of percussion drilling with a helix path of laser pulse movement. Material removal during helical drilling takes place during multiple passes on a defined circular path on the workpiece. The ablation front moves downward in a helix trajectory, and after a certain number of revolutions in the drilling volume the drill hole is completed. The material remove rate per each pulse is much smaller than with the trepanning process. Therefore, helical drilling increases the contour accuracy and enables the best drilling quality. Short and ultrashort pulsed lasers are generally employed in helical drilling process. The ablation process with ultrashort laser pulses is characterized as a vaporization-dominated process. A small volume of material is ablated and removed as vapor during irradiation of the short pulse. Owing to that, thermal load of the workpiece can be decreased. Micro cracks and recast layers can be avoided as a result of a lower heat load in material and vaporization.

The drilling strategies with relative movement between laser spot and workpiece generally provide the advantage of higher precision and make it possible to increase the geometry complexity of holes in terms of hole diameter. Furthermore, helical drilling can change the hole taper by controlling the incident angle of the focused laser beam relative to the workpiece.

2.1.3 Definition of hole geometry and its complexity

The geometry of a rotational symmetric borehole can be described by introducing three parameters as shown in Fig. 6: the hole radius R, the tangential angle θ to the central line of the hole and the drilling depth z. With these three parameters, a borehole with an arbitrary profile can be defined.

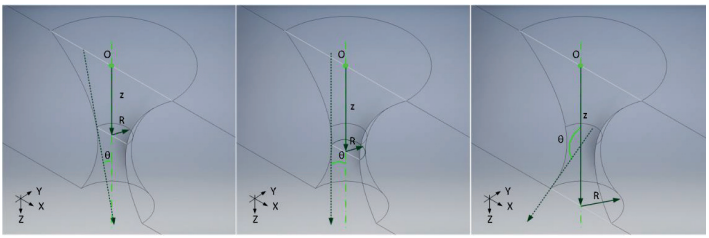


Fig. 6 Schematic diagram of definition of the hole geometric complexity

Note that the tangential angle θ describes the local taper angle on the hole wall as illustrated in Fig. 6. And the conicity of hole can be simply described as follows:

2.1

$$\begin{cases} \tan(\theta) > 0, & positive\ tapered\ hole \\ \tan(\theta) = 0, & zero\ tapered\ hole \\ \tan(\theta) < 0, & negative\ tapered\ hole. \end{cases}$$

For a cylindrical borehole with a depth d, the hole radius is independent of the drilling depth; meanwhile, the tangential angle θ between the hole wall to the central line of the hole is a constant. Thus, the borehole can be described as follows:

2.2
$$\begin{cases} R(z) = const. \\ \tan(\theta) = 0 \\ z \in [0, d] \end{cases}$$

where $R(z)$ is the hole radius at the depth z. Due to that, a cylindrical hole has only one variable, i.e. the drilling depth, which can be defined as a one-dimensional hole in this work.

For a positive or negative tapered borehole with a depth d, the tangential angle θ between the hole wall to the central line of the hole is a constant, but not equal to 0. The hole radius is dependent on the drilling depth. Thus, these kinds of borehole can be described as follows:

2.3
$$\begin{cases} R(z) = R_0 - z \cdot tan\theta. \\ \tan(\theta) = const \\ z \in [0, d] \end{cases}$$

where R_0 is the hole radius at the entrance. In the case of a positive or negative conical hole, the hole diameter varies with the increasing hole depth. For this reason, a positive or negative conical hole can be defined as a two-dimensional hole in this work.

All other kinds of holes can be characterized in the same manner and defined as multidimensional holes. For instance, a converging-diverging conical hole has the tangential angle θ as one variable. The geometry of such holes can be varied in the direction of $\vec{R}$, $\vec{\theta}$ and $\vec{d}$. Therefore, this kind of hole is defined as a three-dimensional hole in this work.

The complexity of hole geometry refers the complexity of the hole profile in cross-section. When the hole dimensions are clearly defined, the complexity of hole geometry can be quantified. The achievable complexity of the borehole is determined by the drilling strategy as shown in Fig. 4. The single pulse drilling and percussion drilling has limitations in fabricating microholes with defined taper angle and diameter, whereas the trepanning drilling and helical drilling can be used to vary the hole diameter. Furthermore, the helical drilling can control the hole taper by changing the inclination angle of focused laser beam relative to the workpiece.

In the helical drilling process, the hole geometry is directly linked to the parameters of the helical drilling optic. The radius of the borehole is determined by the radius of helical path. The local conicity of the hole can be transferred into

the inclination angle of the focused laser beam on the workpiece. The z position is the drill depth and increases with the increase of pulse number during the helical drilling process. Obviously, the hole geometry results from the combination of the parameters of laser source, material and process as explained in 2.1.1.

2.1.4 Multidimensional laser-beam micro drilling

High-precision, multidimensional holes are required in many technical applications, such as fuel injectors, de Laval nozzles or micro filters [RFR16] [Li18] [Lo09]. In the automotive industry, specially shaped, ever smaller bores are required to make fuel injection through certain nozzle shapes even more efficient in order to comply with current environmental standards. The multidimensional microholes are characterized by a complex profile more than one dimension in the cross-section, for instance a converging taper at the hole entrance and a diverging at its exit. Due to their undercut shape, these kinds of holes are usually manufactured from two sides of the workpiece including a time-consuming co-axial alignment as depicted in Fig. 7. To fabricate shaped cooling air holes in a turbine blade, two laser systems are employed, which makes the preparation work much more complicated and time consuming [Be11].

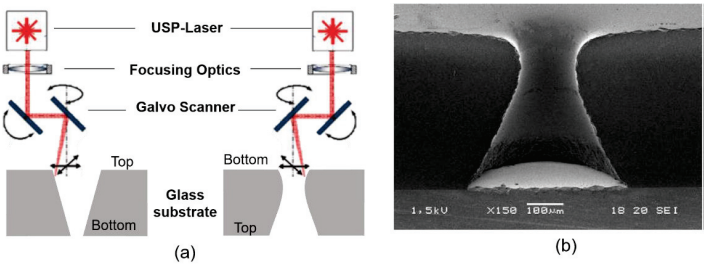


Fig. 7 (a) Fabrication scheme of a glass nozzle in two steps, (b) SEM image of cross-section of the glass nozzle [Lo09]

Compared with current state of the art, a one-sided drilling strategy has numerous advantages regarding flexibility, precision and process efficiency. The procedures for the production of such 3D bores either use the above-mentioned helical drilling optics, in which the beam is deflected on a circular path by an image rotator on the workpiece surface and incident at a certain angle, or by scanner systems. These scanner systems are based on a galvanometer scanner and direct the beam over the workpiece via a mirror system. During the deflection on the specimen, the laser parameters used can be varied, resulting in a more efficient and complex borehole design [BMB13].

A multidimensional hole can be fabricated by using the helical optics with a dynamic drilling strategy. The dynamic strategy is characterized by an increasing helical diameter and dynamically adapted laser parameters during the drilling

process. To fabricate a rotationally symmetrical multidimensional microhole, firstly, a pilot hole with designated taper angle is manufactured via classical helical drilling. Following that, a shaped inlet with a designated profile is concentrically superposed on the pilot hole using a dynamic helical drilling. By means of helical drilling with USP lasers, complex geometries, which cannot be produced by any other mechanical or electrochemical tool, can be achieved.

2.2 Ultrashort pulsed laser material processing

Ultrashort pulsed lasers or ultrafast lasers refer in general to the duration of the laser pulses below 10 ps. Within the past decade, enormous progress has been made in the development of ultrafast laser technology. Nowadays, a KW-class USP laser is available on the market as a commercialized product [Ne13] [AM19], AMP19]. More recently, a new "Cluster of Excellence," namely "Advanced Photon Sources" founded by Fraunhofer Institute for Laser Technology ILT and Fraunhofer Institute for Applied Optics and Precision Engineering IOF, aims to develop ultrashort pulsed laser systems that achieve maximum power up to 20 kW [Fr19].

2.2.1 Ultrashort pulsed laser ablation

In comparison to ablation with short or long laser pulses, ablation with ultrashort pulsed lasers provides two major advantages: a decreased ablation threshold under identical processing conditions and a significant decrease of the heat affected zone, leading to a high-precision in structuring [Ko99] [BRD04]. The comparison between ablation by short pulsed laser and ultrashort pulsed laser is schematically illustrated in Fig. 8.

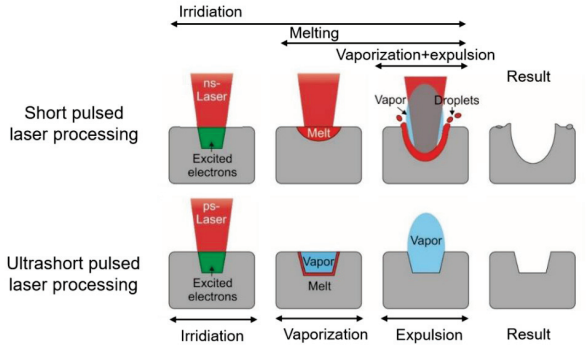


Fig. 8 Comparison of the ablation processing using short and ultrashort laser pulses[STE16]

During the laser processing using short pulsed lasers (~1 ns), a fraction of the incident laser energy is absorbed by the material in a shallow area. Due to a short

optical penetration depth (typically about 10 - 100 nm in most metals and a wavelength in the visible and near-infrared), the material melts and the heat diffuses to the surroundings. With the continuous irradiation of the laser pulse, the temperature of irradiated area keeps increasing and a large temperature gradient is formed. As soon as the temperature reaches the vaporization point, the material is ablated as plasma forms. The further absorption of laser energy by the plasma leads to the plasma expansion and material vaporization, both of which create a strong recoil force. The molten material is expelled by the recoil pressure, which results in the formation of droplets around the irradiated area. As a consequence, the ablation precision is impaired. Moreover, driven by the recoil pressure the so-called shock wave imposes stress due to the large temperature gradients in a relative large volume – the thermal stress. Due to the thermal stress, microcracks appear and spread into the area where is not directly affected by the laser irradiation as shown in Fig. 9. The ablation by short pulsed laser is also characterized as a melt-dominated process [Bi03].

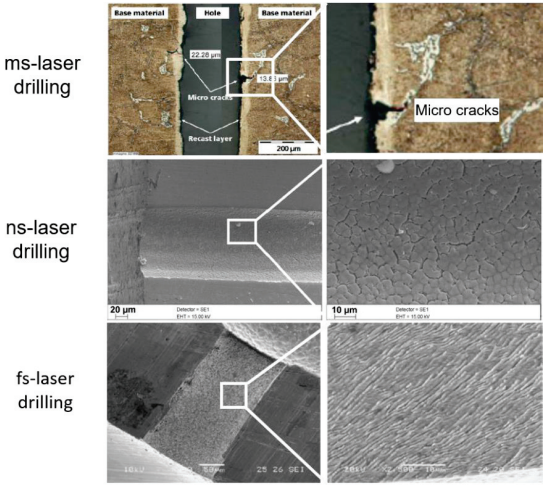


Fig. 9 Comparison of laser pulse duration on morphology of the drilling holes [UFK16] [Wa08] [RRF14]

In contrast to the ablation process by short pulsed laser pulses, during the ablation by ultrafast laser pulse, energy of the photons is deposited in a time period shorter than the relaxation time between the electron system and the lattice. Hence, the electron system exhibits a higher temperature than the lattice. This state and the energy transfer from the electron system into the lattice are described by the two temperature model [Po11]. In metallic material, thermalization within the electronic system by electron-electron collision occurs on an fs-timescale. The vaporization and plasma formation take place much

faster than heat conduction occurs. This contributes to a decreased thermal impact and allows a "cold" material processing without thermally affecting the surrounding material when processing at moderate fluences [SMP10]. Therefore, the ablation process by ultrafast laser is a vaporization-dominated process and attains much higher accuracy and precision. Drilling with ultrafast lasers is one of the established drilling methods to achieve high accuracy and precision [Kn10].

Another characteristic of ultrashort pulsed laser processing is the non-linear absorption in material, such as dielectrics, due to the very high power density. This enables the processing of materials that are normally optically transparent for the wavelengths used.

2.2.2 Thermal effects during ultrashort pulsed laser processing

Processing without thermal affect can be only achieved with the laser fluence near the ablation threshold of the material, where the ablation volume per pulse in material corresponds to the optical penetration depth [No97] [Ne10] [Ja11]. Processing at higher fluences can lead to thermal accumulation in the surrounding material. Therefore, ablation processes based on the two temperature model can be differentiated into a non-thermal (gentle) and a thermal (strong) fluence regime.

For a strong ablation of the material, the energy of the lattice in the ablation volume must exceed the specific evaporation heat. In this case, higher fluence is needed. Theoretically, after the thermalization process of lattice ions and electrons, a certain material volume has a sufficiently high temperature to sublimate. However, the ablation process is far more complex than sublimation assumed. Time-resolved microscopy investigations show that apart from sublimation, so-called spallation and phase explosion occur, which accelerate small particles from the material against the propagation direction of the laser [Fi17]. Also the time period in which the ablation takes place is about seven orders of magnitude longer than the time period of absorption thermalization [Ei15]. In order to achieve highly productive processing, the laser fluence applied is normally significantly higher than the ablation threshold. The SEM images depicted in Fig. 10 show percussion drilling results in stainless steel by fs-lasers with a pulse duration of approximately 200 fs with different laser fluence.

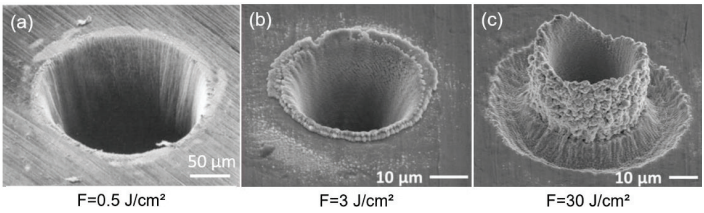


Fig. 10 SEM images of hole entrances with (a) low fluence, (b) medium fluence and (c) high fluence at a pulse repetition rate of 10 kHz in stainless steel [Ch96] [GSL16]

A clean hole entrance without any burr and nearly no debris is achieved by applying laser fluence of 0.5 J/cm². The thermal influence in terms of the formation of burr and particles surrounding the hole entrance increases dramatically in the ablation process from the medium-fluence regime (3 J/cm²) to high-fluence regime (30 J/cm²). The mechanism of material removal at the high-fluence regime using ultrafast laser is dominated by the expulsion of molten material, showing a high similarity to the melt ablation process.

Another effect has been also observed in studies that the ablation at high pulse repetition rate has a significant influence on the ablation results [Fi17] [GSL16] [We14] [Ba15]. Despite that, the ablation with ultrashort laser pulses cannot be simply described by a simple one-temperature model, as the heat diffusion and accumulation still exist in the ablation process. A certain fraction of the pulse energy below the ablation threshold is transferred into heat instead of vaporization. Depending on the local thermal conductivity of the material and the temporal distance between consecutively deposited laser pulses, the heat diffuses or accumulates with time.

The size of heat affected zone can be estimated by calculating the heat penetration depth δ_h in Eq. **2.4** [Po11]

2.4
$$\delta_h = 2\sqrt{\kappa t}$$

Here, κ denotes the thermal diffusivity and t the radiation times

The time-independent temperature increase $\Delta T(t)$ at the focal point with respect to the initial temperature can be given as follows [Ba00]:

2.5
$$\Delta T(t) = \frac{I_a w_0^2 \tau_p}{4\sqrt{\pi\kappa t} k t}$$

where I_a is the average absorbed laser intensity, w_0 the radius of focal spot, τ_p is the laser pulse duration, k the thermal conductivity and κ the thermal diffusivity.

According to WEBER et al. [We14], heat accumulation takes place in the material when the heat does not have enough time to diffuse into colder areas before the next laser pulse again introduces energy into the material. The upcoming pulse then hits a surface with a $T > T_{start}$. The behavior of the temperature development is shown in Fig. 11. If the repetition rate at the same energy of the pulse is different, the heat accumulation is stronger at the higher f_{Rep}. At a lower f_{Rep} the heat is able to dissipate to the T_{start} within the sufficient interval between two consecutive pulses as the black curve shown in Fig. 11. In this case, the ongoing pulses hit the "cold" material. According to the Eq. **2.5**, if the average power of the pulses at a different f_{Rep} is adjusted, there is still a similar behavior

of the heat accumulation. Due to the temperature accumulation, the gentle ablation processing diminishes.

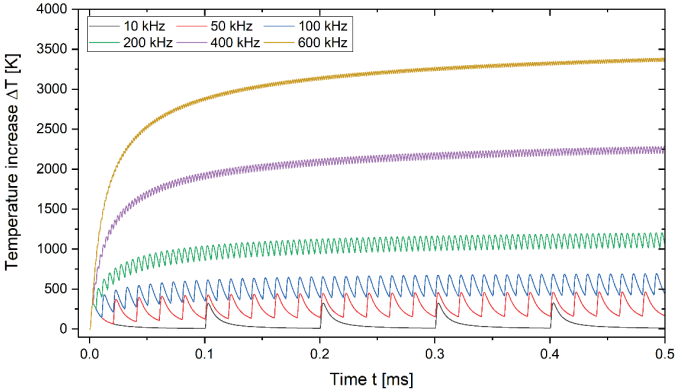


Fig. 11 Theoretical temperature increase on a 0.1 mm thick stainless steel surface with F = 40 J/cm² at varied pulse repetition rates during USP ablation, laser pulse duration: 0.9 ps, spot size: 15 µm

The SEM images depicted in Fig. 12 show percussion drilling results in stainless steel by fs-lasers with a pulse duration of approximately 200 fs with different laser pulse repetition rates [GSL16] [HG09]. Due to the heat accumulation, a significant amount of recast and particles can be observed at the hole entrance by applying a high pulse repetition rate of 1 MHz as shown in Fig. 12(a). Even tempering colors encircle the hole entrance, indicating a high thermal load. As the pulse repetition rate increases, a certain amount of heat accumulates at the bore front. The residual heat dissipates into the surrounding material and causes the heat affected zone (HAZ). In this HAZ, chemical and metallurgical changes occur due to diffusion processes. As pulse repetition rate decreases, the quality of boreholes in aspects of morphology and metallurgical properties can be enhanced with the same fluence applied. The height of burr and the amount of particles/debris at the hole entrance at a 10 kHz pulse repetition rate are significantly reduced, showing a typical vaporization-dominated ablation process.

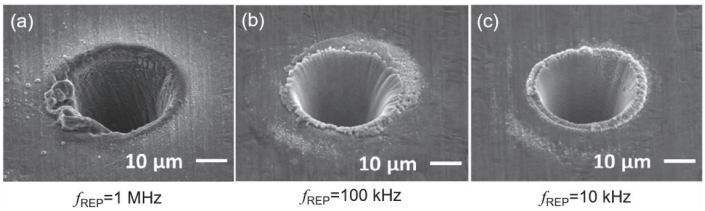


Fig. 12 SEM images of hole entrances with different pulse repetition rates at F=2.7 J/cm² in stainless steel [GSL16]

2.3 Laser-beam helical drilling technology

The process of helical drilling has been described in 2.1.2. In order to fabricate microholes with defined conicity, a high aspect ratio (>10:1) and high circularity, purpose-built drilling optics i.e. helical drilling optics, must be applied. The key characteristic of helical drilling is the rotating movement of the laser beam relative to the workpiece. Instead of the rotational movement of the workpiece, the rotation of laser beam – while the workpiece is stationary during the processing – is considered as more efficiency and flexible. The helical drilling optics enable an independent and precise adjustment of hole diameter and inclination angles of the laser beam to the workpiece [NSD16].

2.3.1 Systems engineering for laser-beam helical drilling

The concepts of mainstream helical drilling optics available for applications can be categorized as scanner-system-based precession optics and rotating-prism-based helical optics as illustrated in Fig. 13.

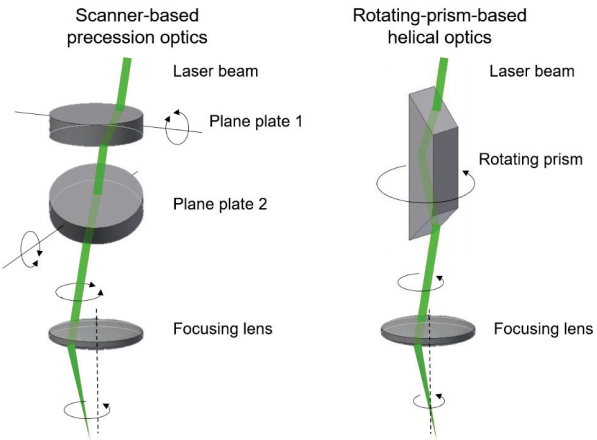


Fig. 13 Main principles of beam rotation for helical drilling

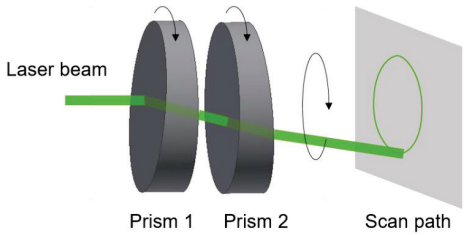
The industrial products and prototypes based on these two principles are listed in Table 1 together with the manufacturers. Other concepts such as trepanning optics based on an eccentrically rotating lens [Po11] can nowadays hardly find its way in the fabrication of high-precision helical drilling

Table 1: Typical products and their manufacturers according to the categorization in Fig. 13

Principle	Industrial products/Prototype	Manufacturer
Scanner-system-based	Precession Elephant series [AR18a]	ARGES
	precSYS 5-axis micromachining system [Au16]	SCANLAB
	5 Axis Micro Drilling Scanhead [Ca16]	Canon
	AGV5D 5-Axis Laser Micromachining System [Ae19]	Aerotech
	LS-Precess [La16]	Lasea
	Trepanning Module[SRA13]	Bayerisches Laserzentrum
Rotating-prism/lens-based	Wedge-prism-based helical drilling optics [Da03]	IFSW Stuttgart
	Prism rotating system [Wa15]	MHI
	Dove-prism-based Helical drilling optics [Wa08] [WG09]	Fraunhofer ILT
	Koala 4D-Laser-Trepanning system [AR18b]	ARGES
	GL.Trepan [NSD16]	GFH

The precession optics based on scanner systems use two independently movable transmission plan plates as the rotator unit. By synchronizing the two plan plates, the precession movement of laser pulses can be performed. Moreover, a parallel offset of the transmission laser beam to the incident laser beam can be generated; thus, the conicity of boreholes is tunable. In combination with a galvanometer scanner system, the geometry of boreholes can be flexibly adjusted. The galvanometer scanner system offers the advantage of guiding the laser beam over the workpiece on any desired scanning path. Therefore, it can be used to fabricate contoured holes. One of the examples of a scanner system tailored to helical drilling applications is the Precession Elephant series built by ARGES. Depending on the helical diameter, the maximum precession frequency of a laser beam is 200 to 600 Hz, corresponding to 12,000 to 36,000 RPM.

The rotating-prism-based helical optics include helical drilling optics based on rotating wedge prisms [Da03], a Dove prism [Wa08] [WG09] and a cylinder lens [MG14]. The core component of the helical optics based on rotating wedge prisms is the Risley prism pair, which consist of a pair of wedge prisms [Ma99]. Their plan surfaces are neighbored and parallel to each other as shown in Fig, 14. The Risley prism pair works as image rotator and rotates in a fixed relationship. Furthermore, by changing the relative angle of the two prisms, it is used as an angle changing unit to adjust the diameter of boreholes.



Fig, 14 Schematic diagram of the working principle of a Risley prism pair

The working principle can be formulated as follows: By rotating one wedge prism in relation to the other, the direction of the output laser beam will be changed. When the wedges' angle of the both wedge prisms is in the same direction, the angle of the refracted beam becomes greater. Whereas when the wedges are rotated to an angle in opposite directions, they cancel each other out, and the laser beam is allowed to pass straight through the Risley prism pair. The early systems for helical drilling comprised merely the Risley prism pair, and to improve the possibilities for setting the drilling parameters, such as helical diameter and taper angle, a third wedge prism has been added in this kind of helical drilling optics. As for a parallel offset unit, one of the classic concepts developed by the Dausinger+Giesen GmbH together with IFSW Stuttgart uses a third wedge prism, which is mounted in front of the Risley prism pair. By adjusting the distance between them, the lateral offset of a laser beam can be changed. MHI Japan used the similar principle and built a prototype of helical drilling optics. After the technical refinement of the concept based on rotating wedge prisms over the last decade, another concept, such as the application of a tiltable plane-parallel plate, is now emerging. One of the examples is the 4D-Laser-Trepanning system marketed as Koala by ARGES. In this system, the inclination angle of the plane-parallel plate determines the lateral offset of the incident laser beam to the Risley prism pair. The maximum precession frequency of laser beam is, however, restricted to 6000 RPM.

The Dove prism is a type of reflective prism and has been used as a beam rotator in helical drilling optics for more than two decades [KS99]. After entering one of the sloped faces of the Dove prism, the incident laser beam is refracted to the bottom surface and undergoes total internal reflection from the inside and then emerges from the opposite sloped face. As a result of a reflection behavior, if the reflection axis of the prism rotates, the image (emerging laser beam in the case of helical drilling) rotates at twice the rotation frequency of the prism [Sm00]. This interesting effect of a Dove prism enables an enhancement of the precession speed in the helical drilling process. The available optical rotational speed of laser beam on the workpiece can reach 36,000 RPM. Fig. 15 shows a new prototype of helical drilling optics system using a rotating Dove prism.

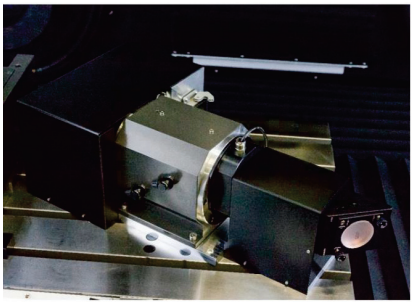


Fig. 15 Prototype of a helical drilling optics based on a rotating Dove prism

Helical drilling optics

Principle:
Rotating Dove prism

Main specifications:
Optical rotational frequency: 600 Hz
Helical diameter: 0~1.3 mm[1)]
Max. taper angle: -7~15 °
Aspect ratio: 30:1

[1)]Using focal length f=60 mm

Instead of using prisms as an image rotator, the equipment manufacturer GFH together with the IFSW developed a trepanning optic using a rotating telescope of cylinder lenses to steer the laser beam in the drilling process [GF18]. In this cylinder lens concept, both spot position and beam intensity profile rotate simultaneously [NSD16]. Additionally, the controlling units for path diameter and inclination angle of laser beam are separate from the rotating components, which allow a laser beam rotation of up to 30,000 RPM.

Besides the helical optics based on image rotator, other concepts such as using beam shaping components to perform an optical trepanning process have been attracting researchers' interest. A refractive-axicon-based optical trepanning system presented by University of Central Florida and University of Liverpool can transform a Gaussian Beam into an annular beam [ZLK06] [Ku14].

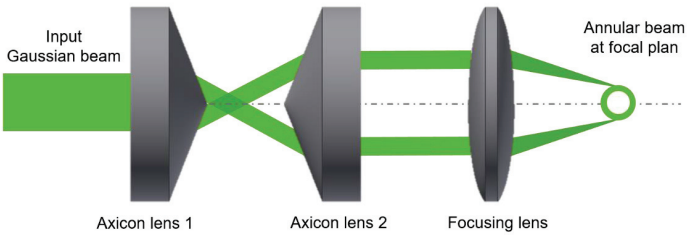


Fig. 16 Schematic diagram of an axicon-based optical trepanning/punching system [ZLK06]

As schematically depicted in Fig. 16, two identical axicon lenses are arranged symmetrically in a line, so that the emerging laser beam is parallel to the incident Gaussian laser beam. The angle of incidence of the focused annular beam is dynamically adapted by adjusting the distance between the two axicon lenses. The control of the diameter of the annular pattern is principally implemented by adjusting the distance between the focusing lens and the workpiece. Without

relative movement of the laser beam to the workpiece occurs, the optical trepanning is characterized as optical punching process. As a result of the beam shaping – from a spot Gaussian laser beam to an annular beam pattern – the optical trepanning/punching works efficiently in thin films or sheets.

2.3.2 Helical drilling of complex microholes

The circularity of a borehole is one of the key performance criteria during microhole drilling [Bh13] [Da17][Ha18b] . The circularity of the microhole ρ_c is defined as the degree of roundness of a circular hole and is calculated as follows:

2.6

$$\rho_c = 4\pi \frac{A_c}{P_c}$$

where A_c and P_c refer the area and perimeter of the through microhole respectively.

By using a quarter-wave plate, the circularity of boreholes can reach 0.95 owing to the circular helical path and the proper rotation of laser spot on the helical path generated by the mechanical precession movement [AR18a].

The major advantage of scanner-based helical optics is the high flexibility of hole geometry as shown in Fig. 17. By means of the synchronization of the galvanometer-scanner, the location of the laser pulses deposited on the workpiece can be precisely guided.

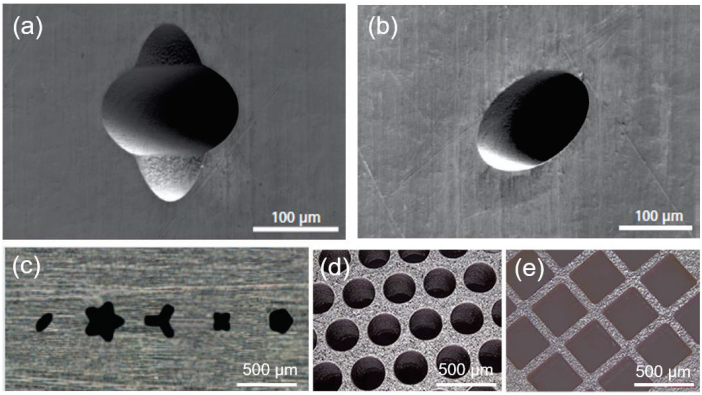


Fig. 17 Microholes with different shapes fabricated by scanner-based helical optics. (a) and (b) flexible hole geometry in 300 µm thick steel [Au16], (c) boreholes with high freedom in 300 µm stainless steel [AR18a], (d) and (e) straight-walled holes in 320 µm thick silicon nitride [Ae19]

The maximum inclination angle of scanner-based and rotating-prism-based helical drilling optics ranges from -7.5° to +7.5° depending on the factors of

focal length and applied laser wavelength [Au16]. The typical aspect-ratio of the microholes that are fabricated by scanner-based helical optics can reach 12:1 [AR18a]. Microholes with a diameter of 50 µm have recently been manufactured in 1 mm thick stainless steel by adapting the drilling strategies [Fü17]. The key objective of the process development for increasing the aspect-ratio of microholes in metals is to control the plasma in the borehole channel, in which the helical optics provides the possibility to control the location of pulse deposition [NSD16].

3 Experimental setup and instruments for characterization

3.1 Helical drilling systems and process

The helical drilling system consists of an ultrashort pulse laser source, the helical optics and a process monitoring system as schematically shown in Fig. 18. Passing through the helical optics, the linear polarized laser beam rotates around optical axis with a certain angular speed and is focused by the focusing lens on the workpiece.

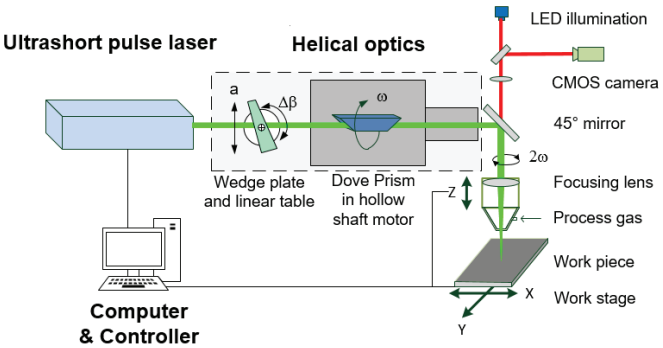


Fig. 18 Schematic diagram of a helical drilling system with an ultrashort pulse laser

3.1.1 Laser beam sources

As for the most part of the investigations in this work, a 7-picosecond laser (TruMicro 5270, TRUMPF) was employed. The ultrashort pulse laser source delivers a second harmonic generation of 515 nm wavelength using a LBO crystal leading to a maximum average output power of 60 W at the maximal repetition rate of 400 kHz. The maximum single pulse energy is 150 µJ. The output power and duration of laser pulse is programmable and, thus, a laser energy deposition can be adapted for drilling geometry during helical process.

In addition, a 12-picosecond laser(PX-series, EdgeWave) having a wavelength of 532 nm, average power 60 Watts (at 100 kHz) was applied for the experiments on 3 mm thick stainless steel. The laser source is a picosecond oscillator and amplifier system based on InnoSlab technology. The specifications of both laser sources are listed in Table 2.

Table 2: Specifications of the ultrashort pulse lasers applied in this work

		TruMicro 5270	EdgeWave PX-2
Wavelength	λ	515 nm	532 nm
Pulse duration	τ_p	7 ps	12 ps
Max. average power	P_{max}	60 W	60 W
Max. pulse energy	E_p	150 µJ	600 µJ
Repetition rate range	f_{REP}	0.4-400 kHz	1 – 1000 kHz
Beam quality factor	M^2	1.3	1.1
Raw beam diameter	d_{raw}	5 mm	3 mm

3.1.2 Helical drilling optics

The helical drilling optics applied in this work is based on a rotating Dove prism as shown in Fig. 19. The Dove prism is located in the hollow shaft motor, which has a maximum rotational frequency of 160 Hz, or rephrased a rotational speed of 160 revolutions per second (rps). The Dove prism works as an image rotator and is the core component in the helical drilling optics. In it the emerging laser beam has a doubled rotational speed of the Dove prism itself. The helical revolution of laser beam is enabled by the spinning Dove prism.

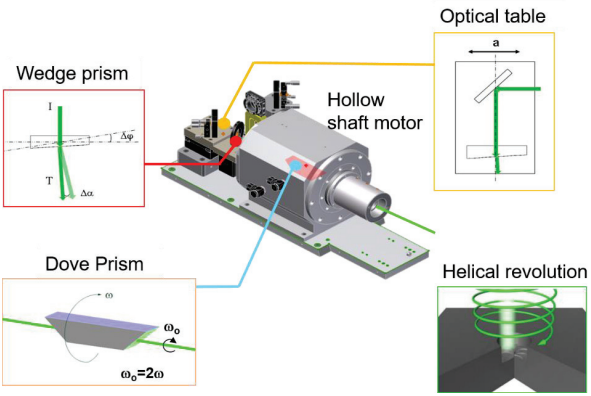


Fig. 19 Layout of the key components in the dove-prism-based helical drilling optics

The wedge prism mounted on a stepper motor in front of the Dove prism can change the inclination angle of the incident laser beam $\Delta\beta$ by deflection in a fixed angle. Thus, the tilt angle of laser beam relative to the focusing lens can be altered. By means of that, the distance between the focused laser spot to the optical axis center, i. e. the helical radius can be regulated. Additionally, an optical table on a linear stage enables parallel offset of the incident laser beam

to the Dove prism Δα. The linearly shifted laser beam meets the same position after it is focused by the focusing lens, but with an altered inclination angle to the surface of the workpiece. With the helical revolution, tiled angle is directly relevant to the hole taper. Thus, the hole conicity can be adjusted. The working principles of the tilt of wedge prism and parallel offset of the optical table are schematically illustrated in Fig. 20. The position and rotational speed of the wedge prism as well as the position of linear stage and its traveling speed can be precisely controlled. The precision of the angle position of wedge prism is 0.1° with a maximum rotation speed of 45°/s. The precision of the position of linear stage is 0.01 mm with a maximum rotation speed of 5 mm/s.

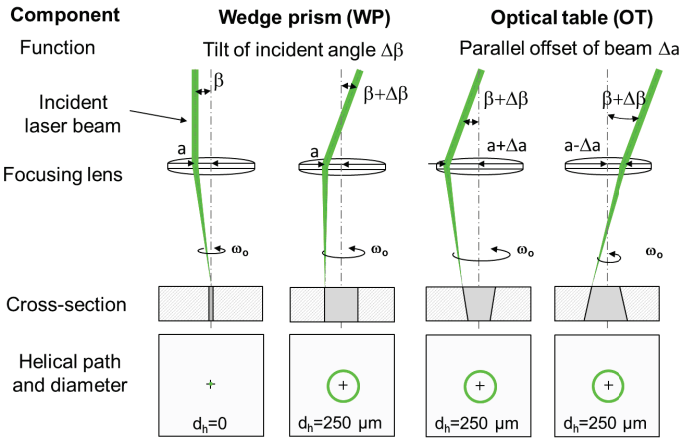


Fig. 20 Schematic of the working principle of the wedge prism in the helical drilling system

After propagating through the helical optics, the laser beam is focused on the surface of a sample by a triplet lens system having a 60 mm effective focal length. The focused spot diameters are 15 µm (TruMicro 5270) and 25 µm (EdgeWave PX-2), each measured with a single pulse energy of 3 µJ at the repetition rate of 200 kHz respectively.

The dynamic helical drilling process is performed in two steps: Foremost a cylindrical stem-hole can be drilled through with a classic helical drilling process. Following that, a wide positive conical entrance was fabricated by a three-dimensional helical drilling process, where the helical diameter was enlarged dynamically during drilling.

3.2 Materials and analysis methods

In the work, micro funnel-shaped holes were drilled in a thin-wall stainless steel (X5CrNi18-10) sheet of 0.5 mm thickness. According to EN 10020, particularly pure steels with mass proportions of iron companion elements of ≤ 0.035% are designated [BA05]. The type designation is X5CrNi18-10 of material identification number 1.4301; the other material characteristics are listed in Table 3.

Table 2: Overview of the properties of the material used in this work [TH06]

Parameter	Symbol	Value	Unit
Density	ρ	7.9	g/cm³
Modulus of elasticity	τ_p[Pa]	200	kN/mm²
Melting temperature	T_m	1670-1730	K
Evaporating temperature	T_v	2650	K
Specific heat capacity	c_p	500	J/(kg·K)
Thermal conductivity	k	15	W/(m·K)

The longitudinal cross-sections of the fabricated microholes were prepared so that the drilling depth and hole profile can be observed and characterized. For the light microscopic analysis of the samples, a microscope (VHX-2000, Keyence) was used. The light microscopic has magnifications from 100x to 2500x and the topographies of microstructures can be viewed and analyzed in 2D and 3D images.

Moreover, a confocal laser scanning microscope (LSM, VK-9700, Keyence) with a depth resolution 0.1 µm was employed to capture geometries and surfaces three-dimensionally. From the images of the LSM analysis, the surface average roughness value was determined, the profile structures at each point of the image could be measured as well.

Scanning electron microscopy (SEM, LEO 1455 EP, Zeiss) was used to characterize the morphological features in the boreholes, as it can be used to image particularly small structures in the nanometer range.

To characterize the heat affected zone (HAZ) of the pilot hole and shaped inlet, the sample was etched in a V2A-Beize bath for 10 s at a temperature of ca. 70°C. Subsequently, the metallurgical microstructure of the ablated areas was analyzed using a scanning electron microscope.

4 Helical path in helical drilling processes

The understanding of the behavior of the laser beam motion and the deposition of the pulses in the helical drilling process is a prerequisite to finding out the relationship between optical parameters and hole geometry as well as to enhancing the controllability of the helical drilling process. This chapter deals with the theory on the helical path and the intensity distribution along the helical path. For an intuitive description the helical path is visualized in two and three-dimensions. Moreover, the behavior of pulse overlap and the superposed laser intensity distribution are analyzed and numerically simulated.

4.1 Helical path

One of the characteristics of the helical drilling process is that the laser beam rotates along an optical axis. The rotation is driven by the spinning dove prism in the hollow shaft motor. As a result of a total internal reflection, which occurs in the Dove prism, the rotational speed of the laser beam is doubled when it passes through the spinning Dove prism. A single revolution of the laser beam corresponds to a 180° rotation of the Dove prism as depicted in Fig. 21.

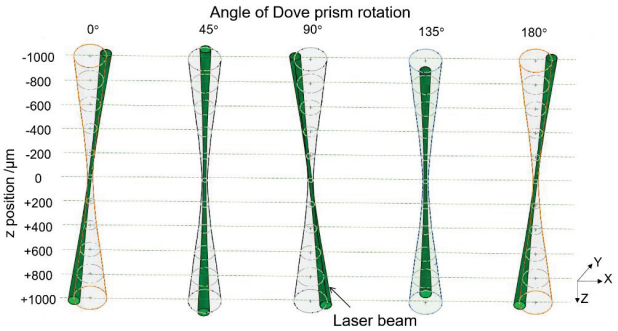


Fig. 21 Schematic diagram of the rotational behavior of a laser beam in relationship to the angle of the Dove prism rotation

As the Dove prism rotates from 0° to 45°, the laser beam rotates along the optical axis for 90°. The laser beam finishes one complete rotation whereas the Dove prism has only the half of a revolution. The 3D envelope of the rotating laser beam is illustrated in Fig. 21. The shape of the 3D envelope can be modulated by changing the rotation diameter and the angle of rotation axis. In the helical drilling, the rotation diameter can be controlled by setting the angle of wedge prism. The angle of rotational axis is controlled by displacing the laser beam with a linear axis. The trajectory of successively incoming laser pulses is defined as the

helical path. Two-dimensional (2D) and three-dimensional (3D) helical pathways are distinguished from each other depending on the observation from different dimensions. The z position z = 0 denotes the focal position of a single laser beam; the positive z position shows the direction of laser beam propagation.

4.1.1 Two-dimensional helical path

In a classic helical drilling process, where the helical diameter is constant, the incoming laser pulses are deposited in a sequence on the circular helical path as shown in Fig. 22. A two-dimensional helical path can be described as the trajectory of the laser beam center of the specific laser pulses distributed in one revolution on the xy plane. The branding marks of laser radiation with an interval of 60° in Fig. 22(b) show the helical rotation on focal plane. As a great number of subsequent laser pulses are applied in helical drilling; a 2D helical path with a diameter d_h on the focal plane is schematically illustrated in Fig. 22(c). The laser pulses have a certain degree of overlap and the angular distance of two neighboring laser pulses $\Delta\theta$ is a matter of pulse repetition rate and rotational speed and independent on helical diameter.

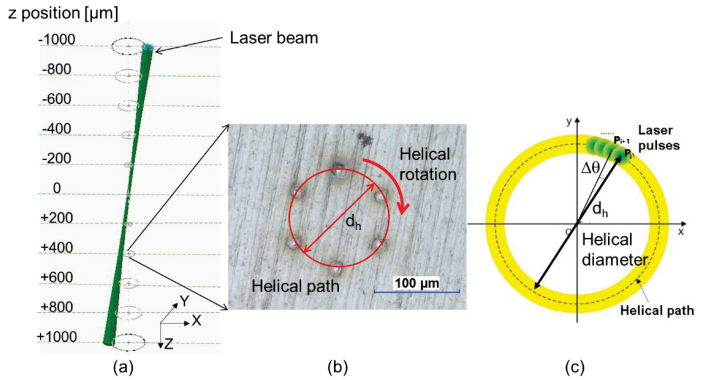


Fig. 22 Illustration of 2D helical path with branding marks on stainless steel at a low output laser power

In Cartesian coordinates, the position of the i[th] laser pulse $P(x_i, y_i)$ can be given as:

4.1

$$\begin{cases} x_i = r_h \cdot \cos\theta_i \\ y_i = r_h \cdot \sin\theta_i \end{cases}$$

where r_h is the helical radius and θ_i is the angular coordinate of the i[th] laser pulse. The angular coordinate θ_i can be expressed as:

4.2

$$\theta_i = 2\pi\omega_b t_i = 2\pi\omega_b \cdot \frac{i}{f}$$

Here, ω_b is the laser beam rotating speed, t_i the time moment of the i[th] laser pulse output and f the repetition rate of the laser pulses.

Since the helical radius is fixed in a classic helical drilling process, the positions of each pulse deposited on the helical path can be described by a polar coordinate system as following:

4.3

$$r(\theta_i) = r_h$$

In a dynamic helical drilling process, the helical radius is a variable. The position of the i[th] laser pulse $P_T(x_i, y_i)$ can be given in the Cartesian coordinates, as:

4.4

$$\begin{cases} x_i = r_{hi} \cdot \cos\theta_i \\ y_i = r_{hi} \cdot \sin\theta_i \end{cases}$$

Here, r_{hi} is dynamic helical radius, which can be continuously varied over the process time. Fig. 23(a) illustrates the spiral helical path with a continuously increased helical diameter. Due to the similar behavior of pulse distribution, this kind of dynamic helical process can be defined as a helical trepanning process.

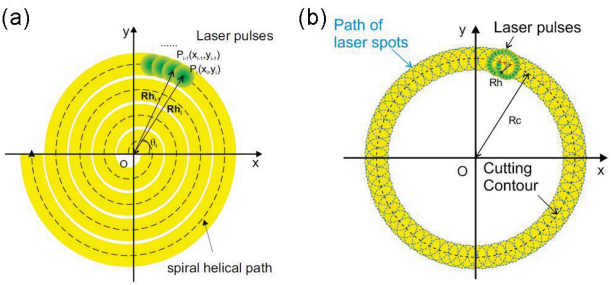


Fig. 23 Two-dimensional helical path of helical trepanning (a) and helical contour cutting (b)

Helical contour cutting is considered to be another dynamic helical process for producing circular holes. In the helical contour cutting process, the laser beam has a helical revolution with smaller helical radius as the classic helical drilling process, meanwhile the center of the revolution moves forward in a defined contour by motion axis. The path of laser pulses in helical contour cutting is depicted in Fig. 23(b). With a given radius of circular contour r_c and cutting velocity v_c, the pulse position $P_C(x_i, y_i)$ at the time moment t can be given as:

4.5

$$\begin{cases} x_i = r_c \cdot \cos\left(\frac{v_c}{r_c}t\right) + r_h \cdot \cos\theta_i \\ y_i = r_c \cdot \sin\left(\frac{v_c}{r_c}t\right) + r_h \cdot \sin\theta_i \end{cases}$$

With the above equations, the helical path of classic and dynamic helical drilling process including helical trepanning and helical contour cutting can be numerically represented. Based on the numeric representation, the laser energy deposition can be quantified in the following sections.

4.1.2 Three-dimensional helical path

The 2D helical path can represent a pulse distribution on the xy plane with a fixed helical diameter at a certain z position. However, a single 2D path is not able to show one of the key characteristics of a borehole – the conicity. In the helical drilling process, the hole geometry is determined primarily by the caustic of the three-dimensional (3D) helical path, in addition to the laser parameters applied. The 3D helical path describes the trajectory of the laser pulse positions in revolutions along the hole depth. Rephrased, by plotting the positions of laser pulses sequentially deposited, the spatial path of laser pulses in the whole drilling channel can be represented approximately as a 3D helix curve – the 3D helical path.

Fig. 24 illustrates the 3D helical paths for three typical hole profiles: positive and negative conical as well as cylindrical. Generally, a 3D helical path of a laser beam in the borehole is determined by the positions of wedge prism and linear table.

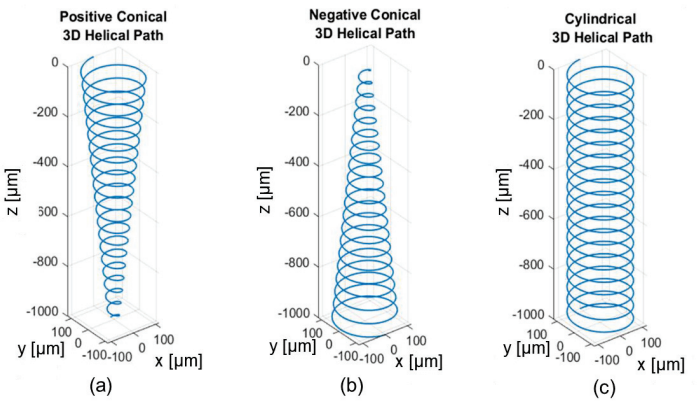


Fig. 24 Simplified three-dimensional helical path in (a) positive, (b) negative conical and (c) cylindrical profiles

In the classic helical drilling process, a cylindrical or positive/negative conical helical path and a helical diameter depending on the desired hole profiles are predefined by setting and fixing proper optical parameters. By means of that, a 2D or 2.5D borehole can be produced. An adapted 3D helical path plays a significant role in helical drilling of 3D shaped holes such as a microfunnel, the helical path is plotted in a Cartesian coordinate system and shown in Fig. 25.

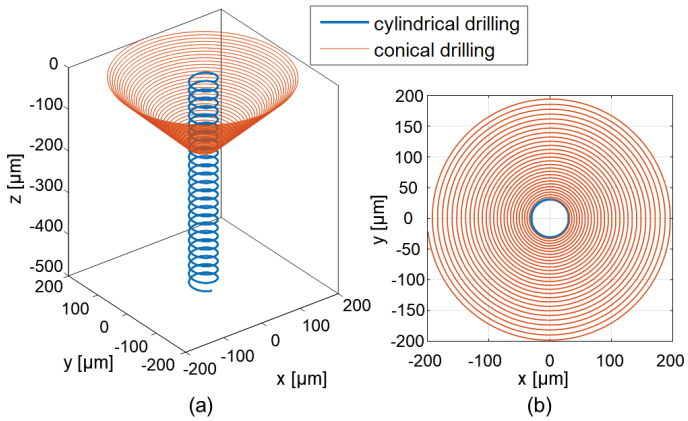


Fig. 25 Combined helical paths for funnel-shaped holes (a) 3D helical path, (b) top view of 3D helical path

4.2 Visualization of helical path

To link the 3D helical path to the final geometry of a borehole drilled by helical optics, an intuitive representation of the abstract helical path is essential. The visualization of helical path can be achieved by means of CAD software and a measurement of helical diameters at varied optical parameter.

One method to record the helical diameter is to produce branding marks by laser radiation with very low single pulse energy on a polished target. The branding marks on stainless steel in Fig. 26(a) show the development of a helical diameter at varied z positions and optical table positions (OT). Instead of a whole revolution, merely two dots at the Dove prism angle of 0° and 90° separately are marked at each z position. The distance of the centers of 0° and 90° branding marks corresponds to the helical diameter at the plane as a result of the doubled angular speed of the Dove prism. Interesting to be noted is that the 2D helical path can roughly be seen in Fig. 26(a) from the angle between axes of 0° and 90°, also at OT=±2.5 mm and ±5 mm. However, in the case when the laser branding marks overlap each other (at OT=0), an intuitive helical path fails to be represented. Due to that, the helical diameters are subsequently measured by means of a digital microscope having a maximum magnification of 2000 and represented in diagram plotting the helical diameter at the z position as shown in Fig. 26(b).

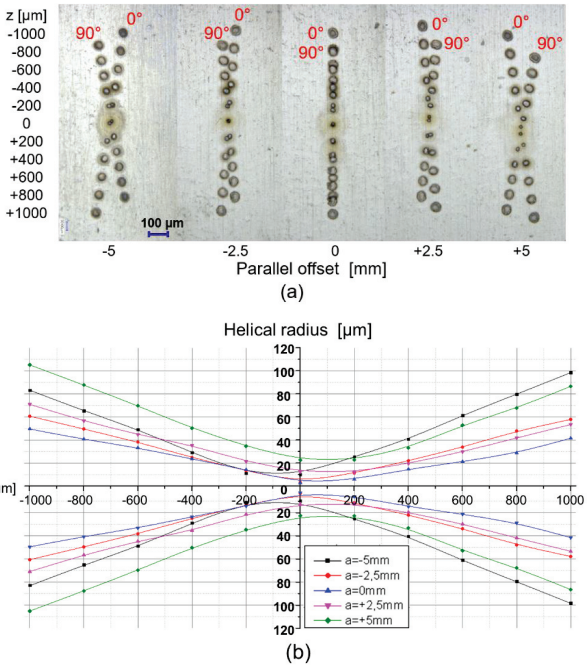


Fig. 26 Development of helical diameters at varied z positions and optical table positions (OT): (a) Diagrams of branding marks, (b) Plotted diagram of helical path

The other method to measure the helical diameter is to record the position of the laser spots at 0° and 90° using a high-resolution CMOS camera. In this work, the camera (IDS, µEye) has a lateral resolution of 1.67 µm. The coordinates of each spot can be precisely recorded and extracted from the software (Laseview) as shown in Fig. 27.

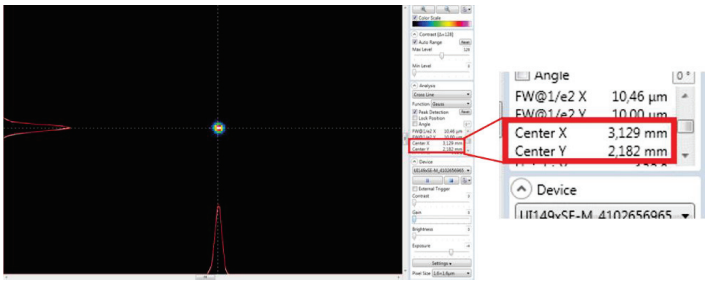


Fig. 27 Record of the position of laser spots by means of CMOS camera and analyzing software

Based on the measured data of helical diameters at z positions and varied position of the wedge prism and optical table, a rotary symmetric 3D helical path can be visualized. Since the longitudinal cross-section of the 3D helical path contains equivalent information as the 3D model, the helical path is depicted mostly as a cross-section profile (caustic).

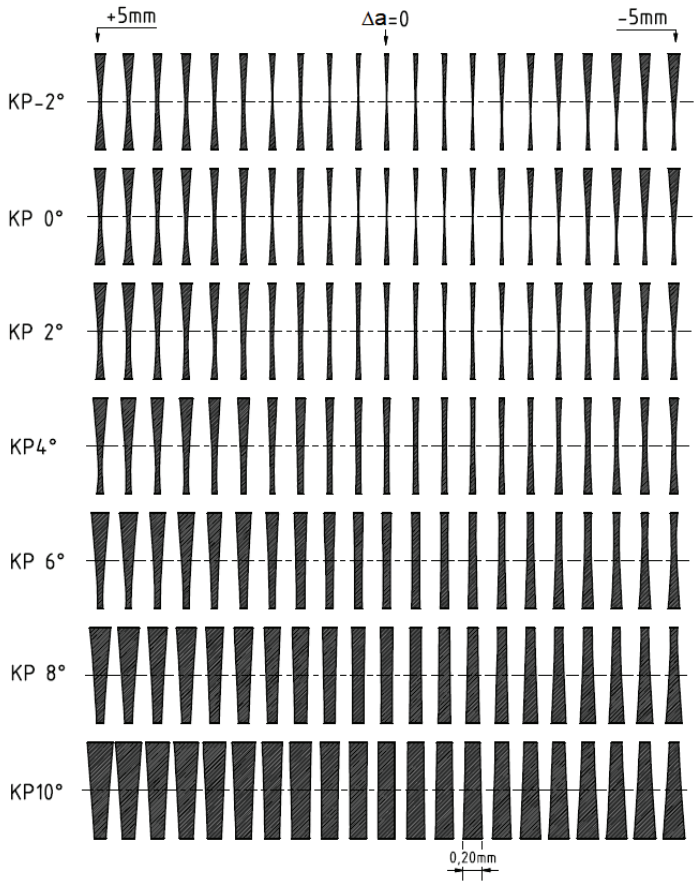


Fig. 28 Road map of helical path in the x/y-z plane with a varied position of the wedge prism (KP) and optical table (OT)

The 3D helical path is adjusted for holes with designated profiles. As aforementioned, the 3D helical path is determined by the position of wedge

prism and parallel offset in the helical drilling optics. Fig. 28 shows the caustic of the helical path with varied parallel offset (Δa) from a = -5 mm to +5 mm with an interval of 0.5 mm at the position of the wedge prism (KP) from -2° to 10° with a pitch of 2°. The z position ranges from -0.5 mm to +0.5 mm. The dashed lines are the z position at 0 mm. From the roadmap of sectional graph of simplified 3D helical path showed in Fig. 28, the dependence of the waist position on the stepping motor angle and linear stage can be extracted.

An intuitive development of the profiles is displayed in Fig. 28, in which the caustic of the helical path is almost cylindrical when the parallel offset OT = 0 mm. The profile, however, evolves to a negative conicity at negative positions OT < 0 mm and a positive conicity at positive positions OT > 0 mm. Noteworthy is that the positions of caustic waist in helical path are not always overlapped with the position of laser beam focus z=0. At the negative parallel offset, the positions of caustic waist are located above the focal position, whereas they are located below z = 0 at the positive parallel position. When the parallel offset OT = 0 mm, the waist position of the caustic of the helical path in the z direction stays almost constant; at z = 0, it is overlapped with the beam waist. The caustics at different wedge prism positions are symmetric on the focal plane. With the increase of stepping motor angle, the helical diameter increases correspondingly.

At a negative parallel offset (OT < 0), the waist position of the caustic of the helical path descends in the z direction as the angle of wedge prism (KP) increases. That means the smallest helical diameter is located further away from the laser focal plane as the angle of wedge prism increases. On the contrary, the waist position of the caustic of helical path rises in the z direction with a positive parallel offset (OT > 0) as the stepping motor angle increases. In addition, the smallest helical diameter is located further away from the laser focal plane as the angle of wedge prism increases. Within the same parallel offset, the helical diameter increases along with the angle of wedge prism.

Within the same angle of wedge prism, the waist position of the caustic of helical path develops from below the focal position (+z) to above (-z) as the parallel offset varies from positive to negative positions. The tendencies can be easily detected, especially at KP≥4°. The caustics of the helical path evolve from a positive conical shape to negative conical ones.

The visualization of helical path gives an intuitive overview of how the caustic of 3D helical path develops. It contributes to a prognosis of the hole profile, which can be indirectly represented by the visualized helical path. However, the fact is that laser helical drilling is a process simultaneously influenced by several factors, such as material properties, overlapping rate of the laser beam, energy loss during drilling process, thermal accumulation in the drilling hole and so on. In order to draw more reliable and accurate conclusions on how the helical path influences hole geometry, drilling experiments were carried out with a series of

different parameters with reference to the simplified 3D helical path diagram. The results are discussed in the following chapters.

4.3 Laser intensity distribution on helical path

4.3.1 Pulse distribution on helical path-pulse overlap

In ultrashort pulsed laser processing, the laser beam sources normally work at a high repetition rate from tens of kilohertz (kHz) to megahertz (MHz). To achieve a well-defined ablation edge, the laser pulses applied for ablation has a certain degree of overlap. The adjacent pulse centers are less than a diameter apart. The overlap of laser pulses is schematically shown in Fig. 29.

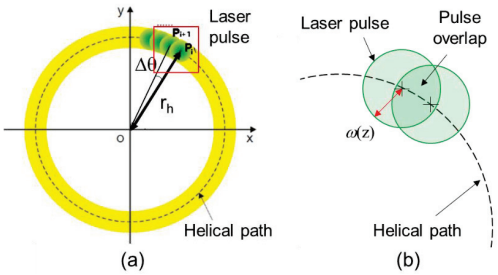


Fig. 29 Schematic diagram of pulse overlap in the helical drilling process. (a) An overview of the laser pulses on helical path. (b) The details of marked in red box in (a)

In analogy to the calculation of laser pulse overlap in a laser beam removing process using a galvanometer scanner published in [VD12], the calculation expression of overlap degree η_{or} in helical drilling is given as the following:

4.6

$$\eta_{or} = 1 - \frac{r_h(z) \cdot \sin(2\pi \cdot \omega_m / f)}{w(z) + \pi \cdot \omega_m \cdot r_h(z) \cdot \tau_p}$$

Here $w(z)$ is the beam intensity 1/e² radius of the laser spot in the z position and z = 0 corresponds to a focal plane of the laser beam, $r_h(z)$ is helical radius of the revolution at z position, ω_m is rotational speed number of the hollow shaft motor or the rotational frequency of the Dove prism, f is the repetition rate of laser pulses, τ_p is the pulse duration.

Considering the employment of an ultrashort pulsed laser that the pulse duration $\tau_p < 10$ ps, and $f \gg \omega_m$, therefore, the phrase $\pi \cdot \omega_m \cdot r_h(z) \cdot \tau_p$ approaches zero and $sin(2\pi \cdot \omega_m / f)$ approaches $2\pi \cdot \omega_m / f$. Thus, the expression of overlap degree in a helical revolution can be simplified as:

4.7

$$\eta_{or} = 1 - \frac{2\pi \cdot r_h(z) \cdot \omega_m}{w(z) \cdot f}$$

The overlap degree of laser pulses in helical processing describes the spatial distance between the laser pulses deposited sequentially on the helical path. To represent the density of laser pulses deposited locally on a single revolution of a helical path, the number of laser pulses per unit length N_{ppl} is introduced and given as:

4.8

$$N_{ppl} = \frac{f/2\omega_m}{2\pi r_h(z)} = \frac{f}{4\pi\omega_m r_h(z)}$$

Helical radius, rotational speed and repetition rate are, first of all, the three key factors that determine the overlap degree in helical drilling process. The development behavior of the overlap degree with the key parameters is shown in Fig. 30(a) and (b). The relationship between two of the key factors and overlap degree are represented, respectively. With a constant pulse repetition rate, the overlap degree drops down with the increase of rotational speed and helical radius. Intuitively speaking, the total number of incoming pulses in a unit time is fewer due to the shortened period of the helical revolution, and meanwhile the circumference of the revolution becomes greater with the increasing helical radius. As a result, the pulse overlap drops down as can be seen in Fig. 30(a).

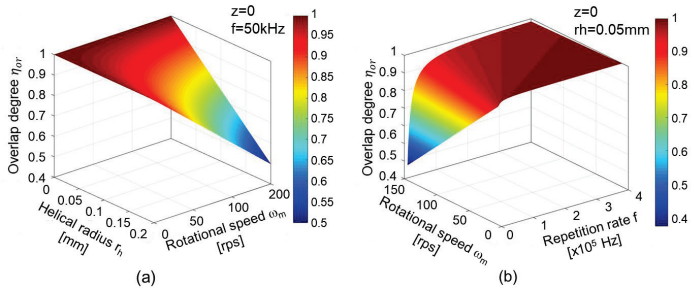


Fig. 30 Correlation between overlap degree and rotational speed, repetition rate and helical radius at focal plane

Whereas when the helical radius stays constant, the overlap degree stays relatively stable, having a value over 0.95 at a higher repetition rate (>100 kHz), but it drops dramatically if the laser pulse repetition rate is reduced, especially below 50 kHz, as shown in Fig. 30(b). Generally, a higher overlap degree is preferred to achieve higher ablation efficiency. For high precision drilling with a minimized heat affected zone, however, a relative low repetition rate of laser pulses is reasonable. Thus, a trade-off between efficiency and accuracy should be taken into consideration. If working at a laser pulse repetition rate over 100 kHz, the rotational speed of the Dove prism plays a minor role in overlap degree, since the part ω_m/f in the Eq. **4.7** only has an extremely slight difference when ω_m rises from 0 to 150 rpm.

4.3.2 Superposed laser intensity distribution

Superposed laser intensity distribution in classic helical drilling

The overlap degree of laser pulses and number of laser pulses per unit length on the helical path describe the spatial behavior of laser pulse deposition in the helical drilling process. From the point of view of laser energy deposition, the higher the overlap degree, the more laser energy is deposited at unit length on the helical path. In a classic helical drilling process, where the helical path is constant, the incoming laser pulses are deposited in a sequence on the circular helical path. The spatial distribution of pulses and the superposed laser intensity distribution are shown in Fig. 31.

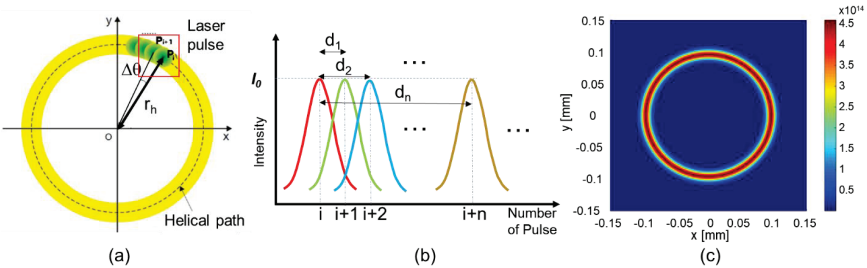


Fig. 31 (a) The distribution of the laser pulses train on helical path, (b) the overlapped intensity of pulses, (c) the calculation of superposed intensity distribution

In the helical drilling process, the angular distance $\Delta\theta$ and that between two consecutive laser pulses are given by:

4.9

$$\Delta\theta = 2\pi \cdot 2\omega_m \cdot \Delta t = \frac{4\pi\omega_m}{f}$$

And the spatial distance between the ith pulse and the $(i+n)^{th}$ pulse d_n is:

4.10

$$d_n = d_h \sin(n\Delta\theta/2) = d_h \sin(2\pi n\omega_m/f)$$

Here, ω_m is the rotational frequency of the Dove prism, Δt is the time interval between two consecutive laser pulses, f refers to the pulse repetition rate, and d_h is the helical diameter.

Depending on the material and specifications of drilling, helical drilling needs several hundreds to tens of thousands of revolutions of laser pulses to fabricate a hole. The intensity of single laser pulse I_0 at focal plane in the revolution is:

4.11

$$I_0 = \frac{P_{peak}}{A_P} = \frac{E_p/\tau_p}{\pi w_0^2}$$

where P_{peak} is laser peak power, E_p is single pulse energy applied, τ_p is pulse duration, A_P is effective focal spot area, and w_0 is the beam intensity 1/e² radius of laser spot on focal plane of laser beam.

A superposed laser intensity (SLI) is defined to describe the laser energy deposition of ultrashort pulses on helical path and the SLI at z position. According to the **4.9** and **4.10** the local superposed laser intensity $I_s(z)$ at a given z position is expressed as:

4.12

$$I_s(z) = \sum_{i=1}^{ft} I(z) \cdot exp\left(-2\frac{d_{i-1}^2(z)}{w^2(z)}\right) = \sum_{i=1}^{ft} I(z) \cdot exp\left\{-2\frac{d_h^2(z)\sin^2[2\pi(i-1)\omega_m/f]}{w^2(z)}\right\}$$

Here, $I(z)$ is the peak intensity of the pulse at z position and t refers to the drilling time. The superposed laser intensity on the focal plane of laser beam z = 0 can be given as:

4.13

$$I_{s0} = \sum_{i=1}^{ft} I_0 \cdot exp\left(-2\frac{d_{i-1}^2}{w_0^2}\right) = \sum_{i=1}^{ft} I_0 \cdot exp\left\{-2\frac{d_h^2\sin^2[2\pi(i-1)\omega_m/f]}{w_0^2}\right\}$$

With the equations and by means of the numeric simulation using Matlab, the superposed intensity distribution with varied helical diameter is plotted and shown in Fig. 32. The single pulse energy, the rotational frequency of the Dove prism and pulse repetition rate as well as the drilling time play a role in the development of local superposed laser intensity.

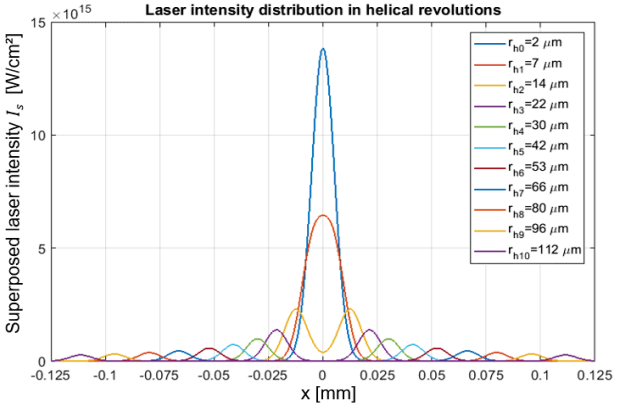


Fig. 32 Superposed intensity distribution with varied helical radii

Main parameters: Laser single pulse energy: 82.5 μJ, f=40 kHz, laser duration: 0.1 s, ω_m=60 rps, ω_0=10 μm

Under the conditions that the laser parameter, rotational speed, and focal position are kept constant during helical drilling, the peak intensity drops down dramatically as the helical diameter increases, showing a strong link to the pulse overlap degree – an anti-proportional behavior. This can also be deduced from the Eq. **4.12**: $I_s \propto f(-d_h^2)$. The superposed laser intensity is a function of $-d_h^2$. When the helical radius is smaller than the laser spot radius w_0, each of the laser pulses has an overlap on other pulses within the helical path, an intensity "peak" is thus formed since all of the pulses contribute to the superposed intensity in the center of helical path (x=0). This means that the whole volume in the borehole is irradiated by laser pulses and a "full-ablation" process occurs. The peak of the superposed intensity splits into two when the helical radius increases to greater than the spot radius, two peaks can be distinguished from the cross-section profile of superposed intensity distribution. However, it does not mean that the interaction of the laser pulses with 180° angular interval is excluded. As can be seen in Fig. 32, the intensity at the center of helical path equals approximately one fifth of the peak intensity at helical diameter of 14 µm. In this case, the whole area with the circumference of the helical diameter plus laser spot size is irradiated by the laser pulses and can be ablated if the superposed intensity exceeds the ablation threshold of the material. As the helical diameter increases further, the peak value of superposed intensity has no significant decrease. Moreover, a "clear separation" of pulse intensity profile can be observed, and the superposed laser intensity distributes symmetrically along the helical center. The outer contour of the boreholes will be ablated without the laser removal of the core part. The drilling process is thus more efficient compared with an ablation process of the full volume of borehole using e.g. a scanner.

Superposed laser intensity distribution in dynamic helical processes

The dynamic helical process is characterized by a dynamically varied helical diameter (helical trepanning) or a process with fixed helical diameter, but dynamic helical center (helical contour cutting) during the helical drilling. As a result of the distinguished spatial distribution of the pulse locations, the ablation behavior differs in different helical processes. Based on the Eq. **4.4** and **4.5**, the single pulse position in the dynamic helical process can be exactly defined and, thus, the numerical calculation of the superposed intensity distribution can be carried out.

In analogy to the classic helical drilling, the results of helical trepanning and helical contour cutting with the initial parameters displayed in Table 3 are represented in a color map as shown in Fig. 33. Helical trepanning and helical contour cutting process can be applied to fabricate highly qualitative microholes (cf. 6.2).

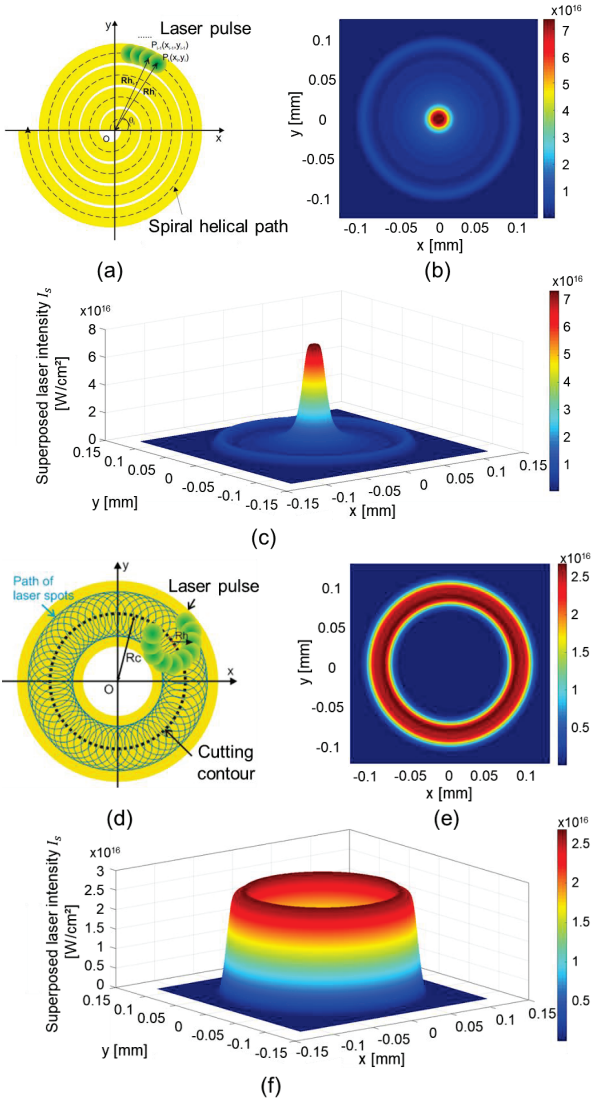


Fig. 33 Superposed intensity distribution in helical trepanning (a-c) and helical contour cutting (d-f) with the parameters in Table 3. (a) and (d) helical path, (b) and (e) intensity distribution from on xy plane, (c) and (f) 3D intensity distribution. Note the different scales of color bar

The helical trepanning is a process with a full-volume ablation. The characteristics of the superposed laser intensity in helical trepanning are, first of all, a peak in the center of the helical path and relative low intensity outside it. Besides a pulse-to-pulse overlap, a path-to-path overlap in the radial direction at varied helical radii is another key feature of helical trepanning. Depending on the laser spot size and path-to-path offset, which is determined by the rotational speed of wedge prism, the path-to-path overlap varies and is not a constant value since the increase of helical diameter has no linear behavior to the angle of wedge prism (see 5.2.1). This is again a distinction between processing using helical drilling optics and a galvanometer scanner.

Table 3: Parameters for the numeric simulation of helical trepanning and helical contour cutting in Fig. 33

Parameters	Helical trepanning	Helical contour cutting
Single pulse energy	82.5 µJ	82.5 µJ
Pulse repetition rate	40 kHz	40 kHz
Rotational speed	60 rps	60 rps
Laser spot radius	10 µm	10 µm
Helical radius	dynamically increased with rotational speed of wedge prism 0.5°/s	30 µm radius of cutting contour: 0.085 mm
Other parameters	dwell of 2 s at r_h = 10 µm	feed rate of motion: 0.05 mm/s

Fig. 34 depicts the superposed intensity of all helical processes. In the helical contour cutting process, the appearance of the superposed intensity distribution in case of the circular cutting is analogous to classic helical drilling (cf. Fig. 31c) – a donut shape.

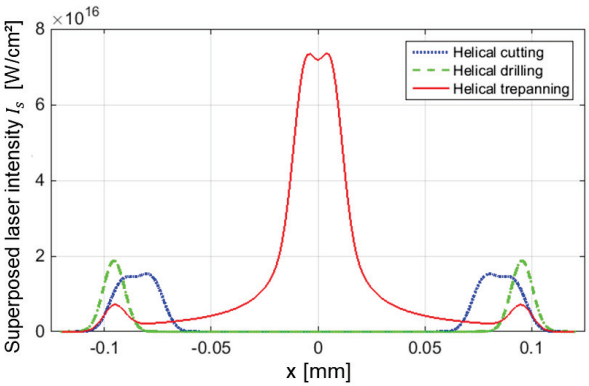


Fig. 34 Comparison of the superposed laser intensity distribution of classic helical drilling (dashed line in green), helical trepanning (solid line in red) and helical contour cutting (dotted line in blue)

The profile of superposed intensity in classic helical drilling can be considered as a symmetric Gaussian distribution and, as a result, a linear accumulation of superposed intensity of laser pulses. However, due to a wobbling motion of the laser beam, the intensity at the inner circular contour is higher than that at the outer contour, as can be seen in Fig. 34. Depending upon the helical radius (the radius of wobbling motion) and feed rate of axis, the deviation of intensity distribution at inner and outer contours can lead to dissimilar results on, for instance, thermal effect and surface roughness on cutting kerf. A path-to-path overlap caused by the wobbling motion is tangential to the center of cutting contour. Compared to helical trepanning, helical contour cutting has a considerably lower ablation volume, but still larger than classic helical drilling, where a single path of laser pulses exists and, therefore, the ablation width is the smallest.

4.4 Summary

The helical path describes the spatial trajectory of laser pulses deposited during helical processing and is a key terminology through all helical processes: the classic helical drilling with fixed helical diameter, helical trepanning with dynamic variation of helical diameter and helical contour cutting. The helical path can be represented in 2D and 3D, providing useful information about helical diameter at different z positions, angle of divergence and convergence, positions of caustic waist (minimum helical diameter), and so on. Therefore, the helical path gives an indication of the hole geometry. With the understanding and mapping of the helical path at different positions of the wedge prism and optical table, the parameter windows for fabricating microholes with specific geometry can be given. The mapping of helical path can be achieved by visualizing the helical path with laser branding marks or camera-based digital measurement. The latter method is more precise and more reliable.

The distribution of laser pulses on helical path determines the pulse overlap and, furthermore, the intensity distribution on the helical path. Superposed laser intensity is introduced to quantify the laser energy deposition during the helical process. Due to the distinction of helical paths among three helical processes, the energy deposition of each process has its own features: Classic helical drilling has minimum ablation volume, helical trepanning is characterized by full-volume-ablation of the borehole, whereas helical contour cutting has a greater kerf compared with classic helical drilling.

5 Classical helical drilling process and influential factors

The classic helical drilling process is the most commonly employed and fundamental manufacturing process to fabricate 2-dimensional or 2.5-dimensional microholes. As aforementioned, the classic helical drilling process is characterized by a fixed helical path and laser parameters applied during the entire process. Generally speaking, the helical path can indicate the hole geometry (hole diameter and hole conicity), however, only under certain conditions. The processing parameters in the classic helical drilling process include parameters of the laser beam (single pulse energy, pulse repetition rate and exposure duration) and parameters of various optical components (rotating speed of the Dove prism, focal position relative to the workpiece) as well as the pressure of the assisting gas and the chemical composition of the assisting gas. In this chapter, the influence of the processing parameters on the classic helical drilling process of stainless steel will be discussed. Furthermore, the temporal evolution of the borehole geometry in the classic helical drilling process is analyzed by means of an exit-situ observation methodology. In addition to the borehole geometry, the thermal effect and diverse metallurgical properties after the drilling process are addressed.

5.1 Laser parameters

The laser beam source, a significant part in laser processing, plays a vital role in classical helical drilling. Modern laser systems make it possible to digitally control the output, such as laser power, laser beam pulse form and trigger modes. In state-of-the-art helical drilling, three parameters of the laser beam – namely single pulse energy, pulse repetition rate and exposure duration (drilling duration) – are the main factors influenced by the laser source and exert a dominating influence on the hole geometry and the total drilling efficiency.

5.1.1 Single pulse energy

Ultrashort pulse lasers with a pulse duration regime from a hundred femtoseconds to tens of picoseconds are dominantly employed in the high-precision ablation process. The absorbed energy per unit volume can be assumed to exponentially drop with the distance to the focus of laser beam as a consequence the often-reported logarithmic ablation law results. The ablation depth can be given as [Ne14]:

5.1
$$D_{ab} = \delta \cdot ln\left(\frac{F}{F_{th}}\right)$$

with the ablation depth D_{ab}, the energy penetration depth δ, the applied fluence F and the threshold fluence F_{th}.

The onset of ablation occurs above a threshold fluence, which will depend on the absorption mechanism, particular material properties, microstructure, morphology, the presence of defects, and on laser parameters such as wavelength and pulse duration [SMP10]. For a pulsed Gaussian beam distribution with single pulse energy E_p and spot radius w_0, the peak flucence F_0 in the center of the beam can be expressed as:

5.2

$$F_0 = 2E_p/\pi\omega_0^2$$

The peak fluence of the laser pulse is determined by the applied single pulse energy. The influence of laser pulse duration and the interpulse heat accumulation on the ablation threshold fluence of stainless steel has been investigated by Raciukaitis et. al. in [Ra08]. With an adaption of laser pulse duration, the fluence of ablation threshold by single pulse is measured to be F_{th}=0.50 J/cm².

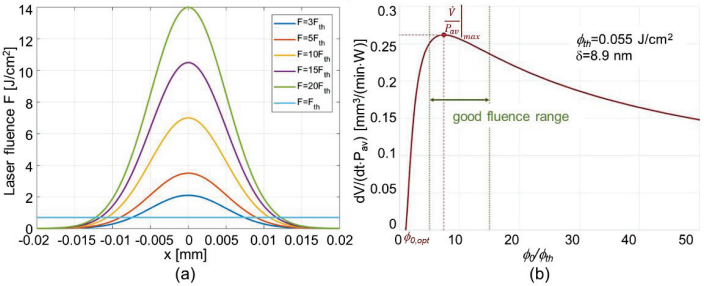


Fig. 35 (a) Ablation threshold and scaling of the applied laser fluence, (b) Removal rate per average power for surface ablation of stainless steel as a function of the peak fluence [Ne14]

Fig. 35(a) shows the scaling of the applied laser fluence with reference to the ablation threshold. As the laser single pulse energy increases, the laser fluence rises proportionally. Thus, the cutoff distance above the threshold fluence becomes greater, and the ablation diameter increases. However, the increment of ablation diameter drops down when the laser fluence increases further. According to [Ne14] the ablation rate increases correspondingly as illustrated in Fig. 35(b). However, with the further increase of laser fluence, the ablation efficiency (ablation rate divided by laser power applied) reaches the maximum at approximately 7.5 times of the ablation threshold fluence, and then it drops. [Ne14] has even given a "good fluence range" which is between five times to fifteen times of the ablation threshold. In the most cases of helical drilling process, the applied single pulse energy exceeds even 20 times the ablation threshold fluence. The materials to be processed have a thickness greater than the working distance of the laser beam (defined as two times the Rayleigh length)

and the aspect ratio to be achieved is normally higher than 1:1. Moreover, due to the defocusing of the laser beam when processing thick material, the laser fluence at different depths within the borehole decreases with the increase of depth. In order to achieve an effective ablation and a specified hole geometry, the laser fluence applied is essential to be adapted properly.

The experiments with varying laser single pulse energy were carried out in a 1 mm thick stainless steel plate. Microscopic images of the hole inlet (entry) and outlet (exit) as well as the diagram of the hole diameters measured against single pulses energy applied are shown in Fig. 36. Both hole entry and exit have excellent sharp edge and circularity (> 0.98). Moreover, the diameter of the hole entry for different single pulse energies that are applied is very stable with a deviation of 4 µm compared to the average values. The exit diameter shows a quasi-linearly rising behavior as the single pulse energy increases. Since the applied laser fluence here (47.7 J/cm²@75 µJ at focus) is considerably higher than the fluence of the ablation threshold (F_{th}=0.50 J/cm²), the diameters of hole inlets do not differ significantly from each other as the single pulse energy is varied. The influence of increased single pulse energy on the exit diameter of the borehole, however, has dramatically increased. The increasing single pulse energy contributes to a growing ablation volume as well as the ablation rate. The conicity of boreholes, defined as the ratio of the diameters of hole inlets and outlets, has been changed from 1.17 to 0.93. The hole profile evolves from a slightly positive conical hole to a slightly negative conical one. With a given helical diameter and parallel offset of incident laser beam, the helical path is determined; despite this, the experiment provides evidence that the single pulse energy applied has a significant influence on the final hole geometry.

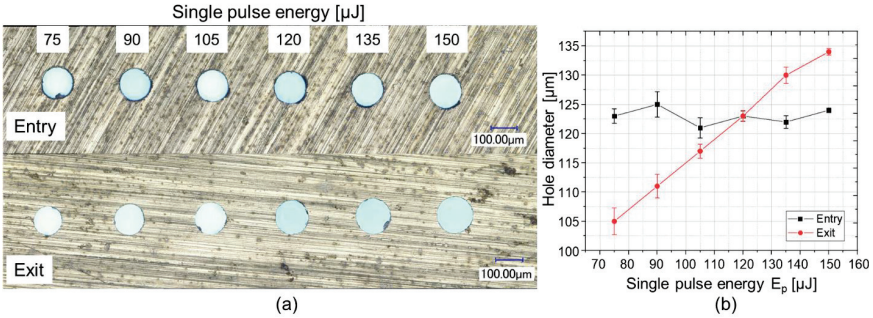


Fig. 36 Helical drilling in 1 mm thick stainless steel with varied single pulse energy. (a) Microscope images of hole entries and exits. (b) Diagram of the hole diameters vs. applied single pulse energy.
Parameters: repetition rate: 100 kHz, drilling time: 15 sec., gas pressure: 3 bar (compressed air), helical diameter: 100 µm, optical table position: Δa = 0 mm, rotational speed: 50 rps, z position: +200 µm in material

The maximum single pulse energy of an ultrashort pulsed laser plays a decisive role particularly in the fabrication of microholes in material thicker than 3 mm with respect to drilling precision, drilling efficiency and achievable aspect-ratio. Fig. 37 shows the distinction of the helical drilling process in 3 mm thick stainless steel material using two picosecond-laser beam sources with a maximum single pulse energy of 150 µJ and 650 µJ, respectively. The focal position for both investigations is at 0.5 mm beneath the top surface of the material. As can be seen in Fig. 37, the microfunnel-like borehole made using Ep_{max}=150 µJ has a taper angle of about 67° and evident striation on the hole inlet. Due to the defocusing of the incident laser beam and the reflection on the narrow inner of the borehole wall, the laser fluence decreases as hole depth increases. Once the laser fluence drops down below the material ablation threshold, the ablation process stops and only thermal energy is brought into the material. For the laser source with Ep_{max}=150 µJ, 3 mm of material thickness is the critical thickness. No broadening phase occurs in during the drilling process even with a drilling duration of 120 seconds. In contrast, the cross-sectional profile of high-aspect microholes drilled by Ep_{max}=650 µJ generally has significantly higher cylindricity and parallelism at different parallel offsets. The right-angled inlets exhibit high surface quality and are free of striation. Moreover, the higher single pulse energy enables a broadening phase of the helical drilling process on the borehole outlet and contributes to a more efficient drilling process. The drilling-through time with the laser source with Ep_{max}=650 µJ can be reduced to 15 seconds. Thus, the impact of material vapors and material plasma, which are driven out from the borehole inlet before the hole is drilled through completely, on the morphology of the borehole inlet can be minimized.

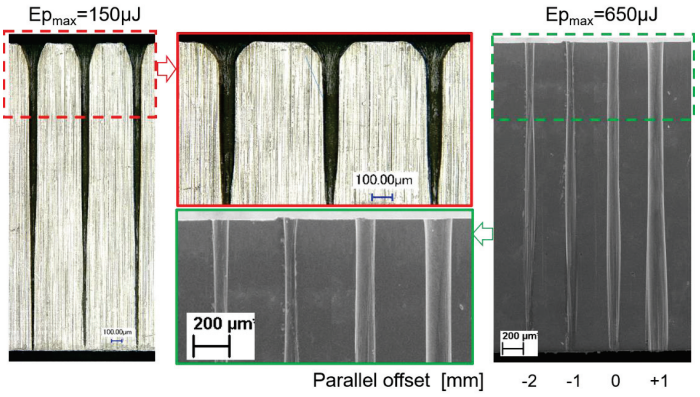


Fig. 37 Comparison of helical drilling of 3 mm thick stainless steel using maximum single pulse energy of 150 µJ and 650 µJ

5.1.2 Pulse repetition rate

The influence of the pulse repetition rate on the borehole geometry with respect to the entry diameter and the exit diameter has been investigated under the same conditions shown in section 5.1.1. Conditional upon the laser system technology, the laser repetition rate is controlled by a pulse picker with an integer divisor. The fundamental repetition rate of the applied laser source is 400 kHz. With the available pulse repetition rate and adapted process parameter, the drilling results are exhibited in Fig. 38. Different from the influence of the single pulse energy depicted in Fig. 36, both the entry diameter and the exit diameter increase with the increase of the pulse repetition rate. The increased single pulse energy has a dominant influence on the exit diameter of the borehole. Worthy of note is that the average power of the laser beam increases either when the single pulse energy or the pulse repetition rate increases and the other parameters stay constant. However, the effect of increasing the single pulse energy is largely different with regard to the geometry of borehole. The higher pulse repetition rate contributes to a more efficient drilling. The so-called incubation effect could be the reason. As a result of that, the ablation threshold of the materials decreases and ablation efficiency rises [Ra08]. Nevertheless, the higher pulse repetition rate could even induce a negative heat accumulation during the drilling process, which is a common phenomenon in processing using ultrashort pulsed lasers at high repetition rates [We14] [FR14]. The thermal influence can be clearly seen on the entry of the borehole at repetition rate of 400 kHz in Fig. 38(a).

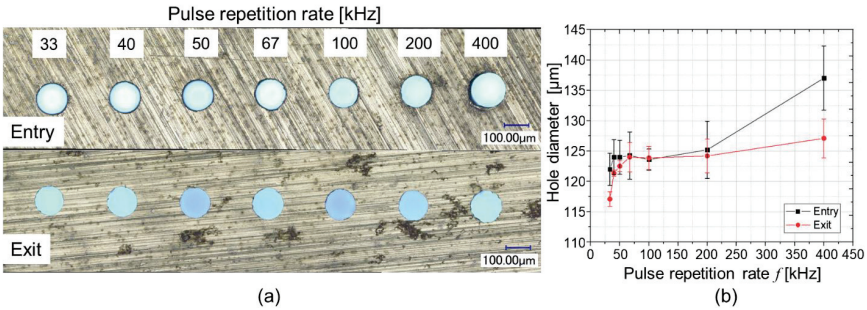


Fig. 38 Helical drilling in 1 mm thick stainless steel with varied pulse repetition rates. (a) microscopic images of hole entries and exits. (b) Diagram of the hole diameters vs. applied pulse repetition rate
Parameters: single pulse energy: 120 µj, drilling time: 15 sec., gas pressure: 3 bar (compressed air), helical diameter: 100 µm, optical table position: Δa = 0 mm, rotational speed: 50 rps, z position: +200 µm in material

The ablation area from laser pulses in the helical drilling process is normally constrained in a diameter of up to several hundred micrometers. Although the laser pulses deposit consecutively on the helical path with a spatial offset, as shown in Fig. 39(a), the heat accumulation is observable when drilling in a

thickness greater than 2 mm; even the pulse repetition rate is not higher than 100 kHz.

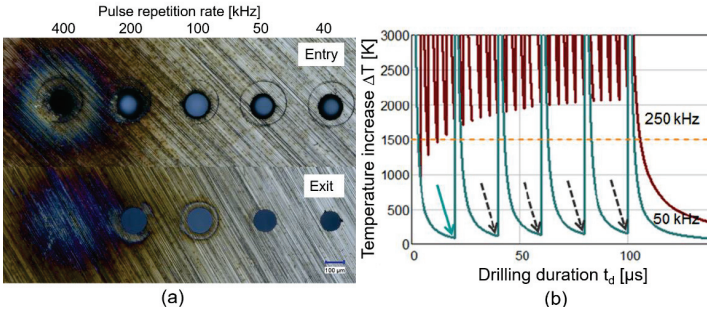


Fig. 39 Helical drilling in 2 mm thick stainless steel with varied pulse repetition rates. (a) microscopic images of hole entries and exits with thermal affect; (b) result of numeric simulation on temporal evolution of the temperature increase with 50 kHz and 250 kHz pulse repetition rate [We14].

Parameters: single pulse energy: 150 µJ, drilling time: 50 sec., gas pressure: 3 bar (compressed air), helical diameter: 50 µm, optical table position: Δa = 0 mm, rotational speed: 50 rps, z position: +1000 µm in material

A thermal ring around the borehole exit gives evidence of a heat accumulation induced by high pulse repetition rate above 100 kHz. A similar development of hole geometry can be seen in the helical drilling process of 2 mm thick stainless steel. It is remarkable that the hole is not drilled through even at a pulse repetition rate as high as 400 kHz and a single pulse energy of 150 µJ. Moreover, a significant thermally affected zone, as tempering colors with a radius approximately three time of the hole radius, can be seen both at the hole inlet and the hole outlet. The tempering colors, which decodes the temperature profile in stainless steel, is a well-known effect [Ve07] [GSL16]. Apparently, the results can be attributed to a plasma congestion in the deep bore channel. The plasma produced by high energy single pulses forms a plasma cloud in the bore channel near the hole inlet, which cannot be driven out from the bore channel. Due to that, the recoil force of the plasma is restricted by the narrow bore channel itself on the one hand, and, on the other, the plasma partly absorbs the incoming pulse energy. Therefore, the kinetic energy against the recoil force increases. As a result, the plasma cloud stays within the bore channel and absorbs even more pulse energy, thus, the local temperature increases dramatically and causes a considerable large heat affected zone around the borehole.

Numeric simulations on heat accumulation can be carried out based on the heat conduction equation. The result from [We14] shows the temporal evolution of the temperature increase with 50 kHz and 250 kHz pulse repetition rate as shown in Fig. 39(b). At a repetition rate of 50 kHz (curve in pine green), the surface temperature after the deposition of the first pulse firstly increases but drops down to a residual increase after an interpulse break before the second pulse is applied. Every subsequent pulse again heats the surface in the same

manner as the first pulse, but the starting point of the temperature is slightly higher due to the previously inserted heat. The effect of an increased repetition rate to 250 kHz (curve in red) shows a dramatic increase of temperature since the surface is not yet significantly cooled down before the subsequent laser pulses deposit on the spot. This yields a much higher heat accumulation and higher resulting temperature than at the lower repetition rate of 50 kHz. This model is still valid for the helical drilling process, where a spatial offset exits between the subsequently induced laser pulses. The pulse overlap ratio is normally over 95 percent of the focused beam diameter in the classic helical drilling process (cf. 4.3.1).

5.1.3 Drilling duration

It is obvious that the drilling duration directly determines the ablation volume and, thus, has a direct influence on the geometrical profile of borehole. The drilling results with drilling time varying from 6 to 16 seconds are shown in Fig. 40. After an adequate volume was ablated during a process time of 6 seconds, the hole was drilled through without a qualified roundness of the exit hole. Moreover, the exit diameter was minimized and not yet enlarged to its final geometry. The increase of the drilling time by 2 seconds to a total process time of 8 seconds led to a larger opening of exit as well as a higher circularity. The exit continued to be broadened when the drilling duration was increased; however, the maximum increase of the exit diameter is terminated at about 14 seconds of drilling time. Afterwards the borehole geometry was independent from the drilling time and appears to be fully stable. In contrast, the drilling duration had less influence on the entry diameter. The entry diameter was finalized after a drilling time for about 8 seconds and stays stable.

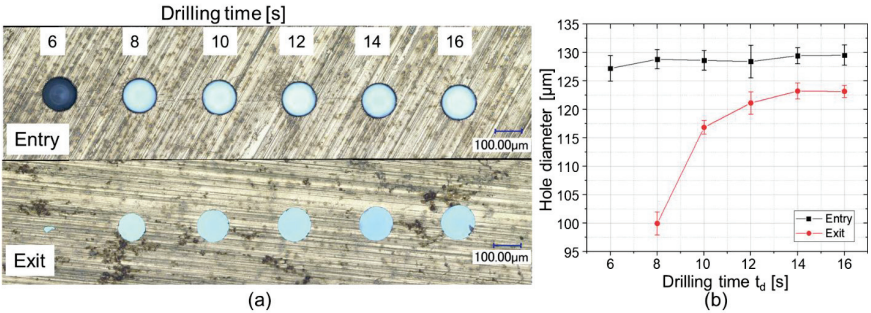


Fig. 40 Helical drilling in 1 mm thick stainless steel with varied drilling time. (a) Microscopic images of hole entries and exits. (b) Diagram of the hole diameters vs. applied pulse repetition rate
Parameters: single pulse energy: 120 µJ, repetition rate: 50 kHz, gas pressure: 3 bar (compressed air), helical diameter: 100 µm, optical table position: Δa = 0 mm, rotational speed: 50 rps, z position: +200 µm in material

The ex-situ analysis on the borehole geometry was performed in order to investigate the temporal evolution of the borehole geometry during the drilling process. The holes' silhouettes of longitudinal sections were extracted from high resolution microscopic images by means of professional photo processing software (see Fig. 41). Only the steps with a significant change in the shape of helical-drilled holes are presented to illustrate the temporal geometric evolution; therefore, the time interval is adapted and does not necessarily show an adequate parameter spacing. The helical diameter was set to be greater than two times the laser post size, so that the helical path can be resolved and represented clearly.

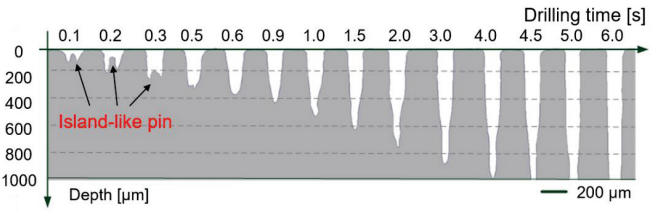


Fig. 41 Temporal evolution of longitudinal sections of holes produced by the helical drilling process

Three drilling phases can be distinguished according to the features of the hole capillary and the ablation behavior. In the first phase (t = 0 ~ 0.9 s), a hole with an island-like pin in the middle is excavated at the shallow surface of the material up to an ablation depth of 0.3 mm. The groove has an ideal longitudinal section with respect to the overlapped laser intensity distribution shown in Fig. 31(c). The successive laser pulses deepen the donut-shaped groove. Thus, the height of the island-like pin initially grows up to a maximum, and then the root of the pin is ablated by the laser pulses reflected on the wall and, as a result, the pin disappears. Instead of the island-like pin, a capillary hole with a dome-like bottom can be observed. With a process time higher than t = 0.6 s, the capillary hole deepens and the ablation front moves forward longitudinally due to the projection and reflection of the laser beams on the inner borehole wall. The second process phase (0.9 < t < 4.0 s) is characterized by the forming of a funnel-like borehole with a slim tip. As a result of the change of the laser ablation behavior, mainly caused by the reflection of the laser energy on the borehole wall to the center of hole, the bottom of the capillary is sharped and finally forms a slim tip at the bottom. This is quite similar to the effect that can be observed on the laser percussion drilling process. Noteworthy is the small change in direction of the capillary bottom at t = 1.0 s towards the left side of the drilling hole. This can be attributed to reflections of the laser beam at the internal wall of the borehole. Once the tip is formed, its length and funnel-like profile stay quasi constant until it reaches the rear side of the sample. The final phase begins at the time when the hole is drilled through. This is the case between 4s and 4.5s. In the final phase the hole exit is broadened to the final geometry and the

hole forms the designed profile. For the drilling hole investigated here, about 100 revolutions of laser pulses were performed to enlarge the diameter of the exit and form a cylindrical hole profile. The number of revolutions depends on the setting of hole diameter and the laser parameters applied (e.g. pulse energy). The ablation behavior in the helical drilling process is investigated and the relationship between drilling time and hole depth is plotted and shown in Fig. 42. This diagram further illustrates the three phases in helical drilling process.

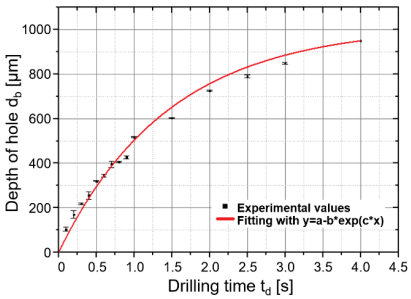


Fig. 42 Helical drilling depth as a function of drilling time with the main parameters: Single pulse energy applied 120 µJ, Repetition rate 50 kHz, Helical radius 50 µm

For the first second an initial phase drills the borehole with a high average ablation rate, and approximately half of the final depth can be reached. The reason for the high ablation rate can be explained as following. The Rayleigh length of the laser beam applied in this experiment is calculated to be 264 µm, and the laser beam focus is located at 200 µm beneath the material surface. Thus, the most effective ablation range extends longitudinally to about half of the material thickness, which is nearby the middle of the material. In the second drilling phase (from 1.0 seconds to 4.0 seconds), the ablation rate of the drilling process is strongly reduced due to the declined laser intensity by a defocused laser beam and energy losses due to internal reflection of the laser beam, as well as energy absorption by vaporized particles and plasma [PN10]. As soon as the hole is drilled through, the mixture of molten and vaporized material can be driven out from the hole outlet by coaxial gas pressure. Thus, the influence on laser intensity deposition on the internal wall of the borehole is weakened and the hole profile, where the sharp capillary was, can be further shaped and broadened to the final geometry.

5.2 Helical optical parameters

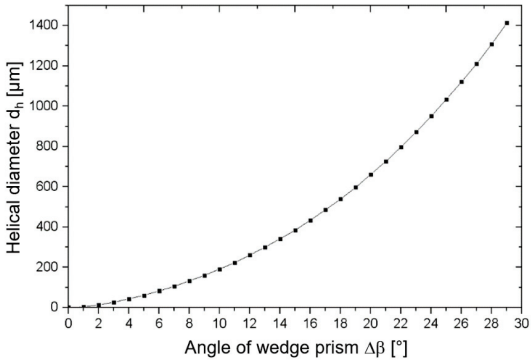
In this section, the positions of the optical table and the angle of wedge prism both relatively to their zero-position, the rotational speed of the Dove prism within the hollow shaft engine, as well as the focal position are categorized into a certain set of parameters of the helical optic system. As introduced in Chapter 3, the position of the optical table has to be linked with the conicity of the

boreholes as a result of a parallel offset of the incident laser beam relative to the rotational optical axis. The angle of the wedge prism is responsible for the variation of the helical diameter. Both the two key parameters determine the helical path for the helical drilling process (please see Chapter 4). The rotational speed of the Dove prism is given as a process parameter and limited to about 160 rps by the system configuration. The focal position plays a role in the helical drilling process and can be adjusted by a high precision z axis with a minimum pitch of less than one micrometer.

5.2.1 Tilted angle of incident laser beam to Dove prism

The principle of altering the helical diameter for the helical drilling process has been introduced in Chapter 3. The helical diameter in the helical drilling process is dominantly determined by the declination of the wedge prism. By changing the angle of the wedge prism, the inclination angle of the incident laser beam relative to the Dove prism and to the focusing optics changes and, thus, the focusing position on the respective image plane varies. With the helical revolution, the helical radius can be adjusted. The development of the helical diameter with declination angles of the wedge prism is depicted in the diagram in Fig. 43.

Fig. 43 Diagram of helical diameter vs. angle of wedge prism



Due to the imaging property of the focusing lens, the increase of the helical diameter does not behave in a linear correlation to the increase of the inclination angle of the wedge prism. By means of polynomial fitting, the relationship between the helical diameter d_h on the focal plane and the wedge prism angle a_{wp} can be given as:

$$d_h = 3.02 + 9.73a_{wp} + 1.24a_{wp}^2 \quad \textbf{5.3}$$

Without regard to the helical error caused by geometrical deviations of the Dove prism [Zi15], the final borehole diameter is determined by the sum of helical diameter and the laser beam spot size. The laser beam has to have an applied fluence above the ablation threshold of the specified material.

5.2.2 Parallel offset of incident laser beam to Dove prism

The conicity of holes is defined as the ratio between the entry diameter and the exit diameter and describes the taper of the holes. For an intuitive representation of the conicity, three different types of holes – negative conical, positive conical and cylindrical shaped geometries – are demonstrated within the longitude cross-section shown in Fig. 44.

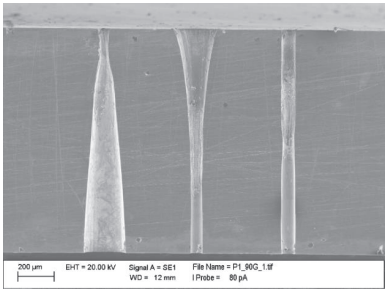


Fig. 44 Helical drilling in 1.2 mm thick stainless steel with a negative (left), positive (middle) and quasi-zero (right) conicity.

- For negative conical drilling, the conicity $\chi \in (0,1)$;
- For cylindrical drilling, the conicity $\chi = 1$;
- For positive conical drilling, the conicity $\chi > 1$.

With the variation of the position of the optical table from +3 mm to -3 mm, the evolution of the hole geometry on the exit can be clearly extracted from Fig. 45. When the entry diameter decreases slightly, the exit diameter increases from ca. 60 µm at an optical table position of +3 mm to about three times that diameter at a position -2 mm. In the drilling experiments, the drilling time was kept 15 seconds consistent. Since the ablation volume was increased with the parallel offset in negative direction, the hole was not drilled through at a table position -3 mm within the 15 seconds. The evolution of the borehole conicity with the parallel offset of the laser beam to the Dove prism can be clearly seen in Fig. 31. With the parallel offset +3 mm the conicity of boreholes is $\chi \approx 2.2$, at around -0.25 mm $\chi \approx 1$, a cylindrical borehole can be fabricated, and with the parallel offset of -2 mm $\chi \approx 0.67$. Supposing that the hole could be drilled through with the parallel offset of -3 mm, the conicity could reach a value of $\chi = 0.5$. At increased optical table positions in both positive and negative directions, the available conicity of the laser drilling can be extended further. However, the

maximal achievable conicity is limited by the clear aperture of the Dove prism, the focal length of focusing optics and the raw beam diameter, etc.

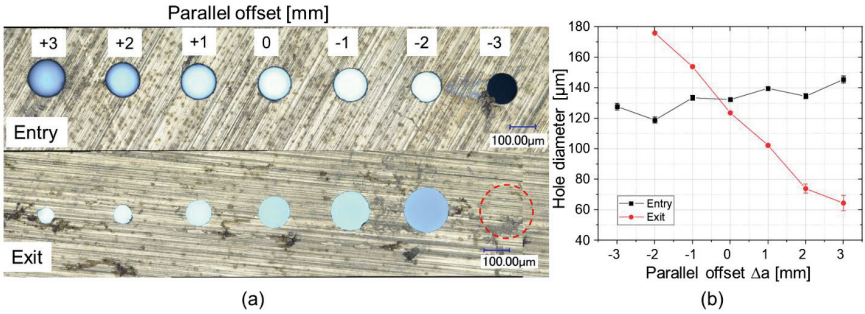


Fig. 45 Helical drilling in 1 mm thick stainless steel with varied parallel offsets. (a) Microscopic images of hole entries and exits. (b) Diagram of the hole diameters vs. applied pulse repetition rate

Parameters: single pulse energy: 120 µJ, repetition rate: 50 kHz, drilling time: 15 sec., gas pressure: 3 bar (compressed air), helical diameter: Δa = 100 µm, rotational speed: 50 rps, z position: +200 µm in material

It is to be noted that the parallel offset of the laser beam to the Dove prism has a direct influence on the conicity of the drilling geometry. However, it is not the single influential factor. The focal position of the laser beam relative to the workpiece, for instance, can be a factor that changes the conicity of boreholes.

5.2.3 Focal position of the laser beam

The intensity of a single laser beam has the maximum at the focal position. For the helical drilling process, the caustic of the laser beam is a part of the caustic of the helical path. The intensity of superposed laser pulses applied on the helical path is determined by the intensity of the laser beam on the respective plane, and on the overlap degree of the laser pulses. As interpreted in Chapter 4, the caustic waist of the helical path is independent of the laser beam focus. Rephrased, the location of the maximum superposed laser intensity within the helical path may offset from the focal position of the laser beam. Furthermore, the variation of the focal position modifies the laser intensity distribution applied on the front surface of the sample, where the inlet of the borehole is located, as well as on the rear surface, where the outlet of the borehole is located. The modified laser energy deposition can also be represented as the change of the helical diameter and the incident angle of the laser beam. The influence of different focal positions relative to the front surface of the material has been systematically investigated and the results are depicted in Fig. 46. With a fixed helical path, which is determined by a fixed optical table position and a fixed angle of the wedge prism during the helical drilling process, the focal position of

the laser beam is moved from 200 µm above the front surface of the sample to 800 µm beneath. Due to strong defocusing, the laser intensity decays as the distance from the focal plane increases. As a result, the hole outlet at the focal positions from-200 µm to +200µm are not completely drilled through. The incomplete circular shapes of the exits can be seen in Fig. 46(a). Another possible reason is that the higher density of laser energy at the focal plane ignites plasma with higher density, which can absorb a certain part of the incident laser intensity (plasma shielding). If the focal position of the laser beam is located at the inlet of the borehole, the intensity of the upcoming laser pulses is impaired. Due to that, the ablation volume per pulse decreases and the drilling efficiency drops. When the laser beam is focused within the material, the shielding effect of laser induced plasma is weaker and the drilling process can be improved.

The geometry of the borehole has been varied from a negative conical hole to positive conical ones, which can be observed from the longitudinal cross-section of the boreholes seen in Fig. 46(a). A more significant influence on the exit diameter by changes of the focal position can be seen in Fig. 46(b), compared with the variation of the optical table position as shown in Fig. 45(b). As the laser focal position approaches the rear surface of the material, the diameter of the hole entry increases in a quasi-linear behavior from a minimum diameter of 90 µm to about 260 µm. The exit diameter enlarges to about 125 µm, which is about the half of entry diameter at this position.

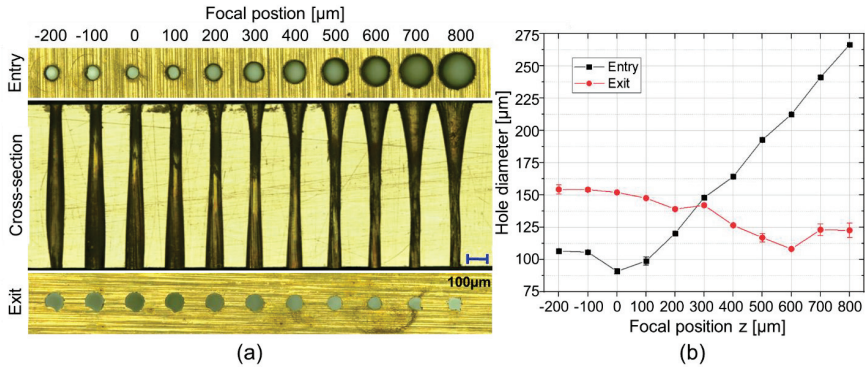


Fig. 46 Helical drilling in 1 mm thick stainless steel with varied focal position. (a) Microscopic images of hole entries and exits. (b) Diagram of the hole diameters vs. applied pulse repetition rate
Parameters: single pulse energy: 120 µJ, repetition rate: 50 kHz, Drilling time: 15 sec., gas pressure: 3 bar (compressed air), helical diameter: 50 µm, optical table position: Δa = 0 mm, rotational speed: 50 rps

The combined influence of the optical table position (offset) and the focal position (z position) on the hole geometry can be seen from the evolution of the longitudinal cross-sections in Fig. 47. By shifting the focal position from 0.25 mm

beneath the front surface of the material to the middle of the material bulk, the profiles of the holes show a significant change, especially for optical table positions with greater absolute value (i.e. ±3 mm).

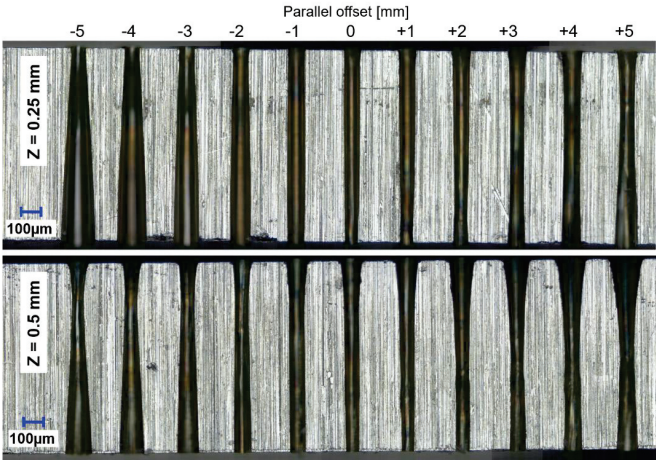


Fig. 47 Cross-section of bore-holes at focal positions of z = 0.25 mm and 0.5 mm in material with varied parallel offset, applied laser single pulse energy 125 µJ, pulse repetition rate 60 kHz, drilling time 10 seconds, helical rotating speed 3600 rpm

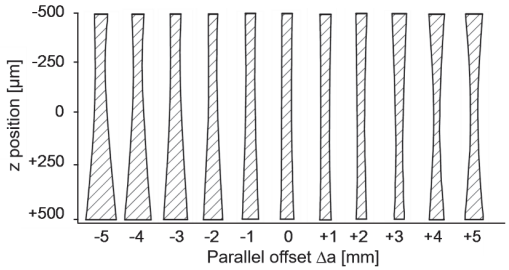


Fig. 48 Two-dimensional caustic of helical path with varied parallel offset for experiments depicted in Fig. 47

By using the parameter setting for the helical path displayed in Fig. 47, holes are fabricated in 1 mm thick stainless steel with the focus of the laser beam at 0.25 mm and 0.5 mm under the front side of material, where the inlets of laser beam is located. As can be seen from the longitudinal cross-sections of the boreholes in Fig. 47, the focal position plays an important role in the hole profile. Compared with the hole profile drilled with the focal position at z = 0.5 mm, the entrances of boreholes with the focal position at z = 0.25 mm are sharper. In addition, a more distinct evolution of hole profile from negative conical profile over cylindrical to positive conical profile is shown in the drilling results at

z = 0.25 mm. The main part of the borehole at this z position is generally dominated by a single art of taper, i. e. negative, positive or zero taper.

Due to the strong defocusing of laser beam at z = 0.5 mm, converging-diverging holes can be fabricated with a larger parallel offset in both a plus and minus direction, especially at offset Δa ≥ +4 mm and Δa ≤ -4 mm as shown in Fig. 47.

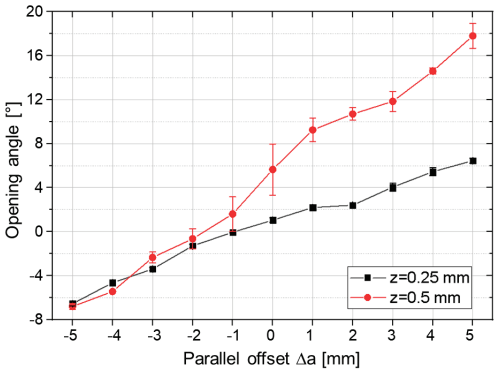


Fig. 49 Opening angle of the main part of holes at varied parallel offsets in the helical drilling process with the focal plane at z = 0.25 mm and 0.5 mm

The hole profile drilled at z = 0.5 mm in the material are in an excellent agreement with the 2D caustic of helical path displayed in Fig. 48. The full opening angle of the main part of the boreholes is plotted by the parallel offset in Fig. 49. A greater positive taper can be obtained by focusing the laser at a deeper position in the material. An opening angle of 18.6° can be achieved at offset of +5 mm and z = 0.5 mm, while the opening angle is about 6.6° at z = 0.25 mm. However, the achievable negative taper stays approximately the same (6.5°) in both z positions. The achievable maximum negative taper in 1 mm stainless steel is limited by the aperture of the Dove prism and the maximum single pulse energy of the laser beam.

5.2.4 Rotational speed of the Dove prism

The helical revolution of the laser beam was generated by the mechanical rotation of the Dove prism in the helical drilling optics. The rotational speed is one of the influential factors on the overlap degree of the laser pulses deposited on helical path. Additionally, the rotational speed together with drilling time determines the number of helical revolutions in the whole drilling process.

Generally, at least one completed helical revolution is essential to achieve a borehole with a designated helical diameter. Moreover, as discussed in Section 5.1.3, the fabrication of a borehole with a designated conicity needs three complete drilling phases, for which multiple revolutions normally take place.

Depending on the factors – for instance material thickness, laser specifications and designated hole geometry – the number of helical revolutions necessary for the drilling differs case by case. The influence of rotational speed of the Dove prism in drilling 1 m thick stainless steel is shown in Fig. 50 and Fig. 51. At 10 rps rotational speed and drilling time of 15 seconds, the exit diameter is not broadened to the final geometry, although the material is drilled through and with a high roundness, because the number of revolutions amounts to 300. The last phase of helical drilling is not complete. By accelerating the rotational speed to 20 rps, the diameter of borehole exit is broadened to about double the sized compared with that of 10 rps. The stability of diameter of borehole entries and exits shown in Fig. 51 gives evidence for that, and the broadening process completes within fewer than 600 revolutions since the further increase of rotational speed no longer has any influence on the hole geometry.

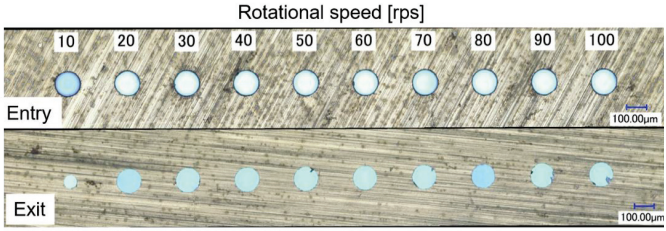


Fig. 50 Helical drilling in 1 mm thick stainless steel with varied rotational speed of the Dove prism. Microscopic images of hole entries and exits

Parameters: single pulse energy: 120 µJ, repetition rate: 50 kHz, drilling time: 15 sec., gas pressure: 3 bar (compressed air), helical diameter: 50 µm, optical table position: Δa = 0 mm, z position: +200 µm in material

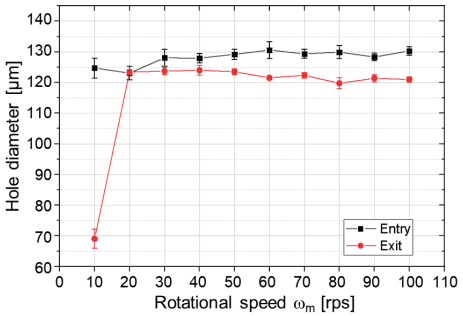


Fig. 51 Diagram of the hole diameters vs. applied pulse repetition rate

In helical drilling of thin material, the higher rotational speed is generally advantageous in order to maximize the drilling speed. Within the same drilling duration, the number of revolutions increases as the rotational speed rises, and the number of revolutions plays an important role in shaping the hole geometry.

Fig. 52 shows the drilling results of helical drilling in 0.1 mm thick stainless steel foil with 60 and 150 rps rotational speeds and varied drilling duration. The laser pulses are deposited on merely a 12% of one single helical path in the first 1 ms drilling time with the rotational speed 60 rps. And a complete single helical path can be formed after at least 8.33 ms. In the case of 150 rps, the necessary time for one complete helical revolution can be reduced to 3.33 ms. As can be seen in Fig. 52, the stainless steel foil is pierced through in the first 1 ms at 60 rps. Due to that, the first helical revolution is completed after 8 ms and the boreholes from 1 ms to 8 ms have random "through-positions" on helical path depending on the location of the first laser pulse deposited on the material. After 9 ms laser duration, the boreholes have targeted positions. Instead of piercing through in 1 ms at 60 rps, a "C-shaped" trench is ablated on the surface of the foil at 150 rps due to a slightly decreased overlap degree and ,thus, dropped superposed laser intensity. A stable targeted drilling position can be achieved after 3 ms. The roundness of borehole entries and exits is improved to some extent when 150 rps rotational speed is used since the number of helical revolutions in a unit time increases with higher rotational speed.

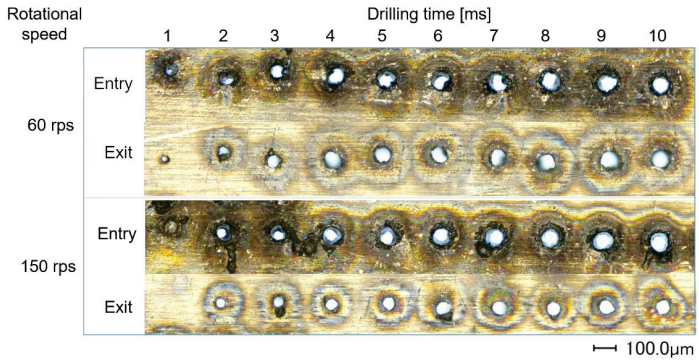


Fig. 52 Comparison of helical drilling in 0.1 mm thick stainless steel foil at 60 and 150 rps rotational speeds and varied drilling duration

5.3 Process ambient conditions

It has been reported by other researchers that the ambient pressure and type have an effect on the hole formation and quality [Dö13] [Ok10] [Br10]. The helical drilling process is normally performed with a coaxial gas jet for three main reasons. Firstly, the process gas assists in material removal, expelling molten material and vapor/plasma material from the hole cavity. Secondly, the focusing lens can be protected from vapor and ejected debris generated by laser beam. Last but not least, the process gas creates a local convection environment leading to faster heat conduction and, thus, a cooling effect at the borehole inlet.

5.3.1 Type of process gas

The influence of the type of process gas on geometry of the hole entry by helical drilling is represented in Fig. 53. Compressed air, nitrogen and helium as process gas were employed in the investigation. The development of the hole diameter with three gas types is of high similarity. The hole diameter decreases about to the half of that without process gas (0 bar) as the gas jet works at 1 bar. This can be explained by the effect of molten/vapor/plasma material removed by the gas jet. However, the diameter increases with the increase of gas pressure. The reason for that will be discussed in 5.3.2. Moreover, the increase rate of hole diameter with compressed air is approx. twice of that with nitrogen and helium. Obviously, the oxygen in the compressed air contributes to the higher ablation rate by means of an oxidation process. Nitrogen and helium are normally working as protection gas. Despite a comparable effect on the hole geometry, the behavior of the diameter development in helical drilling with helium appears to be more linear than with nitrogen.

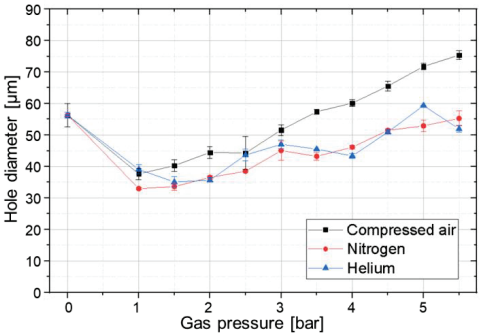


Fig. 53 Relationship between hole diameter of hole entry and type of process gases. Parameters: single pulse energy: 120 µJ, repetition rate: 50 kHz, drilling time: 15 sec., helical diameter: 30 µm, drilling, optical table position: Δa = 0 mm, rotational speed: 50 rps, z position: +200 µm in material

The comparison of morphology on borehole walls as drilled without post-processing is shown in Fig. 54. The dark oxidation can be clearly seen on the borehole wall of the drilling with compressed air since the content of oxygen amounted to approx. 20 percent. The existence of oxygen promotes the oxidation process during the drilling and generates more heat in the workpiece as a result of exothermic reaction [Po08]. Whereas the appearance of borehole walls with nitrogen as process gas are smoother and less oxidized. The pure atmosphere of nitrogen contributes to a protection of the ablated area from oxidation. In addition, since the exothermic reaction of oxygen does not occur in this case, the hole size is smaller than when drilling with compressed air under the same parameter. Noteworthy is that, longitudinal striations in the direction of laser beam propagation are present on the borehole wall near the exit by nitrogen. No explanation about the phenomenon has been reported yet. A possible reason of the formation of striation could be the nitridation of the

material by laser irradiation. The viscosity of the molten material differs from the oxidation and is driven out from the drill channel in a different behavior. The criteria for choosing the appropriate process gas depend on the property of the material to be drilled as well as the requirements and expectations on the precision, drilling efficiency, and metallurgical quality of the boreholes.

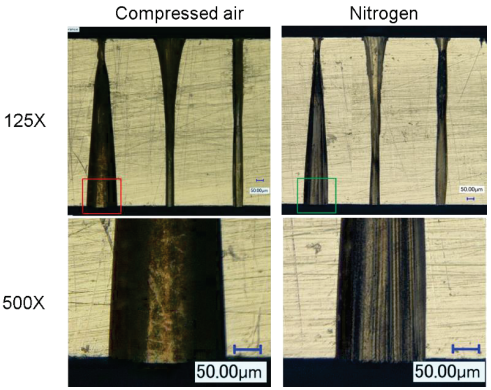


Fig. 54 Microscopic image of helical drilling in stainless steel with compressed air and nitrogen as process gas

5.3.2 Pressure of process gas

By employing compressed air as a process gas for the helical drilling, the influence of pressure on hole geometry especially on longitudinal cross-section was investigated.

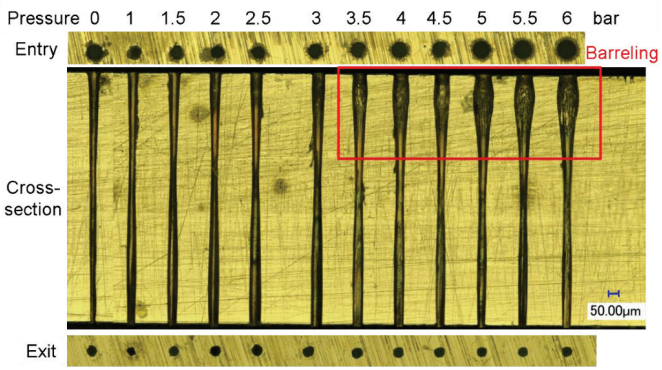


Fig. 55 Helical drilling in 1 mm thick stainless steel at varied gas pressure. Parameters: single pulse energy: 120 µJ, repetition rate: 50 kHz, drilling time: 15 sec. gas art: compressed air, Helical diameter: 100 µm, optical table position: Δa = 0 mm, Rotational speed: 50 rps, z position: +200 µm in material

The development of hole entry diameter at varied gas pressure is quantified and depicted in Fig. 53. The hole profiles are represented in Fig. 55. The SEM image of the hole barreling is shown in Fig. 56.

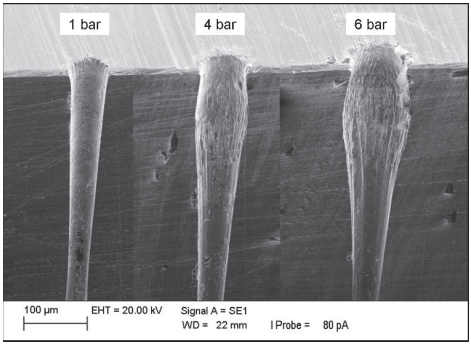


Fig. 56 SEM image of hole inlets in stainless steel drilling by 1, 4 and 6 bar compressed air extracted from Fig. 55

The effect of increased gas pressure seems to be minimized on the hole exit. No significant distinction can be seen on the hole exit and the profile of the part between middle and outlet of borehole. However, barreling with increasing dimensions is present near the inlet of boreholes once the gas pressure increases to 3 bar. Furthermore, the volume of barreling expands with the increase of applied gas pressure. Due to this, the ignited plasma behavior changes at different gas pressures. A balance of gas pressure and recoil force of ignited plasma by laser irradiation exists near the inlet in the material during the drilling process. The density of plasma becomes greater due to a higher mechanical confinement of ablated particles, plume and the laser generated shock-wave by the ambient gas at increased pressure [Dö13] [Me12] [BE03] [WZZ11] The accumulated plasma with high temperature etches the holes wall and enlarges the dimension until the balance is disturbed by changed boundary conditions, for instance the drilling-through or termination of laser irradiation. The presence of barreling impairs the geometric as well as morphologic quality of drillings with respect to verticalness of the hole profile and roughness of the borehole wall as shown in Fig. 56.

5.4 Hole geometry and surface morphology of classic helical drilling

Based on the investigation and analysis on the influence of laser energy deposition on drilling geometry, the processing parameters in helical drilling can be optimized and a high precision is achievable. Fig. 57 shows the hole entrance and exit qualified with high circularity and well-defined edge. Additionally, the profile of longitudinal cross-section having an aspect ratio (ratio of hole depth to hole diameter) of 10:1 exhibits a high parallelism and cylindricity along the depth. The inlet and outlet of boreholes present excellent verticalness. Optical inspection

and statistical analysis of the hole produced with ps-pulses reveal a tolerance of diameter within ±2 µm.

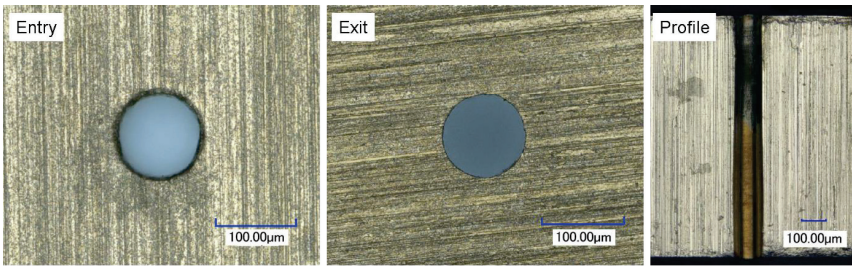
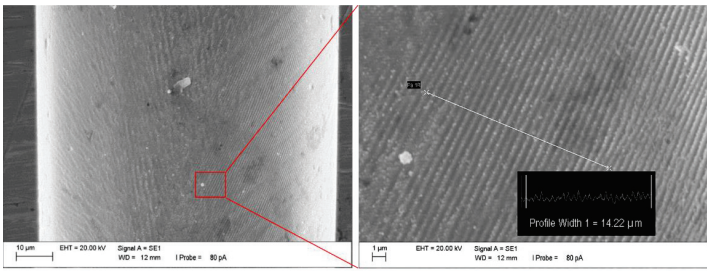


Fig. 57 (a) Top view of helical drilled borehole entry with diameter 100 µm and roundness 0.92. (b) Top view of borehole exit with diameter 100 µm and roundness 0.94. (c) Cylindrical hole profile in longitudinal cross-section. Material: 1 mm thick stainless steel (1.4301)

To evaluate the drilling quality, the topography of hole wall was analyzed by means of SEM and confocal laser scanning microscope (LSM). The SEM images of the cross-section of hole wall with 1000X magnifications (Fig. 58a) show a clean and uniform surface, on which a laser induced periodic surface structures (LIPSS) is present. The measurement of the periodicity of LIPSS in a higher magnification seen in Fig. 58(b) shows an almost constant periodicity of approximately 570 nm. As reported in [Ka03] [RRF14] [We08] [NG10], the mechanism of LIPSS formation is supposed to be an interference of laser and surface plasmons (surface electromagnetic waves). Depending on the laser fluence applied, the periodicity and contrast of the LIPSS on the borehole wall can be varied.

Fig. 58 (a) SEM images of the helical drilled hole wall in Fig. 57, (b) relative details of the obtained surfaces with Laser Induced Periodic Surface Structures (LIPSS)



To investigate the evolution of hole wall surface roughness along the hole depths, five points at different areas were measured and evaluated by LSM as

shown in Fig. 59. The inlet zone has the highest roughness value compared with other locations since all the vaporized material and plasma is driven out from the inlet before the hole is completed. The vapor or plasma flow etches the surface of borehole channel in a disorderly manner, and thus the smoothness of the original surface direct after ablation is impaired. As borehole deepens, the newly generated hole wall in greater depth suffers less impact of the vapor and plasma, and the roughness is correspondingly improved dramatically. At the middle depth of the profile, the root-mean-square (RMS) surface roughness Rq value is at the minimum of about 30 nm. Once the hole is drilled through, vapor and plasma can be driven from the hole outlet. Due to the broadening phase of helical drilling, the outlet area remains as the surface is ablated, which means although the impact of the vapor and plasma flow, the affected area is ablated by the following laser pulses. As a result, the surface still has a lower roughness than that on the inlet area. The average value of roughness Rq in the full length on hole wall amounts to ~290 nm. It is competitive to other micro machining techniques such as micro electrical discharge machining (μ-EDM) [RRF14] [FRR16].

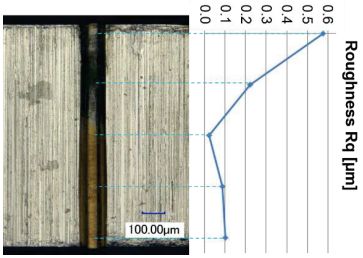


Fig. 59
Characterization of the roughness on borehole wall at five locations along the hole depth

The investigation of the heat affected zone (HAZ) is aimed at morphological changes in the surrounding drilling material. The basic structure of the stainless steel (X5CrNi18-10) shows the characteristics typical for austenitic chromium-nickel steels in the form of polyhedral grain boundaries and twin grain boundaries [BA05] as shown in Fig. 60.

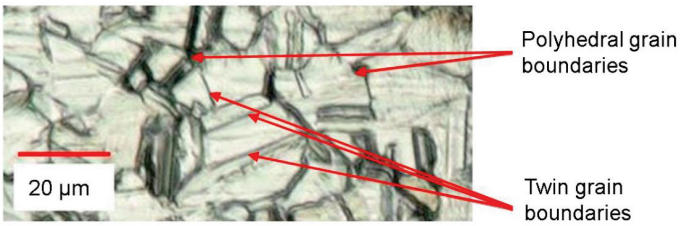
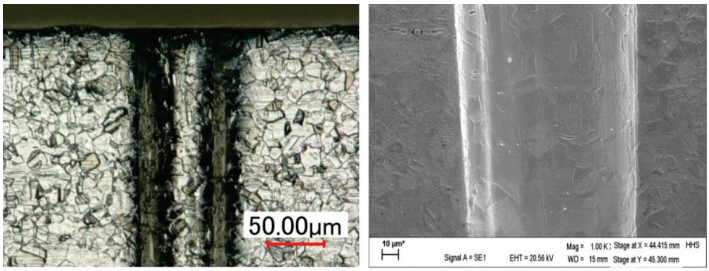


Fig. 60 Exemplary representation of the typical austenitic basic structure of stainless steel (X5CrNi18-10)

As aforementioned, the area of borehole inlet is exposed to laser radiation and vapors/plasma for a longer time than elsewhere, thus the highest probability of a visible heat influence is assumed to be there. Fig. 61 shows an example of an etched channel of a borehole drilled by an ultrashort pulse laser with pulse duration of 900 fs. The applied single pulse energy is 125 µJ and pulse repetition rate 600 kHz.



(a) (b)

Fig. 61 (a) Basic structure in the drill channel in the middle and basic material after etching. (b): SEM image of etched borehole

The austenitic grains of the basic structure have been precisely cut through by the laser at the transition into the drilling channel. It should be particularly emphasized that the microstructures of the polyhedral grain boundaries and twin grain boundaries, which are the typical characteristics of basic material of austenitic chromium-nickel steels, are also very clearly visible in the drilled channels. Not only can no deposits be found around the boreholes, but it is also evident that the helical drilling with ultrashort laser pulses is a sublimation-dominated ablation process with minimized HAZ. The SEM image of the drilling channel in Fig. 61 (b) also provides evidence that a HAZ with an effect on the basic structure cannot be seen.

5.5 Summary

The final geometry of a borehole made with classic helical drilling has several comprehensive influential factors. First of all, the laser parameters determine the peak laser fluence (single pulse energy), temporal interval between pulses (pulse repetition rate) and the number of total pulses (drilling time) for the helical drilling process. With the increase of single pulse energy and drilling time, the diameter of the borehole exit increases while the diameter of entry does not change significantly. Both entry and exit are enlarged by increasing the pulse repetition rate due to heat accumulation. Plasma congestion and strong thermal affect in deep hole drilling using a high repetition rate (>200 kHz) present a demand that the pulse frequency in the helical drilling process should be optimized. Ex-situ diagnosis on the temporal evolution of hole geometry by helical drilling distinguishes three phases of hole formation: The first phase is characterized by the presence of a pin-like island in the middle of the drilling. In

the second phase, this island disappears and a capillary with sharp tip is formed, extending to the rear side of material and the end of this phase. The third phase works as a broadening process to shape the hole outlet to the final geometry.

Helical optical parameters regulate the helical path and the pulse distribution on the helical path. Helical diameters and conicity of the caustic of the helical path can be controlled by a wedge prism and optical linear table, respectively. The final borehole shape is in good agreement with the helical path mapped in advance, when appropriate processing parameters are applied. In order to up-scale the drilling speed, higher rotational speeds of the Dove prism are of great advantage.

Last but not least, the process ambient condition is an important influential factor for drilling geometry and quality. The drilling efficiency can be enhanced by employing compressed air compared with nitrogen and helium as process gases; however, the metallurgical quality is impaired by the presence of oxidation layers. Furthermore, a gas pressure higher than 3 bar places higher mechanical confinement of ablated particles and thus leads to the formation of barreling in material bulk near the borehole inlet.

As a final remark, the characterization on borehole geometry and metallurgical morphology shows a high precision drilling with minimized heat-affect-zone. The roughness on borehole wall is location dependent, linked to the driven-out mechanism and dynamics of material vapors and plasma generated by laser pulse irradiation.

6 Adaption of energy deposition and its applications

The classic helical drilling using optimized processing parameters can achieve high-precision drilling microholes with an opening angle of 18.5° at the entrance and 6.5° at the exit in 1 mm thick stainless steel with an aspect-ratio more than 10:1. However, due to the fixed laser propagation with preset parameters of optical components and ablation behavior on the fixed helical path, classic helical drilling shows major limitations on fabricating microholes with properties such as greater taper angle and aspect ratio as well as specific profiles with shaped inlets. In this chapter, dynamic helical processes, which are characterized by a variation of one or multiple process parameter during the process, are introduced as feasible strategies to adapt laser energy deposition and, further, to transcend the aforementioned limitations of classic helical drilling. The objectives of employing adaption of energy deposition in both classic and dynamic helical drilling processes include the following:

- Extension of the maximum aspect ratio of cylindrical microholes,
- Enhancement of hole quality together with precision of geometry,
- Extension of the maximum opening angle of positive conical microholes and
- Increase of the hole complexity.

This chapter will deal with the adaption of energy deposition both in classic and in dynamic helical drilling processes. The strategies for adaption of energy deposition during the drilling process for each object above mentioned are presented. In addition, quantitative and qualitative analysis on drilling precision and efficiency using the dynamic helical processes is compared with that of classic helical drilling.

6.1 Adaption of energy deposition in classic helical drilling

As discussed in Chapter 5, the final geometry of the microhole (diameter at entry/exit and profile) is predominantly determined by the helical path and laser parameters applied in the classic helical drilling process. Once the helical path is set in advance, the borehole geometry can be adjusted by varying the laser parameters and vice versa. To take the advantage of the possibility for adapting the helical path and laser parameters, two strategies – namely, multi-step helical drilling strategy and dynamic focus shifting – were adopted and implemented. The helical path at each step was fixed during the drilling process, thus these two

strategies were employed for the adaption of energy deposition in classic helical drilling of cylindrical microholes with high aspect ratios.

6.1.1 Multiple-step strategy

By definition, high aspect-ratio holes are characterized as cylindrical microholes with small diameter in larger material thickness. Furthermore, a broadening phase should take place to shape the borehole outlet. This raises critical requirements on a helical path having minimized caustic waist and minimized divergent angle. Despite that, such a helical path is available in the overview of helical paths in Fig. 28. With this helical path, the maximum aspect ratio of microholes is constrained by 10:1 as discussed in the last section. By taking advantage of the caustic of helical path, a multiple-step strategy can be adopted in the helical drilling process. In each step, helical path or laser parameters or both can be specifically adapted. The working principle is schematically described in Fig. 62.

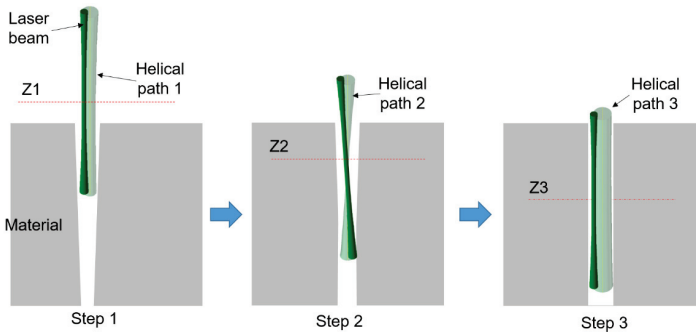


Fig. 62 Schematic diagram of a multi-step strategy for helical drilling of cylindrical holes

In the first step, the laser beam is focused at the position Z1, a "slim" helical path with a slightly convergent angle. A small helical diameter is applied to fabricate a pilot borehole so that the vaporized material generated in further steps can be driven out from the outlet without any secondary damage to borehole inlet. Following that, the focus of the laser beam shifts to the position Z2. Moreover, the helical path with minimized diameter at the caustic waist is located at the borehole inlet. With that, the laser beam on the helical path passes through from borehole inlet, without any ablation processes occurring at the inlet. Thus, the minimized diameter of borehole inlet remains, while the borehole outlet is broadened nearly to the final exit diameter by the divergent part of helical path. Due to the defocusing of laser beam, not only does the laser fluence decrease, but the ablation area and volume per pulse do as well, correspondingly. Therefore, the broadening process is very precise and the exit diameter can be controlled. The last step serves as post processing to remove the possible

constriction part, where the transitional area of the convergent and divergent parts is located. A helical path having a quasi-cylindrical caustic and diameter as small as possible is suitable for post-processing. In addition, the focal position should be adapted.

The two-step classic helical drilling is performed in 1 mm thick stainless steel with varied drilling durations at each step. The focal position of laser beam is located at Z1 in the first step and at Z2 in the second step. Fig. 63 shows the longitudinal cross-section of drilling using the parameters listed in Table 4. In addition to the parameters of focal position (Z) and drilling duration, the angles of the wedge prism are 4° at step 1 and 6° at step 2. The parallel offsets of the laser beam are 0 mm at step 1 and -1 mm at step 2. Holes No. 1 and No. 11 in the Fig. 63 are indeed fabricated by a single step with the focal position at 400 µm in the material and 100 µm above the top surface, respectively. Despite the minimum hole diameter, hole No. 1 has the profile of poor cylindricity and evolves from a hyperbolic curve at the inlet via barreling in the middle and a convergent part at the outlet of borehole. By utilizing a two-step strategy, the cylindricity of the borehole can be significantly improved. Moreover, the diameters can be further decreased in comparison to hole No. 11. The boreholes drilled in two steps have quite straight and sharp outlets overall compared with those made in one step.

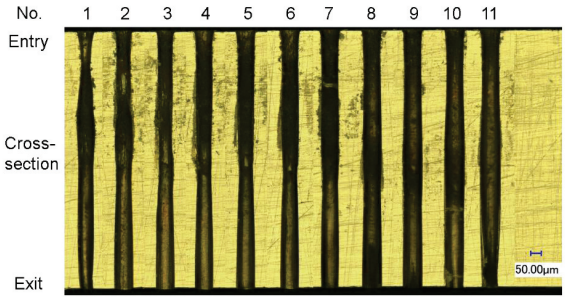


Fig. 63 Longitudinal cross-section of drillings with two steps and varied parameters as described in Tabel 1

Table 4: Parameters for drilling holes in Fig. 63

No.		**1**	**2**	**3**	**4**	**5**	**6**	**7**	**8**	**9**	**10**	**11**
Drilling duration/s	Z1 = -100 µm	0	1	2	3	4	5	6	7	8	9	10
	Z2 = +400 µm	10	9	8	7	6	5	4	3	2	1	0

For the further improvement of the cylindricity, a third step is introduced between the two steps. The laser beam is focused at 150 µm beneath the top surface of the material. The parallel offset of the laser beam is +2 mm and angle of wedge prism is 4°. The drilling duration for three steps is varied with the

constant total drilling duration of 10 seconds. The drilling results on longitudinal cross-section of borehole are shown in Fig. 64 and the parameters applied in Table 5. As can be seen, the drilling duration of each step has a mild influence on hole cylindricity. A remarkable difference can be found in boreholes No. 4, 8 and 12 with 1 second drilling time in the first step. The inlets of boreholes are not sharp and with great cone angle as hole No. 1 in Fig. 63. By prolonging the drilling time, the diameter of inlet increases slightly; however, the verticality of the inlet is enhanced. The optimal cylindrical drilling results are holes No. 5 and 6, for which the drilling duration at each step is averaged. The aspect ratio of 20:1 can be achieved in 1 mm thick stainless steel with further optimized parameters.

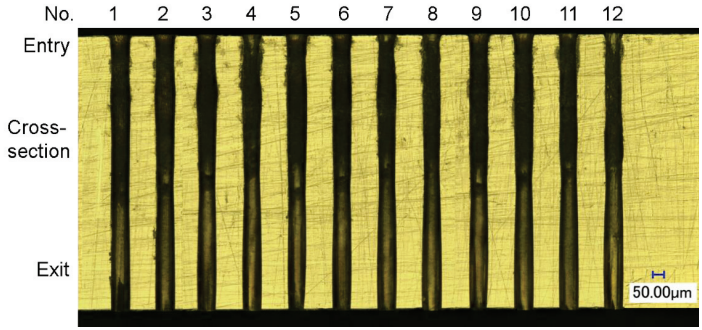


Fig. 64 Longitudinal cross-section of drillings with three steps and varied parameters as described in Table 5: Parameters for drilling holes with three steps in Fig. 64

Table 5: Parameters for drilling holes with three steps in Fig. 64

No.		**1**	**2**	**3**	**4**	**5**	**6**	**7**	**8**	**9**	**10**	**11**	**12**
Drilling duration/s	Z1 = -100 µm	4	3	2	1	4	3	2	1	4	3	2	1
	Z2 = +150 µm	4	4	4	4	3	3	3	3	2	2	2	2
	Z3 = +400 µm	2	3	4	5	3	4	5	6	4	5	6	7

The multi-step strategy is an effective approach to adapting the laser energy deposition at varied depths of boreholes. The adaption of energy deposition by means of adaption of the helical path contributes to the ablation of the targeted parts in the drilling channel and a minimization of hole diameter. Therefore, the multi-step strategy is widely applied in fabrication of high aspect-ratio microholes.

6.1.2 Dynamic adaption of focus position

As material thickness increases, the achievable aspect ratio is limited by the laser ablation behavior in the drilling channel. The removal rate decreases sharply with increasing drilling depth due to the decreased laser intensity as a result of the beam divergence and the multiple reflections, as well as the effect of laser ignited plasma. Therefore, it poses a major challenge to the fabrication of high aspect ratio microholes in thick material, although the multi-step drilling strategy can adapt the laser energy deposition to a certain depth of a borehole. Nevertheless, the strategy with the dynamic focus shifting provides a possibility to fabricate high-aspect-ratio microholes in 2 mm thick stainless steel. In this strategy, the focus of laser beam shifts along the laser propagation direction from material top side into material bulk during the drilling process. The 3D helical path and laser parameters such as single pulse energy can be adapted to maximize the laser intensity and minimize the helical diameter at the ablation front of the laser pulses.

The peak intensity of a Gaussian laser beam, as is well known, decreases as the distance away from focus increases due to defocusing. The iso-intensity line of a laser beam represents the laser intensity distribution along the propagation direction (z) as shown in Fig. 65 [Ko11]. The position Z_0 refers to the focal plane of a laser beam, having the maximum laser peak intensity and an effective working diameter of Ω_0 according to the ablation threshold. With a varied offset from focal plane, the laser peak intensity decreases to $I(Z_1)$, $I(Z_2)$ and $I(Z_3)$. Since $I(Z_3) < I_{th}$, no ablation beneath the Z position takes place. And the effective working diameter $\Omega_1 > \Omega_2 > \Omega_0 > \Omega_3 = 0$, whereas $Z_3 > Z_2 > Z_1 > Z_0 = 0$. Rephrased, the effective working diameter of the laser beam further from focal plane can be smaller than that near the beam focus.

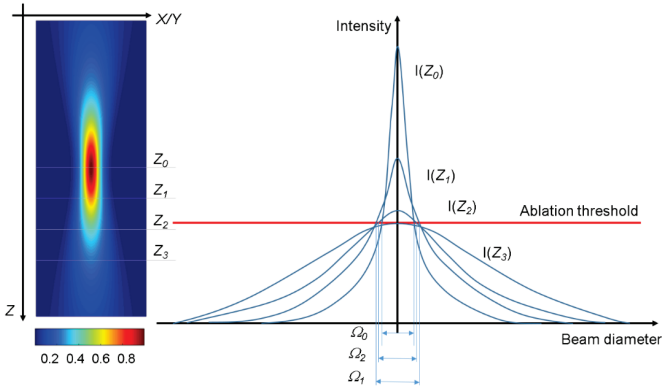


Fig. 65 Iso-intensity line of a Gaussian laser beam with the schematic diagram of ablation threshold and working diameter of laser beam

Ablation experiments on the surface of stainless steel by a static single laser beam with low single pulse energy as shown in Fig. 66 are in excellent agreement with the iso-intensity line. The laser beam moves from Z = -2 mm via focus to +2 mm. The darkness of the ablation area and the width of ablation lines reveal the degree of ablation intensity and effective working diameter of laser beam, respectively. The ablation lines are symmetric and have the identical characteristic such that ablation in the form of branding occurs as the z position approaches the focus. The degree of ablation intensity increases gradually together with an enlargement of ablation width. At Z = -1 mm, the ablation width reaches the maximum and then drops down to the in-between minimum at focal plane Z = 0. The same ablation behavior can be seen in the positive range.

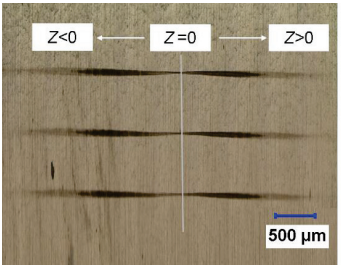


Fig. 66 Ablation of a static single laser beam in the z direction on a surface of stainless steel with a single pulse energy of 3 µJ and three repetitions.

Fig. 67 exhibits the longitudinal cross-section of helical drilling in 2 mm thick stainless steel using dynamic z shift with varied feed rate.

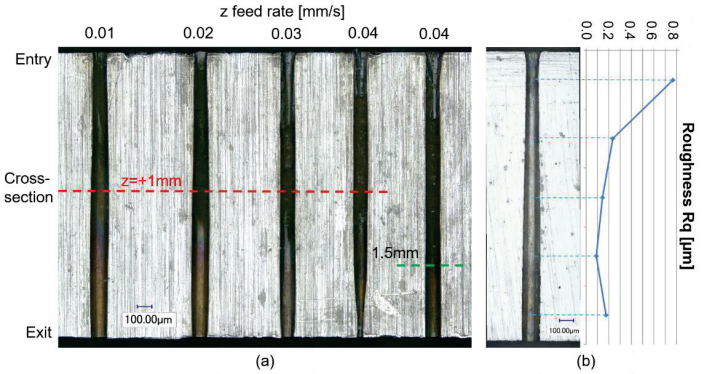


Fig. 67 Longitudinal cross-section of helical drilling in 2 mm thick stainless steel using a dynamic z shift with varied feed rate. (a) longitudinal cross-section (b) Measurement of roughness on borehole wall

By taking advantage of the behavior of effective ablation diameter ruled by the iso-intensity line of a Gaussian laser beam, together with the flexibility of the helical path, effective ablation can be maintained by means of a dynamic shifting

of focal plane with the development of an ablation front at the bottom of the drilling channel. Boreholes with excellent cylindricity can be obtained by dynamically moving the laser beam focus from the top surface to Z = 1 mm in the middle of the material with a feed rate up to 0.03 mm/s. The further increase of feed rate leads to a convergent outlet as a result of insufficient energy deposition. On the one hand, the drilling time is too short to enable the broadening phase of helical drilling. On the other hand, the ablation efficiency at a higher feed rate drops since the forward moving speed of ablation front lags behind the feed rate of focus. By further shifting the focus to Z = 1.5 mm, the outlet of the borehole can be broadened to be cylindrical. However, the entry diameter only increases slightly. The roughness of the borehole wall along the drilling depth is shown in Fig. 67(b). Compared with the result of 1 mm in Fig. 59, the roughness value overall in 2 mm drilling has been increased by about 20 percent while having Rq = 0.75 µm in the inlet area. The tendency of roughness development along the hole depth are comparable. Furthermore, the cylindricity of drilling in 2 mm is significantly improved with the same aspect ratio of 20:1.

Noteworthy is that the helical path is kept constant in the whole drilling process with a helical diameter of 50 µm and parallel offset 0. The adaption of laser energy deposition takes place primarily at the ablation front in order to enable an effective ablation and a minimized effect on the hole entry. Therefore, the preferable helical path should be of high cylindricity in the caustic.

6.2 Dynamic helical drilling process

Dynamic helical drilling is primarily applied for the purposes of fabricating of microholes with high complexity and enhancing geometric and qualitative properties of the microholes. In this subsection, the ablation behavior of laser pulses in the dynamic helical process is discussed. The helical diameter is varied during dynamic helical drilling. The dynamic helical drilling process makes it possible to shape the profile of the entrance and to change the dynamic of the vaporized /molten material driven out during the drilling process.

6.2.1 Ablation behavior in dynamic helical drilling process

In the subsection 4.3.2, the relationship between the superposed laser intensity I_s and the helical diameter d_h was discussed. In dynamic helical drilling, the helical diameter is a temporal variable. According to the Eq. **4.12**, with the condition that the processing parameters are kept constant except the temporal varied helical diameter, the superposed laser intensity in the dynamic helical drilling I_{sd} can be simplified as:

6.1
$$I_{sd} \propto \cdot\, exp\{-d_h^2(z,t)\}$$

where $d_h(z,t)$ denotes the helical diameter at time t and the focal position of the laser beam at z. The helical diameter is determined by incident angle of the

laser beam relative to the Dove prism. It is regulated by the angle of the wedge prism, which is motorized and can rotate with an angular speed V_{wedge}. Combined with the Eq. **5.3**, the helical diameter at focal plane in a dynamic helical process with a fixed given angular speed (V_{wedge}>0) can be given by:

6.2

$$d_h(t) = 3.02 + 9.73V_{wedge} \cdot t + 1.24(V_{wedge} \cdot t)^2$$

With the increase of the helical diameter, the circumference of helical path at the helical diameter increases whereas the total pulse number is identical, thus, the pulse overlap decreases. Eq. **6.1** indicates that the peak intensity of superposed laser pulses drops dramatically in a verse-proportional behavior. By means of the numeric analysis, the superposed laser intensity distributions with the discrete helical diameters and dynamically varied helical diameter are plotted and shown in Fig. 68(a) and (b), respectively. The cross-section in Fig. 68(c) illustrates the development of ablation depth at greater helical diameter by means of a classic helical drilling process.

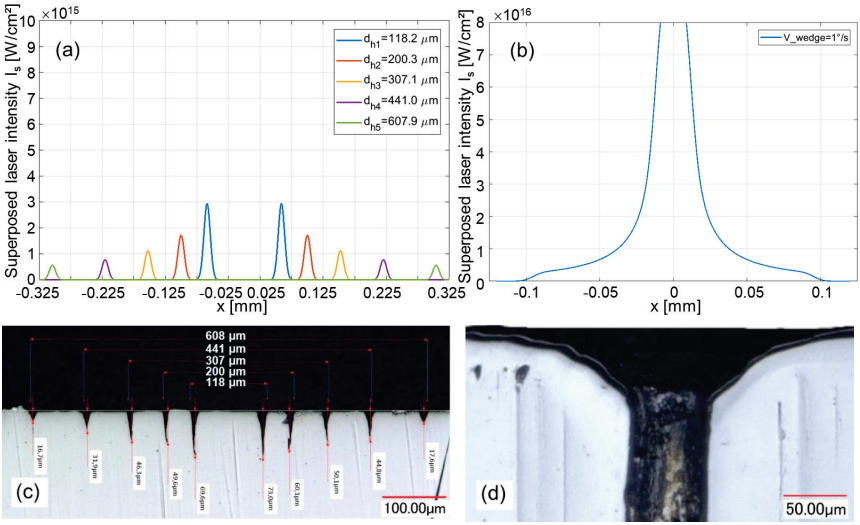


Fig. 68 Comparison of ablation behavior between classic helical and dynamic helical drilling: (a) numeric simulation of the superposed intensity distribution at different helical radii, (b) numeric simulation of the superposed laser intensity distribution of dynamically varying helical radius, (c) ablation depth at different helical radii, (d) ablation profile of dynamically varying helical radius.

The laser single pulse energy applied is 6.25 μJ and the drilling time is 0.5 s at each helical diameter. The helical paths at each diameter are concentric; therefore, the ablated trenches are symmetrically distributed. This reveals once again that the ablation depth decreases with the increase in the helical diameter.

The development of the ablation depth at varied helical diameters is in excellent agreement with that of superposed laser intensity as shown in Fig. 68(a). Akin to the results of classic helical drilling, the ablation depth by continuously increasing helical diameter has the same tendency as exhibited in Fig. 68(d). The helical diameter increases by increasing the deflection angle of laser beam by the wedge prism with a velocity of 0.5°/s. The ablation depth decreases with the increase of the helical diameter. As the helical diameter increases further, the ablation depth at radial direction has no significant decrease, showing a homogenous ablation result.

Since the pulse overlap and the track overlap of scanning across the ablation area is generally kept constant in processing with a galvanometer scanner, the ablation depth is homogenous in this area. In contrast, the degree of pulse overlap is dependent on the helical diameter and keeps changing in the dynamic helical drilling process without any adaption. This dependence is caused by the increase of the circumference, but constant pulse number on the helical revolution. As a result, the pulse overlap decreases with the increase of helical diameter. Moreover, the nonlinear increase of the helical diameter over time leads to a time-dependent track overlap of the neighboring helical paths (cf. 4.3.1). Both the two facts explain the reason for the spatial inhomogeneity of laser energy deposition in the dynamic helical drilling process. The laser energy deposition determines not only the ablation behavior, but also the hole profiles. The influential factors on the ablation behavior in the dynamic helical drilling process have been investigated in the following subsections.

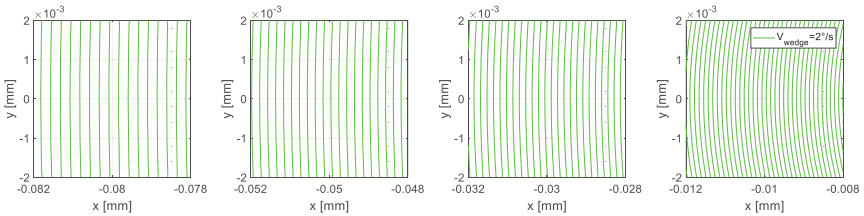


Fig. 69 Helical paths at different helical diameters in dynamic helical drilling. Rotational speed of the Dove prism: 60 rps, velocity of the wedge prism 2°/s

6.2.2 Influential factors in dynamic helical drilling

Influence of applied single pulse energy on hole profile

The correlation between superposed laser intensity and single pulse energy is numerically simulated and displayed in Fig. 70. The curves are characterized by two evident zones: the middle part with a sharp-edged donut top and flank part with a gentle slope. These two zones correspond to the stem hole and the positive conical entrance of the funnel-shaped hole. Due to a higher pulse

density, the superposed laser intensity in the central area of the helical diameter within 0.05 mm is significantly higher than that of areas with greater diameters, where the superposed laser intensity drops much more gently. In addition, a linear relationship between the applied laser pulse energy and the superposed laser intensity exists in the range of helical diameters greater than 0.05 mm as shown in Fig. 70.

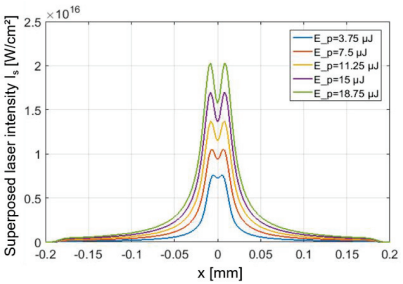


Fig. 70 Simulation of superposed laser intensity in the dynamic helical drilling with (a) varied laser pulse energy at Vwedge = 1.5°/s, ω_m=50 rps

The results of experiments are in excellent agreement with the simulation as can be seen in Fig. 71 and Fig. 72. Within the same single pulse energy applied, the ablation depth decreases with the increase of the helical diameter. The higher single pulse energy contributes to a deeper ablation of the material, especially in the middle area of slope (helical radius around 120 µm), forming a straighter profile.

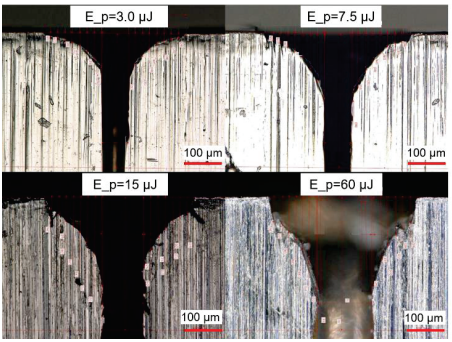


Fig. 71 Longitudinal sections of funnel-shaped holes drilled with varied single pulse energy of 3.0, 7.5, 15 and 60 µJ at a rotational speed of wedge prism 0.5°/s, ω_m = 50 rps

As depicted in Fig. 71 the curvature of slope profiles becomes smaller as laser pulse energy increases. Additionally, the depth of the truncated cone extends when higher single pulse energy is applied. Therefore, the opening angle of the taper declines with the same entrance diameter. In the range of single pulse

energy below 10 µJ, the increasing tendency of ablation depth on the measured position appears to be linear by and large. The cross-section of holes shows a very well-defined profile. The laser beam with higher laser intensity generates more molten material and impairs the quality of the hole wall. The applied single pulse energy has not only an effect on the ablation depth during the helical drilling, but also plays a role in the morphological property of the hole profile fabricated by a dynamic helical drilling process.

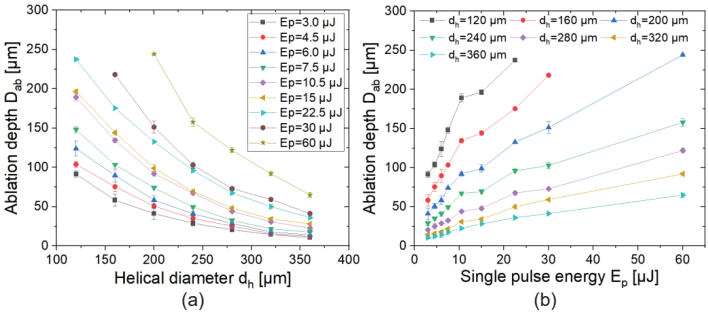


Fig. 72 Diagram of the relationship of ablation depth to helical diameter by varied single pulse energy Ep and the adaption, Vwedge=0.5°/s, ω_m=50 rps

The correlation between the position-dependent ablation behavior and the applied single pulse energy is shown in the diagrams in Fig. 72. In Fig. 72(a), the development of the ablation depth at different helical diameters and varied single pulse energy is represented. The single curve corresponds, by and large, to the hole profile fabricated by dynamic helical processing. With the increase of helical diameter and constant pulse number, the pulse overlap on the helical revolution decreases. Furthermore, due to the parabolic development of the helical diameter with the angle of the incident laser beam to the Dove prism (see Fig. 43), the track overlap between the neighboring helical paths becomes smaller at greater helical diameters. This is the other reason for the decrease in the superposed laser intensity with increasing helical diameter. Consequently, the locally superposed laser intensity decreases and leads to the decrease of ablation depth. By increasing the applied single pulse energy, the ablation depth increases globally over the helical path. The development of the ablation depth at different helical diameters with the increasing single pulse energy can be seen in Fig. 72(b). The slope of the curves shows the increasing rate of the ablation depth. The curves have in common that the increase of the ablation depth has two distinguished zones as shown in Fig. 73(a). In the first zone from 3 µJ to 10 µJ, the ablation depth increases linearly. The smaller the helical diameter, the steeper the slope of the curves. That indicates that the ablation depth increases faster with the single pulse energy applied. In the second zone from 10 µJ on, the increase of the ablation depth shows a quasi-linear behavior, but with a greater deviation and a gentler slope than that in the first zone. The calculated

superposed laser intensity increases linearly with applied single pulse energy and corresponds to the result of the simulation described in Fig. 70.

Compared with the linearly increasing superposed laser intensity, the development of ablation depth at the same helical radius in dynamic helical drilling with increased laser pulse energy shows "abnormal" behavior. The increase rate of ablation depth stays constant at the lower applied single pulse energy. However, with the further increase of the applied single pulse energy, it slows down. The ablation efficiency is defined as the ratio of the ablation depth and applied single pulse energy. An overall decrease of ablation efficiency with increased single pulse energy at different helical diameters can be seen in Fig. 73(b). One possible reason is the enlarged volume of the laser ignited plasma by the higher laser pulse fluence/energy. The plasma absorbs a greater proportion of laser energy, leading to impaired ablation results. The ablation results at the smaller helical diameter show a more efficient process, which is again attributed to the greater overlap between pulses and ablation tracks.

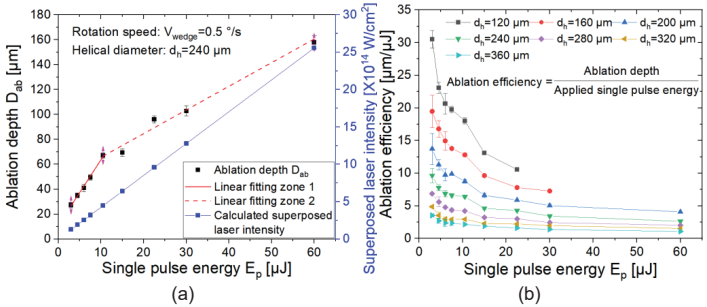


Fig. 73 (a) Development of ablation depth and calculated superposed laser intensity with applied single pulse energy, (b) ablation efficiency. Rotational speed of wedge prism 0.5°/s, ω_m = 50 rps. Measured position helical diameter 240 µm.

Influence of increasing rate of helical diameter on hole profile

The rotation speed of the wedge prism describes the increasing rate of the helical diameter in the dynamic helical drilling process. For the specified diameter of hole entrance, the duration of the process as well as the track offset in the radial direction between the neighbored helical revolutions are determined by the rotation speed of the wedge prism.

The correlation between superposed laser intensity and the rotating speed of the wedge prism is simulated and visualized by a numeric methodology seen in Fig. 74. The higher the rotation speed is, the shorter the process duration and the broader the track offset. As a result, the local superposed laser intensity declines sharply after the start of dynamic helical drilling as shown in Fig. 74.

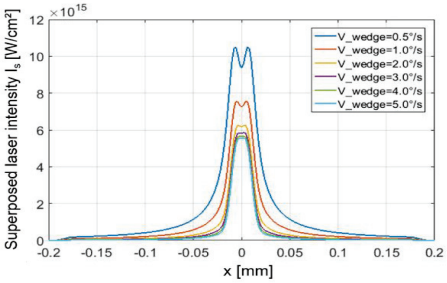


Fig. 74 Simulation of superposed laser intensity in dynamic helical drilling with varied rotation speed of wedge prism at Ep = 7.5 µJ, ω_m = 50 rps.

By varying the rotation speed of the wedge plate, the energy deposition of laser pulses can be spatially modulated during dynamic helical drilling. The faster the increasing rate of helical diameter is, the wider the distance between the neighboring tracks in the helical path as shown in Fig. 75. The offset of the neighboring tracks increases with the rotation speed of the wedge prism in linear behavior.

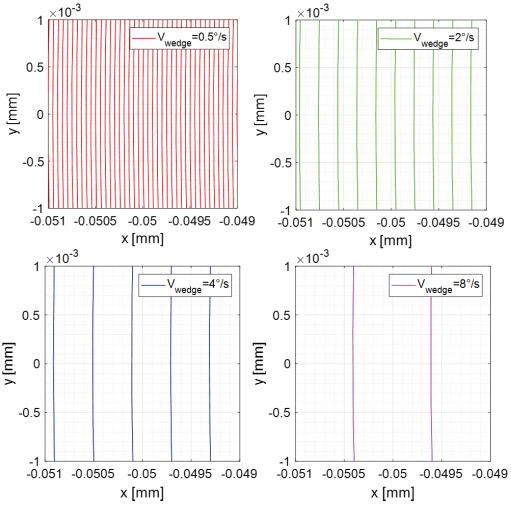


Fig. 75 Track offset of the helical path with varied rotation speed of wedge prism shown in a 2 µm x 2 µm area of the whole 2D helical path, ω_m = 50 rps, laser spot size 15 µm

The longitudinal sections in Fig. 76 show the profile of the entrance of the drilled hole with different rotation speeds of the wedge prism at the same single pulse energy. The correction between the ablation depth over different helical diameters as well as over different rotation speed of wedge prism is plotted in Fig. 77. It is clearly represented that the ablation depth reduces dramatically as

the rotation speed of wedge prism increases from 0.5°/s to 2°/s. By further increasing the rotation speed of wedge prism to 8°/s, the profile of the hole entrance becomes shallower and the difference of hole profiles can hardly be seen. Despite the same ratio of the track offset of four times, the differential of ablation depth between 0.5°/s and 2°/s is much greater than that between 2°/s and 8°/s.

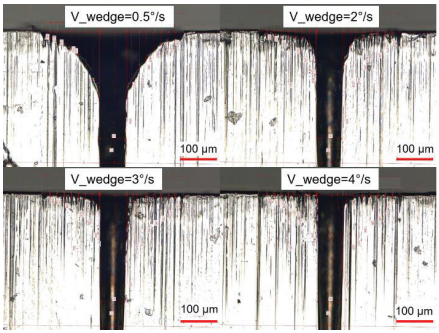


Fig. 76 Longitudinal sections of funnel-shaped holes drilled with varied rotation speeds of the wedge prism: 0.5, 2, 3 and 4 °/s at a single pulse energy of 7.5 µJ, ω_m = 50 rps

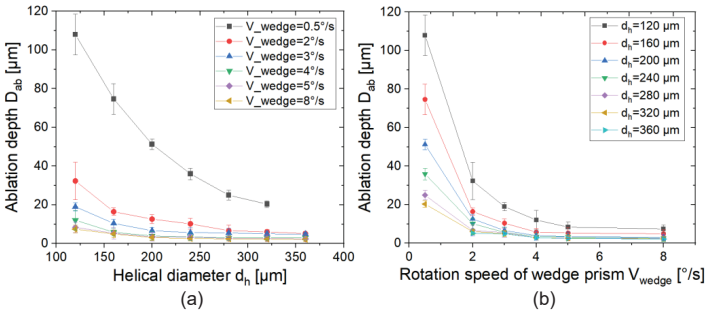


Fig. 77 Diagram of the relationship of ablation depth to helical diameter by varied rotation speed of wedge prism, single pulse energy Ep=7.5 µJ, ω_m=50 rps

The ablation depth is dependent on the local superposed laser intensity. Fig. 78(a) depicted the tendency of ablation depth and the superposed laser intensity against different rotation speed of wedge prism at the position of helical diameter 240 µm. The developing tendency of the ablation depth is in an excellent agreement with the curve of the simulated superposed laser intensity, showing an exponential descending development. By plotting the ablation depth against the superposed laser intensity, a linear relationship as can be seen in Fig. 78(b). The ablation depth as well as the hole profile at varied rotating speeds of the wedge prism can, therefore, be predicted by a numeric simulation based on the ablation results.

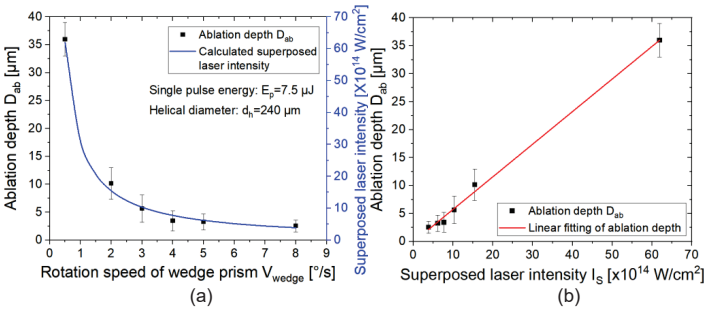


Fig. 78 (a) Ablation depth for various rotation speeds of the wedge prism at a single pulse energy 7.5 µJ. (b) linear relationship between superposed laser intensity and ablation depth. Measured position was 120 µm from the center line, helical radius 120 µm, ω_m = 50 rps

Influence of rotational speed of Dove prism on hole profile

The rotational speed of the Dove prism describes the rotational speed of the laser beam in the dynamic helical path relative to the workpiece. Similar to the rotation speed of the wedge prism, the track overlap in the helical path can be modulated by the variation of the rotational speed of the Dove prism. However, in contrast to that, the density of the tracks increases linearly with the increase of the rotational speed of the Dove prism, as can be seen in Fig. 79. Noteworthy is that the track density is constant on the condition that the ratio of the rotational speed of the Dove prism to the rotation speed of wedge prism remains constant.

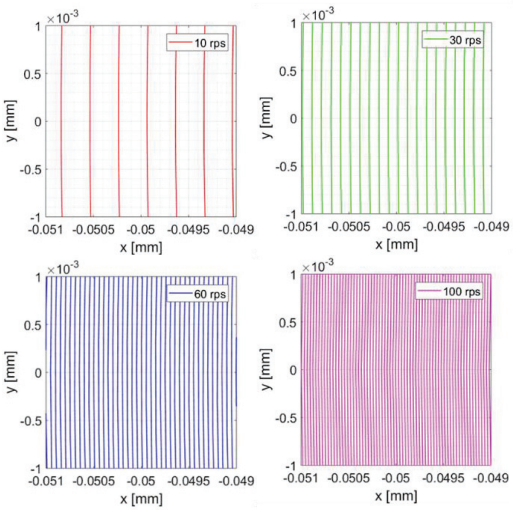


Fig. 79 Track offset of the helical path with varied rotational speed of the Dove prism shown in a 2µm x 2 µm area of the whole 2D helical path, Vwedge = 0.5°/s, laser spot size 15 µm

Despite that, the increase of the rotational speed of laser beam contributes to a higher density of laser beam tracks, and the pulse overlap on one single revolution decreases. Additionally, the pulse number in a unit time remains the same, which means the laser energy deposited locally is independent of the rotational speed of the laser beam. The drilling results shown in Fig. 80 and Fig. 81 provide evidence to the quasi-independency of ablation depth of rotational speed of the Dove prism. The profiles of the shaped entrances drilled with different rotational speeds of the Dove prism show no significant dissimilarity in spite of the deviation in the ablation depth. All the shaped hole entrances exhibit a funnel-like profile.

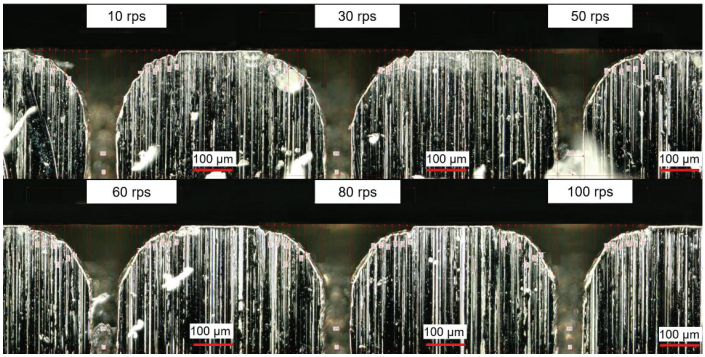


Fig. 80 Longitudinal sections of funnel-shaped holes drilled with varied rotational speeds of the Dove prism at a single pulse energy of 7.5 µJ and a rotational speed of the wedge prism 0.5 °/s

The influence of the increasing rotational speed of the Dove prism on the ablation depth is shown in Fig. 81(a) and (b). As the rotational speed of the Dove prism increases from 10 rps to 100 rps, the ablation depth drops from 110 µm to about 90 µm at the helical diameter of 120 µm. However, as the helical diameter increases, the influence of the rotational speed of the Dove prism weakens and can even be ignored as the helical diameter reaches 360 µm. The spatial dependence of the fluidic dynamic of the ablated material in the drilling process can be one of the main reasons. The ablated material in the near-central area is mainly driven out from the pilot borehole by the pressure of the assistance gas. At the outer area, the ablated material is vaporized vertically from the ablation interface due to a strong recoil force. Furthermore, the overlap degree of the laser pulses on the helical path is higher at a 10 rps rotational speed of the Dove prism than at 100 rps as can be seen in Fig. 30. The ablation works more efficiently with the contribution of higher overlap of laser pulses and thus has a stronger incubation effect. As a result, the ablation depth falls with the increasing rotational speed of the Dove prism despite a constant superposed laser intensity, as shown in Fig. 81(c).

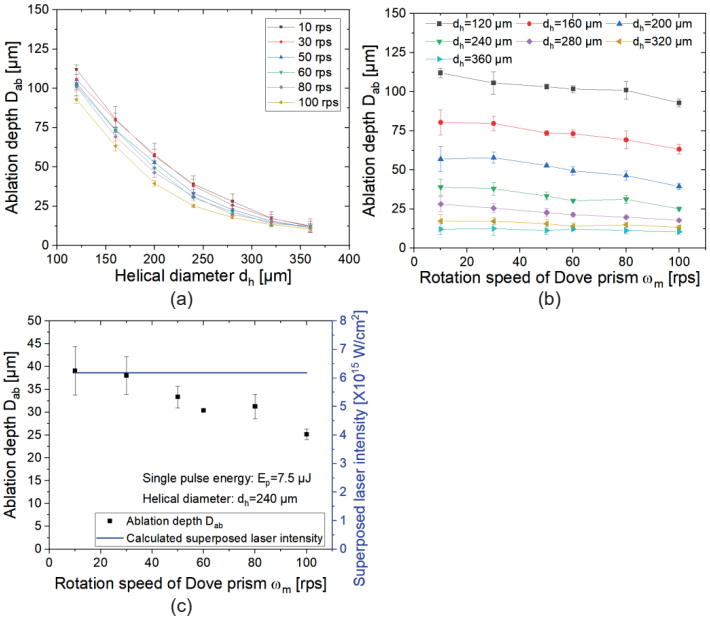


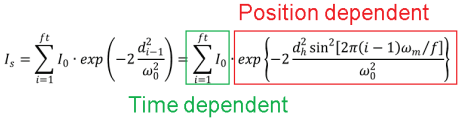
Fig. 81 Diagram of the relationship of ablation depth to helical diameter by varied rotational speed of the Dove prism, Vwedge=0.5°/s, single pulse energy Ep=7.5 μ

6.3 Adaption of energy deposition in dynamic helical drilling

Since the ablation depth of the laser pulses depends on the local energy deposition, the parameters of laser beam and helical optics during the helical drilling process must be dynamically adapted in order to achieve a designated profile.

According to Eq. **4.12** in 4.3.2, the superposed laser intensity is determined by the single pulse energy applied, by the drilling time, the helical diameter, the pulse repetition rate and the rotational speed of the Dove prism. The five influential factors can be categorized into two types, as depicted in Fig. 82: time-dependent and position-dependent factors.

Fig. 82 Categorization of influential factors in the dynamic helical drilling



The helical diameter, the pulse repetition rate, and the rotational speed of the Dove prism determine the pulse position and the location of energy deposition. Thus, the three factors are categorized as position-dependent factors. And the single pulse energy and drilling time belong to the time-dependent influential factors. Spatial and temporal adaption of laser energy deposition in the dynamic helical drilling process to achieve a designated hole profile with defined depth is discussed in this subsection.

6.3.1 Adaption of single pulse energy

As discussed in 6.2.1 and 6.2.2, the single pulse energy is directly linked to the energy deposition and the hole profile. To achieve a designated profile at the hole entrance, the laser energy deposition needs to be adapted. Based on the ablation behavior with the varied single pulse energy depicted in Fig. 83, a so-called reduced model can be built with sparse data.

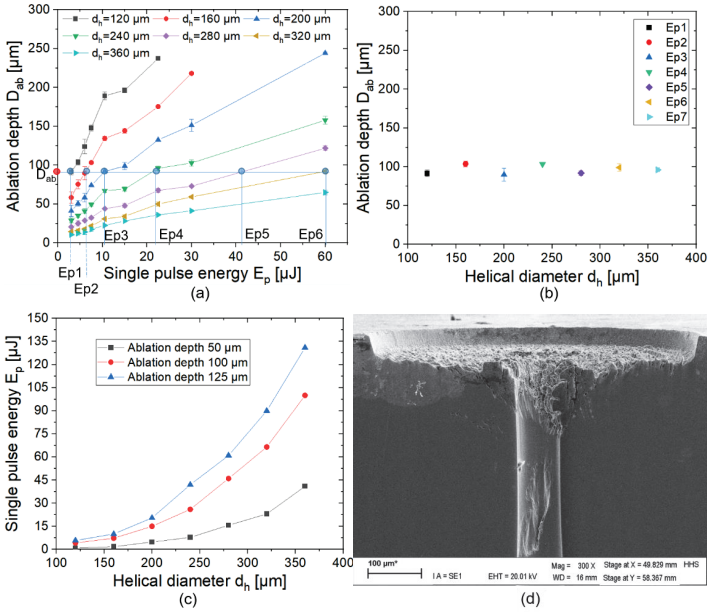


Fig. 83 Adaption of single pulse energy in the dynamic helical drilling process based on Fig. 72. (a) An example of determination of single pulse for a defined ablation depth at different helical diameters. (b) required single pulse energy for the defined ablation depth, (c) adaption of single pulse energy for a „T-shaped" hole entrance with different depth. (d) T-shaped" hole

With this model, the values of the ablation depth at any helical diameter and with any single pulse energy can be interpolated and extrapolated. For a designated profile, for instance a "T-shaped" hole entrance, the function of depth over helical diameter is given, and the required single pulse energy to

achieve such a profile can be reversely derived from the reduced model. The defined ablation depth D_{ab} at different helical diameters can be coordinated in the diagram describing the correlation of the single pulse energy, the helical diameter and the ablation depth, as can be seen in Fig. 83(a) and (b). By plotting the required single pulse energy over the helical diameter as shown in Fig. 83(c), the approach to adapt single pulse energy for different ablation depth can be developed. The curves in Fig. 83(c) show the development of required single pulse energy at the helical path for three different depths – 50 µm, 100 µm and 125 µm – at the entrance of the T-shaped holes. The diagram demonstrates that the approach of adapting spatial single pulse energy based on the reduced model is applicable for other arbitrary 2/2.5 dimensional hole profiles as well (See in 0). The SEM image in Fig. 83(d) shows a T-shaped microhole made with the dynamic helical drilling process and having an ablation depth of approximately 80 µm. The single pulse energy at the helical path is adapted according to the results in Fig. 83(c).

6.3.2 Adaption of drilling duration

According to Eq. **4.12**, the drilling time has a direct link to the local intensity distribution as well, in addition to the single pulse energy. Together with the pulse repetition rate, it determines the total number of laser pulses deposited on the helical path. The number of pulses per unit length N_{ppl} on the helical path is in inverse proportion to the helical diameter. The local superposed laser intensity decreases with the increase of the helical diameter. By extending the drilling duration, the total pulse number at one position increases linearly. The time-dependent number of pulse per unit length $N_{ppl}(t)$ can be given by:

6.3

$$N_{ppl}(t) = \frac{f \cdot t}{2\omega_m \pi d_h} = \frac{ft}{2\pi\omega_m d_h}$$

where f denotes the repetition rate of laser pulses, d_h the helical diameter, ω_m is the rotational speed of the Dove prism, and t is the drilling duration.

The influence of the drilling time on the ablation depth at varied helical diameters is shown in Fig. 84(a). With constant laser pulse energy and the repetition rate, the ablation depth at different diameters increases with the increase of the drilling time. The curve marked as "unadapted" uses a constant drilling duration at different helical diameters. A reduced model can be built in analogy to the adaption approach for single pulse energy. By means of that, the drilling duration at a certain helical diameters can be read out for a designated hole profile based on the model. As shown in Fig. 84(b) and (c), a constant ablation depth at different helical diameters can be achieved after the adaption of drilling duration with the parameters shown in Table 4.

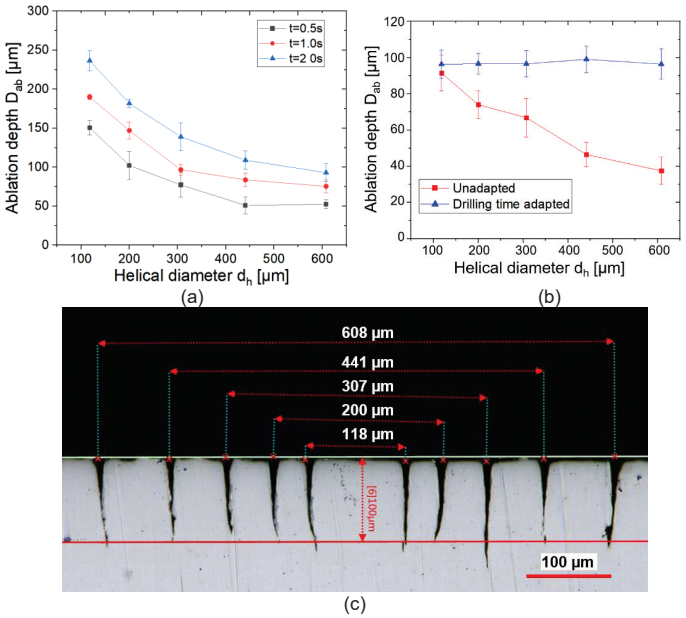


Fig. 84 (a) Diagram of the relationship of ablation depth to helical diameter by varied and drilling time. (b) comparison of the ablation depth with and without adaption of the drilling time. (c) cross-section of ablation depth with adapted drilling time

Table 6: Adaption of drilling time in dynamic helical drilling

*Measurement precision ±2 µm

d_h[µm]*	E_p[µJ]	t_d[s]	f_{REP}[kHz]	$\mathbf{d_h/t_d}$	N_{ppl}
118	12.5	0.500	75	**236**	**0.8430**
200	12.5	0.847	75	**236**	**0.8425**
307	12.5	1.300	75	**236**	**0.8424**
441	12.5	1.860	75	**236**	**0.8391**
608	12.5	2.565	75	**236**	**0.8393**

In the condition that the ratio of the drilling duration and helical diameter is constant, the time-dependent number of pulse per unit length is identical. In the experiment, the specific value d_h/t is kept constant at 236. The calculated number of pulses per unit length is approximately 0.84.

6.3.3 Adaption of pulse repetition rate

Analogous to the adaption of the drilling time, according to Eq. **6.3**, if the rotational speed ω_m and drilling time t are kept constant, the number of pulses

per unit length N_{ppl} has a correlation with the pulse repetition rate f and the helical diameter d_h as following:

6.4
$$N_{ppl} \propto f/d_h$$

With a constant drilling time and applied single pulse energy, the superposed intensity is also scalable by adapting the spatial distance between two consecutive laser pulses d_1 according to Eq. **4.10**. In the helical drilling process, the component $\omega_m << f$, thus, the distance between two neighbored pulses $d_1 \approx 2\,\pi\, d_h\, \omega_m/f$. If the rotational speed ω_m is kept constant,

6.5
$$d_1 \propto d_h/f$$

From Eqs. **6.4** and **6.5**, the same conclusion can be drawn that the ratio of the pulse repetition rate and helical diameter determines the spatial distribution of laser pulses, and further plays a major role in the deposition of the laser energy in the dynamic helical drilling process. Therefore, the energy deposition for the dynamic helical drilling process can be adapted by scaling the pulse repetition rate over different helical diameters.

The parameters for adaption of a pulse repetition rate for a T-shaped hole profile are listed in Table 7. The single pulse energy applied is 12.5 µJ and the drilling duration at different helical diameter is set as 1.333 seconds. Due to the technical condition, the devisor of fundamental frequency must be always an integer; the available pulse repetition rate at each tested helical diameter cannot be given as theoretical calculation. As a result, the term of d_h/f can only be adapted with a minimized deviation. The calculated values of N_{ppl} at different helical diameters are between 0.8 and 0.885 with a standard deviation of 0.0317.

Table 7: Adaption of the pulse repetition rate in dynamic helical drilling
*Measurement precision ±2 µm

d_h[µm]*	E_p[µJ]	t_d[s]	f_{REP}[kHz]	$\mathbf{d_h/f_{REP}}$	N_{ppl}
118	12.5	1.333	28.57	**4.1**	**0.8524**
200	12.5	1.333	50	**4**	**0.8820**
307	12.5	1.333	75	**4.1**	**0.8619**
441	12.5	1.333	100	**4.4**	**0.8000**
608	12.5	1.333	150	**4**	**0.8704**

Fig. 85 shows the ablation behavior with adaption of parameters in Table 7 compared with the ablation development without adaption. The parameters for the curve marked as "unadapted" employs a constant pulse repetition rate of 75 kHz at different helical diameters. The curve using the unadapted parameter is a typical ablation result in dynamic helical drilling without any adaption of laser energy. The ablation depth drops down with the increase of helical diameter. In contrast to that, the ablation depth remains constant at approximately 100 µm over the different helical diameters when the drilling time and pulse repetition

rate are increased, correspondingly. The noticeable deviation of ablation depth can be linked to the deviation between the calculated parameter and technical available parameters. However, the model matches well with the experimental results, and the hypothesis is validated that homogenous ablation is achievable by keeping a constant local superposed laser intensity distribution.

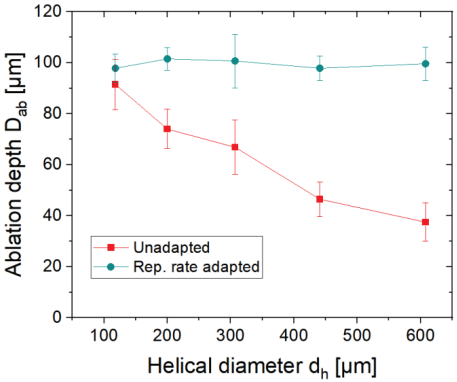


Fig. 85 Ablation depth at varied helical diameters by unadapted process (red square), adapted repetition rate (dark green circle) and drilling time (yellow triangle).

There are other approaches for the adaption of energy deposition in dynamic helical drilling, such as the adaption of the rotational speed of the Dove prism and wedge prism. However, the feedback speed of the motors is due to the acceleration and deceleration out of the range of the ablation process, which is normally in a millisecond regime. Therefore, despite a theoretical feasibility, the strategies for the adaption of laser energy deposition by the adaption of rotational speed of the laser beam and the increasing rate of the helical diameter in the dynamic helical drilling process are not discussed.

6.4 Application examples of energy-deposition-adapted dynamic helical drilling

Extension of the fabrication limitation of classic helical drilling

As aforementioned, the capability of classic helical drilling is limited by the construction of the optical setup of the helical drilling optics. One limitation is the opening angle of a conical hole, which is caused by factors such as the clear aperture of the Dove prism and the maximal parameter offset of the incident laser beam to the Dove prism. The dynamic helical drilling process makes it possible to transcend the limitation of the classic helical drilling process in the fabrication of positive conical holes.

The working principle of a hybrid helical drilling process is depicted in Fig. 86. Firstly, the core hole is made with the classic helical drilling process and the

maximal opening angle. Following that, the hole entrance is shaped by means of the dynamic helical drilling process. With the adaption of the energy deposition as introduced in 6.3.1, the shaped hole profile is as straight as that of classic helical drilling. Thus, the opening angle of a positive conical hole can be extended.

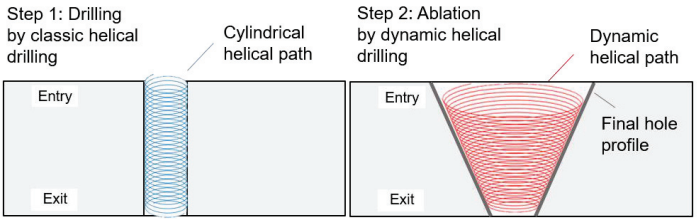
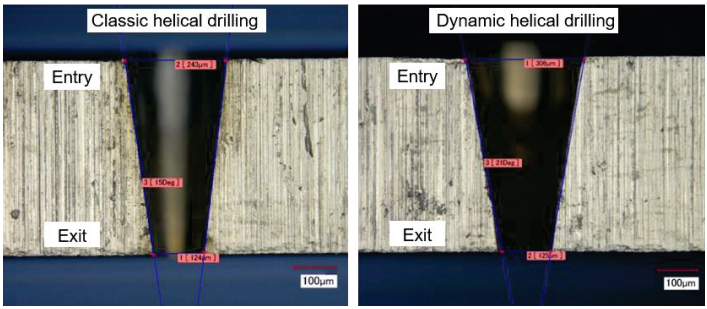


Fig. 86 Schematic diagram of increasing the opening angle using hybrid helical drilling process

The maximum opening angle of about 15°can be achieved by classic helical drilling in a 500 µm thick stainless steel using a f = 60 mm focusing lens, as shown in Fig. 87(a). The entrance and exit diameter are 243 µm and 124 µm, respectively. The cross-section of the positive conical hole shows a very linear profile. The opening angle can be easily extended to 21° by the dynamic helical drilling process with spatially adapted single pulse energy subsequent to the classic helical drilling process (see in Fig. 87(b)). Apparently, the opening angle can be further increased by ablating more volume with a larger entrance diameter. Theoretically, a maximum opening angle of ca. 100° with an exit diameter of 125 µm is achievable by using the existing helical drilling optics and ultrashort pulsed laser system.



(a) (b)

Fig. 87 (a) Cross-section of a hole fabricated with classic helical drilling and a maximum opening angle in 500 µm thick stainless steel.(b) increasing the opening angle by dynamic helical drilling

Increase on the complexity of hole profile

The complexity of the profile of a microhole, by definition, refers to the number of the dimensions of hole profile in respect to hole diameter, depth and conicity (or opening angle). It indirectly demonstrates the possibility of the variation on the above-mentioned three parameters (diameter, depth and conicity). The classic helical drilling process is able to fabricate a 2.5-dimensional hole with specified opening angle along the depth. The dynamic helical drilling process makes it possible to alter the opening angle with the drilling depth. Therefore, the dynamic helical drilling process, in this context, can be considered as a three-dimensional drilling approach.

Rotationally symmetric 3D-shaped holes can be fabricated in one single process step by employing the dynamic helical drilling process. Firstly, a pilot hole with a small diameter (in most case smaller than 100 µm) is manufactured by the classical helical drilling process. Subsequently, a shaped inlet and outlet with a designated profile is concentrically superposed on the pilot hole with a dynamic helical drilling strategy. All relevant process parameters can be varied and adapted dynamically during the dynamic helical drilling process.

With the parameters for negative and positive conical holes and the static strategy, a rotational symmetric converging-diverging hole can be fabricated by concentrically superposing a positive conical hole upon a pre-bored negative conical hole, as shown in Fig. 88(a). The drilling time is about 15 seconds. The position of the throat lies at z = 170 µm beneath the surface (approximately 1/6 of the material thickness) and its diameter is 120 µm. The diameter of the hole entrance and exit are both 180 µm. In order to improve the controllability on the shaping of converging hole and the depth of the throat position, a dynamic drilling strategy is chosen for the converging part.

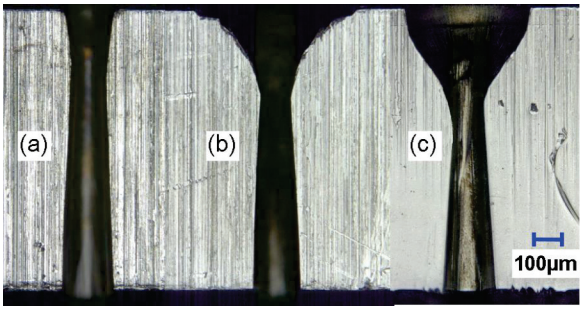


Fig. 88 Converging-diverging holes fabricated by (a) multi-step classic helical drilling and (b)(c) dynamic helical drilling strategies with adapted energy deposition

By means of the dynamic helical drilling process, a hole entrance with designated profile is feasible. Fig. 88(b) and Fig. 88(c) show the converging-diverging holes

with entrance of a funnel and de Laval nozzle form – different curvature of entrance. For the funnel-like hole depicted in Fig. 88 (b), the helical diameter increases from 40 µm to 570 µm within 30 seconds. Accompanied by that, the laser pulse energy decreases from 12.5 µJ to 2.5 µJ in five steps with a decrement of 2.5 µJ and duration of 6 seconds at each step. The single pulse energy remains the same (12.5 µJ) during this process for the hole in Fig. 88 (c). The total drilling time is 40 seconds. The throat positions of both converging-diverging holes are located at z = 330 µm, about 1/3 of the material thickness under the top surface. The opening angle of the converging parts are 91° and 58°, respectively. The diverging part of the holes are of the same geometry: hole-exit diameter 180 µm, divergence angle 6.6°. The dynamic drilling approach manifests a higher flexibility in shaping the entrance part of a converging-diverging hole.

The converging-diverging holes in Fig. 88 exhibit an excellent symmetry of hole profile owing to a helical path with a fairly good circularity achieved by using the helical drilling optics. By varying the pulse energy and increasing the rate of helical diameter for the converging part, the position of throat can be adjusted in the depth direction of the hole.

The morphology of the boreholes is analyzed by an examination on the hole wall under a scanning electron microscope and laser scanning microscope. As the SEM image in Fig. 89 depicts, neither recast layer nor heat affected zone (HAZ) can be detected on the hole wall. Furthermore, the root mean squared (RMS) roughness Rq on the hole wall is measured to be 0.35 µm, which provides evidence of a very smooth hole-wall. On the one hand, the application of an ultrashort pulsed laser having a pulse duration 900 femtoseconds contributes to the high-precision ablation and minimized HAZ [FD03]; on the other hand, as a result of the helix revolution of laser pulses, the local thermal accumulation is weakened [Ba15] [We14]. Both two factors are essential for a high-quality drilling process.

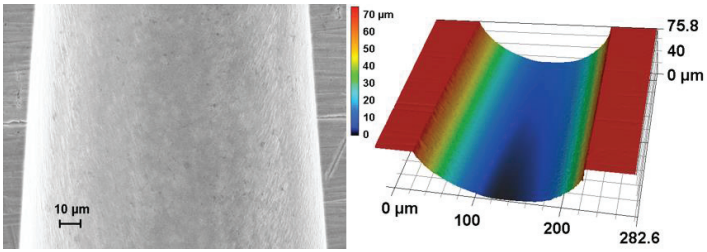


Fig. 89 (a) SEM image and (b) confocal laser scanning microscopy of the cross-section of the diverging part in a converging-diverging hole

With the adapted laser energy deposition, the dynamic helical drilling can be used to fabricate multidimensional microholes with designated profiles, showing

the high controllability in shaping the hole profile. The SEM images of cross-sections of drilling in Fig. 90 show two examples of multidimensional holes fabricated in stainless steel, i. e. a T-shaped hole and Y-shaped microfunnel. Based on the results and discussion presented in previous sections, the applied single pulse energy was adapted in the fabrication of these two shaped holes.

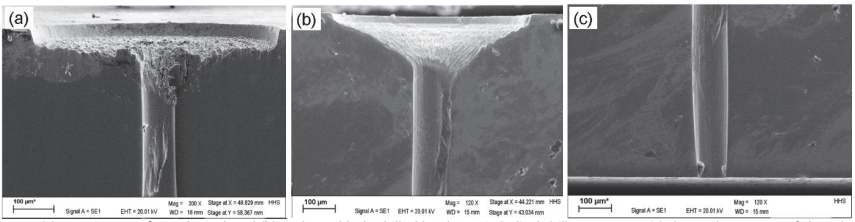


Fig. 90 (a) SEM image of a T-shaped and (b) Y-shaped hole drilled by dynamic helical drilling process, (c) the outlet section of the pilot hole in Y-shaped drilling

The T-shaped hole in Fig. 90(a) shows an inlet with uniform depth of about 80 µm and diameter about 600 µm. The single pulse energy applied in this area was increased from 6.25 µJ near the pilot hole to 18.75 µJ at the outer contour, so that more volume of material could be ablated at larger helical diameter. The microfunnel in Fig. 90 (b) exhibits a well-defined profile of truncated cone with a linear slope and a full opening angle of 126 degree. Compared to drilling results with unadapted energy deposition shown in Fig. 68(d), Fig. 90 (b) demonstrates a linear ablation behavior over the hole diameter. In more details of the adaption strategy, the increase of applied single pulse energy is a factor of 0.8 of in the T-shaped holes. The surface on the hole inlet has a fish-scale-like morphology and the root mean square roughness Rq = 2.43 µm is measured by laser scanning microscopy. Whereas the roughness on the lower pilot hole section at the outlet has a Rq < 0.35 µm. The smooth surface of the borehole is visible in Fig. 90(c). The distinction of surface quality of the shaped hole inlet and the lower section of pilot hole is very clear. The shaped inlet is fabricated by a helical ablation process in one to two repeats. The ablation rate is very high to achieve the depth of multiple tens of microns. In addition, the offset of neighboring helical paths at varied diameters is very fine: about a couple of hundred nanometers due to the high rotational speed of the Dove prism of 100 rps. Thus, the material vaporized by the laser radiation moves towards the neighboring finished area as a result of the recoil force from the material to be ablated in the following beam revolution. Another possible reason can be the projection of laser intensity on the tapered ablation front, and the reflection of the laser beam on the finished area impairs its surface quality. Metallurgical analysis is conducted after the chemical etching process on the shaped inlet as well as the transition part where dynamic helical drilling starts, as shown in Fig. 91. The investigation of the heat affected zone is to characterize the morphological changes in the surrounding drilled material.

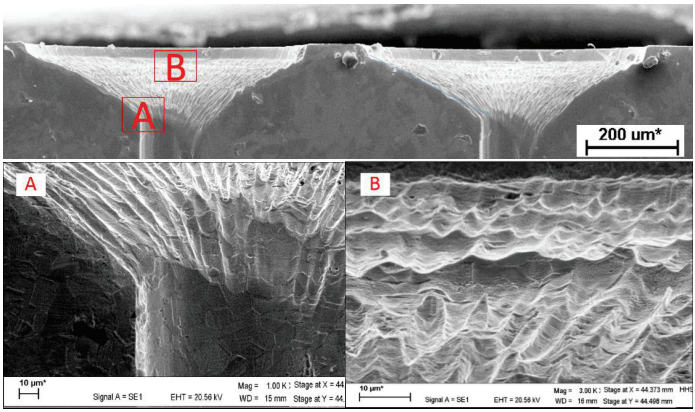


Fig. 91 Metallurgical analysis using SEM on walls of pilot holes and shaped inlets. The areas A and B are shown in higher magnification for detail.

The matrix of the stainless steel used shows the typical features of austenitic chromium-nickel steels in the form of polyhedral grain boundaries and twin boundaries [15]. If the material suffers thermal affect by heat accumulation, the properties such as grain size and phase of matrix change. The SEM images in Fig. 91 in a magnification of 1000 and 3000 times show that the polyhedral grain boundaries and twin boundaries still exist on the ablated surface. It gives evidence that no visible HAZ can be found on the hole wall and shaped inlet as shown in Fig. 91(a) and (b). The austenitic grains of the matrix have been precisely cut through by the laser at the transition into the drill channel. It should be emphasized that the matrix of the drill channels itself can be seen very clearly. Furthermore, no deposits are detectable. Therefore, the dynamic helical drilling process can be characterized as a clean, sublimation-dominated ablation process.

Enhancement of drilling efficiency and quality

In the classic helical drilling process, the vaporized or molten material by laser radiation must be driven out from the inlet of the borehole before the hole is drilled through. As a result, a part of the mixture of vapors and molten material deposit at the entrance and the recast is formed around the entrance. As soon as a through hole is formed, the fluidic dynamic of the molten material changes. Most of it can be driven out from the exit. The recast at the entrance impairs quality of the drilling, especially the optical quality of transparent materials. Fig. 92 shows the drilling results in 500µm thick fused silica with three different processes. The hole with a number of recast layers at the hole entrance shown in Fig. 92(a) is fabricated by the classic helical drilling process with a fixed helical diameter of 170 µm. Even after the sample is bathed in ultrasonic cleaner for two minutes, the hierarchy of the recast layers is very clear to be seen. The width of these layers reaches nearly 100 µmin the radial direction, and the height

approximately 8 µm as the LSM analysis shows in Fig. 92(d). By employing the dynamic helical drilling process (Fig. 92(b) and (d)), no recast layer can be observed. The entrance is well-defined and has a sharp edge. Similarly, the helical contour cutting can fabricate the borehole with negligible recast layers as shown in Fig. 92(c) and (f).

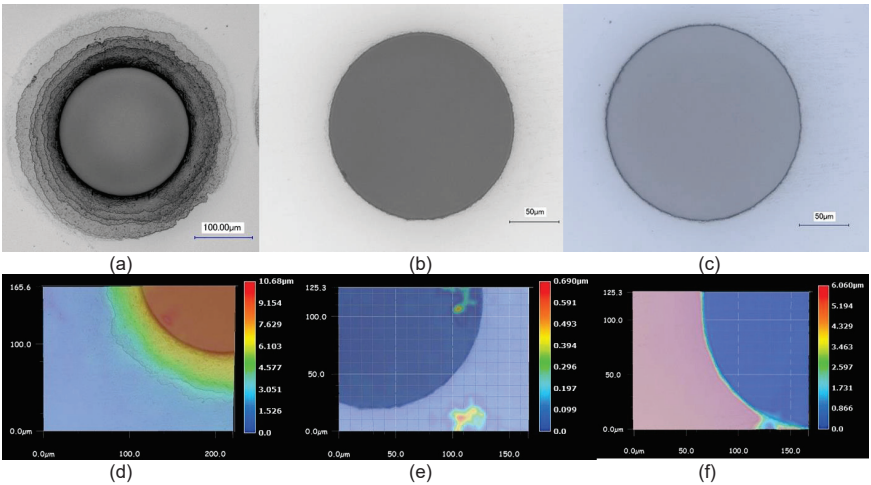


Fig. 92 Comparison of the drilling quality and height of recast layers in fused silica using (a and d) classic helical drilling, (b and e) dynamic helical drilling) and (c and f) helical contour cutting

Processing parameter: single pulse energy: 150 µJ, pulse repetition rate: 200 kHz, parallel offset: -3 mm, focal position z = 0, gas pressure: 2 bar, rotational speed of the Dove prism: 60 rps. For classic helical drilling process: rotation speed of wedge prism: 4°/s. For helical contour cutting: feed rate: 0.4 mm/s, 2 repeats.

During the classic helical drilling process, the molten materials are ejected from the drilling channel and deposit at the entrance. The recast layer is formed as a consequence of the solidification of the molten fused silica. As the ablation front moves deeper in the drilling channel, the range of the spattering of the molten fused silica decreases. Moreover, the recast layers are deposited near the hole entrance and forms a lamination structure, which leads to an increase in height. The height and width of the recast layers at the entrance of the borehole made by classic helical drilling and dynamic helical drilling are characterized by laser scanning microscopy and depicted in Fig. 93. Apparently, the classic helical drilling process produces much more recast volume than the dynamic helical drilling process. The height and width of recast layers both reach the maximum in the classic helical drilling of a hole diameter of 200 µm. With the further increase of the hole diameter, both the height and the width of the recast layer drop and become stable with an insignificant fluctuation. The recast layer

produced in the dynamic helical drilling process can be neglected at drilling with a diameter smaller than 1 mm. Despite that, the recast layer is about 20 µm wide along the radial direction of the hole entrance having a diameter of 1 mm. The average height is less than 3 µm, which is about one third of the recast layer in classic helical drilling. In the fabrication of hole diameters greater than 1 mm, increasing width of the recast layer will be produced as can be seen in Fig. 93(b).

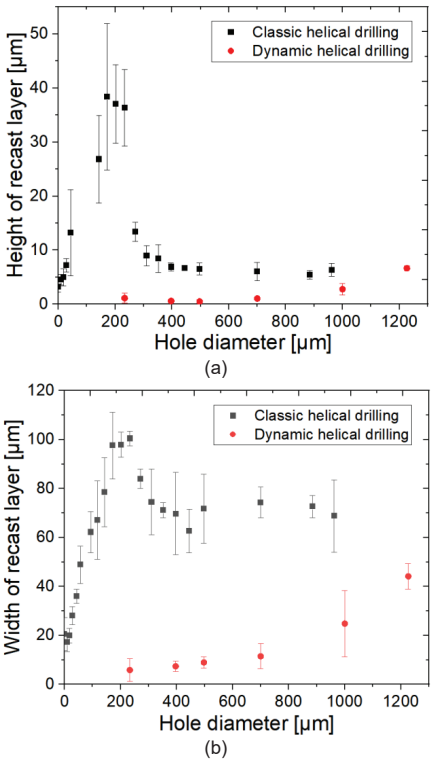


Fig. 93 Comparison of the drilling quality by the classic helical process and dynamic helical process.in aspect of (a) height of the recast layer and (b) width of the recast layer

The dynamic of the molten material by the laser radiation is one of the ways to explain the difference. In the processes of the dynamic helical drilling and helical contour cutting, an initial hole is drilled within one second due to higher concentrated laser energy at a small helical radius. With the relative movement of laser beam to the workpiece, a cutting front is formed with a dynamic direction in the xy plane. Molten material in the volume irradiated by laser pulses

will be driven out from the exit of cutting kerf with assistance of the processing gas (3 bar).

Furthermore, the thermal accumulation during the drilling processes is the other reason for the formation of the recast layer. The laser pulse energy absorbed by material can be divided into different parts: the ablation energy for material evaporation and kinetic and thermal energy in the vapor, and the residual heat [Ba15]. With greater density of laser pulses in ablation area, the deposited residual heat does not fully dissipate, accumulates and heats the base material; finally, a certain amount of residual heat attributes to ablation. In this case, the efficiency of ablation energy is greater than that in a larger helical diameter and lower overlapping degree. It can also explain why the ablation rate is higher at the smaller helical diameter than at the larger helical diameter. The ablation in the classic helical drilling with a helical diameter of 200 µm produces a large number of recasts due to a large amount of local thermal accumulation

The adaption of the dynamic of the molten material in the dynamic helical drilling process and the helical contour cutting process not only contributes to reducing of recast layer volume, but also enhances the drilling efficiency. The classic helical drilling as a static process is more efficient in fabricating microholes with diameters smaller than about 170 µm, as shown in Fig. 94. However, the increase in hole diameter demands a longer drilling time and more laser pulses by the classic helical drilling than the dynamic helical drilling processes. The fabrication of a 1 mm diameter hole requires approximately 60 seconds. Due to that the molten material is fast driven out from the pilot hole, the drilling time for the larger hole diameter is significantly reduced to between 15 seconds and 20 seconds by means of dynamic helical drilling and helical contour cutting process.

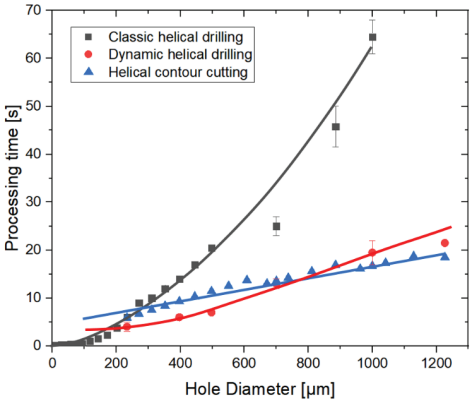
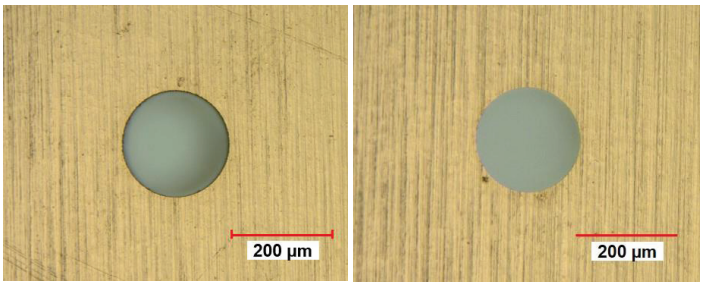


Fig. 94 Comparison of the drilling efficiency by the classic helical process, dynamic helical process and helical contour cutting of fused silica

Fittings of processing time over different hole diameters are done to show the development of processing efficiency by different helical processes. For classic and dynamic helical drilling, a polynomial fitting is applied. For the helical contour cutting a linear fitting is used since the processing time is linear to the perimeter of the hole. The fitted lines divide the hole diameter into three zones and indicate the most efficient drilling process in each zone. For the microhole having a diameter smaller than 170 µm, the classic helical drilling process should be chosen. For diameter between 170 µm and ca. 800 µm, the processing efficiency as well as the drilling quality can be enhanced by employing dynamic helical drilling. The helical contour cutting has the advantage over the other helical processes in fabrication holes with diameter larger than 800 µm.

The quality enhancement from the dynamic helical drilling process is applicable to the processing of metallic material as well. The drilling results shown in Fig. 95 exhibit recast-free borehole entrances without cleaning. No particles produced by the laser ablation can be detected at the entrance. Both entrance and exit show sharp edges and a circularity > 0.98 by microscopic inspection. This process is suitable for applications where post-processing for cleaning must be avoided.



(a) (b)

Fig. 95 Dynamic helical drilling in 0.3 mm thick stainless steel shows equivalent quality as in fused silica with a negligible recast layer. (a) hole entrance, (b) hole exit. Sample without cleaning

6.5 Summary

The main purposes of adapting the laser energy deposition in the classic helical drilling as well as dynamic helical drilling processes are generating microholes with higher precision, aspect ratio and complexity.

In the classic helical drilling process, the core idea for the adaption of energy is the optimization of the correlation between the 3D helical path and iso-intensity distribution of the laser beam. Based on that, strategies using multiple steps and continuously shifting of the laser focus in the depth direction are developed and adopted. The aspect ratio can be improved from 10:1 to 20:1. Meanwhile the cylindricity of holes has been significantly improved.

In the dynamic helical drilling process, the single pulse energy, increasing rate of helical diameter, the pulse repetition rate and the rotational speed of laser beam are the main factors that influence the hole profile. The number of pulses deposited on one position is a characteristic number in the dynamic helical drilling process and is directly linked to the ablation depth at different locations on the helical path. By building a reduced model based on the experiments data, a roadmap of the adaption of energy deposition can be drawn for the fabrication of designated hole profiles. The adaption of the single pulse energy over different helical diameter is the most direct and practical method. A micro hole with T-shaped profile at the entrance is achieved and demonstrated. In addition, the adaption of the local drilling duration and the pulse repetition rate have been proved to be feasible, too.

By taking advantage of the dynamic helical drilling process, the performance of the available helical optics can be improved. First of all, the maximal achievable positive opening angle by using classic helical drilling can be extended. Moreover, holes with more complex profiles such as microfunnels or de Laval nozzles can be fabricated owing to the flexible adaption of laser energy deposition as the hole entrance forms. Last but not least, by adapting the dynamic of molten material in the drilling channel, the drilling speed for hole diameter > 170 µm can be increased by means of dynamic helical drilling and helical contour cutting. Meanwhile, the drilling quality with respect to recast layer can be significantly enhanced.

7 Conclusion and outlook

Microholes in steel, glass, and ceramics find applications as spinning nozzles, injector nozzles, injectors, or venting holes. Soon, such precision holes will also be used in sensor and filter technology. The helical drilling technology together with ultrashort pulsed lasers is an established process for the fabrication of the high-precision microholes, now after it has been under development for more than a decade. In comparison with other laser drilling technologies, the helical drilling process has the following advantages: First of all, it offers higher precision in the hole geometry through the layer-by-layer ablation strategy and the helical movement of the laser pulses. Moreover, the helical drilling technology demonstrates a greater controllability and flexibility in fabricating microholes with different diameters and conicities. In addition, the helical drilling technology is able to shape the hole profile, enabling the fabrication of more complex microholes.

The helical drilling optics based on the rotating Dove prism is characterized by the doubled rotating speed of output laser beam to the Dove prism itself. The Dove prism works as an image rotator and is the core component in the helical drilling optics. The wedge prism in front of the Dove prism can change the tilt angle of the incident laser beam by deflecting it in a fixed angle. By means of that the helical diameter can be controlled. Additionally, an optical table on a linear stage enables a parallel offset of the incident laser beam to the Dove prism. By means of that, the tilt angle of the incident laser beam prior to the focusing lens can be adjusted. This tiled angle is directly relevant to the hole taper, i.e. the hole conicity. By using an ultrashort pulsed laser with maximum single energy 150 µJ and a focal length of 60 mm, a maximum positive opening angle of 15° and negative angle of -6.6° can be achieved by the classic helical drilling process.

The helical path describes the spatial trajectory of laser pulses deposited during the helical processing and plays a vital role in all of the helical drilling processes. It is regulated by the tilt angle and the parallel offset. The 2D helical path in classic helical drilling is a circle, whereas a 3D helical path can be a spiral in the form of a cylinder, negative or positive cone. The classic helical drilling is the process mostly commonly employed to fabricate 2/2.5 dimensional holes, where the helical path as well as the processing parameters are unaltered. The helical trepanning process and helical contour cutting are categorized as dynamic helical processes. In dynamic helical drilling, the helical diameter or focal position to workpiece varies. The helical contour cutting process can be applied to fabricate round holes and can be understood as a classic laser cutting process with a wobbling laser beam. Based on the visualization of the 3D helical path, a process for a designated hole geometry can be simplified. The visualized helical path

works as a road map and indicates how the final hole geometry should roughly look like. Nevertheless, the final hole geometry is the result of combined action of the helical path and the energy deposition on the helical path.

The energy deposition in the helical drilling process can be quantified by the superposed laser intensity on the helical path. It is determined by the parameters of laser pulses and the helical optics. The laser parameters determine the peak laser fluence calculated by the single pulse energy and laser spot diameter, temporal interval between pulses (pulse repetition rate) and the number of total pulses (drilling time) for the helical drilling processes. The rotational speed of the Dove prism has an influence on the pulse-to-pulse overlap. In this work the influence of local superposed laser intensity on hole profile were investigated by a numeric simulation on the laser pulse energy and the increasing speed of helical diameter. The experimental results are in good agreement with that of the simulation and demonstrate how the energy deposition determines ablation depth and hole profile.

A reduced model for dynamic helical ablation was built by investigating the development of ablation depth at varying processing parameters over the whole helical diameter. The single pulse energy, the drilling time, and the pulse repetition rate are in principle the parameters available for the adaption of energy deposition. Other possible strategies such as adaption of the focal position of laser beam relative to the workpiece and the rotational speed of laser beam are theoretically feasible as well. Based on the reduced model of the helical ablation, the laser energy deposition can be adapted for the fabrication of designated hole profile by the spatial and temporal synchronization of the laser pulsed energy. A multidimensional borehole with a flat enlarged hole entrance having a depth of 80 µm can be fabricated by means of adaption of laser pulse energy.

By taking advantage of the dynamic helical drilling process with adapted energy deposition, the performance of the present helical optics can be enhanced. Firstly, the limitations such as the maximal achievable positive opening angle by using classic helical drilling can be extended. Moreover, holes with more complex profiles such as microfunnels and de Laval nozzles can be fabricated thanks to the flexible adaption of laser energy deposition while hole entrance forms. The development of the hole complexity within this work is shown in Fig. 96. The classic helical drilling process has improved the drilling dimension and precision of the laser percussion process. The hole complexity is further increased by means of dynamic helical drilling. As a perspective, irregular holes, which exhibit even higher complexity, can be fabricated by integrating a high-frequency optical deflector in front of the Dove prism. Last but not least, by adapting the dynamic of molten material in the drilling channel, the drilling speed for hole diameter > 170 µm can be increased by means of dynamic helical drilling and helical contour cutting. The advantage is even more obvious at greater hole diameters. To drill a 1-mm-diameter hole, the dynamic helical drilling process need merely

1/4 to 1/3 the time of classic helical drilling. Meanwhile, the recast layer around the hole entrance can be effectively avoided due to the fluid dynamics of the molten material in the dynamic helical drilling process. The height of recast layer is below 5 µm and the width is about 2% of hole diameter.

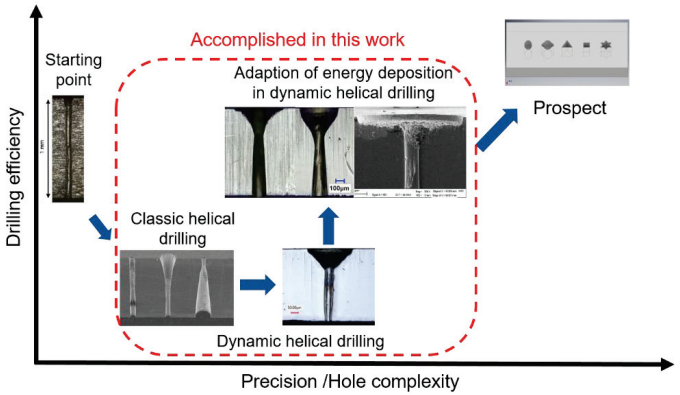


Fig. 96 Development of the achievable hole complexity using Dove-prism-based helical drilling optics and ps ultrashort pulsed lasers.

The morphological analysis with SEM on the helical-drilled hole wall shows a sublimation-dominated and recast-free ablation process with a negligible heat affected zone by taking advantage of the ultrashort pulsed laser. The matrix and grain size remain on the hole wall after drilling process. The typical average roughness of the helical drilling is in the submicron regime. In future work, investigations should be done on improving the surface roughness and homogeneity of the shaped entrance.

Currently, two of the main challenges of the current helical drilling technology are enhancing the drilling efficiency and increasing the hole aspect ratio. The trade-off of drilling precision and efficiency still exists since the requirements increase continuously. However, the efficiency or productivity has been significantly improved owing to the process development of helical drilling as well as the rapid development of the laser source technology. Ultrashort pulsed lasers with high single pulse energy of more than 650 µJ in second harmonic generation (SHG) have been available for a couple of years. They enable even higher laser fluence and, thus, a faster ablation in the helical drilling process. This contributes to enhancing the efficiency not only in the drilling of greater hole diameters, but also of thicker material. A promising technology for upscaling the process efficiency is a multi-beam technology using such as a diffractive optical element (DOE), which has proved to be feasible in the helical drilling process [Gi19]. The laser beam can be split into many identical parallel sub-beams,

making it possible to use the laser pulse energy to full capacity. Therefore, the productivity of the helical drilling process can be up-scaled correspondingly.

The other issue in the further development of the helical drilling process is the increase of the hole aspect ratio. High-aspect-ratio microholes have wide applications, such as venting holes for injection molds. The achievement of the aspect ratios in stainless steel is shown in Fig. 97.

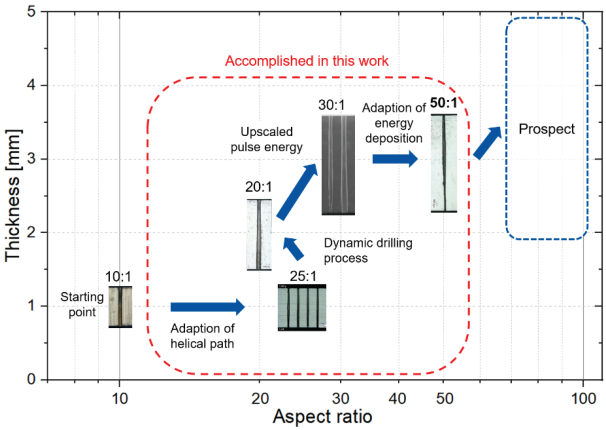


Fig. 97 Development of the achievable aspect ratio using Dove-prism-based helical drilling optics and ps ultrashort pulsed lasers.

By adapting the helical path in the classic helical drilling, the aspect ratio can be increased from 10:1 to about 25:1 in 1 mm thick stainless steel. And the aspect of 20:1 can be achieved in 2 mm thick stainless steel by the dynamic helical drilling process. The helical drilling optics make it possible to control the multiple reflection behavior along the borehole, which is an important phenomenon in the fabrication of high aspect-ratio holes. The high pulse energy of an ultrashort pulse laser is another key factor in achieving a cylindrical microhole with a high aspect ratio. The aspect ratio of 50:1 in 3 mm stainless was achieved in this research work by using the up-scaled laser single pulse energy and the adaption of the laser energy deposition. The development of laser single pulse energy is considered to be the most effective way to further increase the aspect ratio of microholes. Moreover, the manipulation of the modes or forms of output laser pulses has the potential to improve the heat accumulation and the behavior of ignited plasma in the drilling channel, thus minimizing the hole diameter and increasing the hole aspect ratio. Optical elements such as axicon prisms, multi-foci DOE as well as elongated focus DOE have been applied in the processing of transparent materials to elongate the working distance of the focused laser beam. The spatially modulated focused beam has a comparable spot size; however, the effective working distance can be extended up to ten times [Ho20].

This type of spatial light modulator has an enormous potential to increase the hole aspect ratio made with the helical drilling process.

Further investigations are still to be carried out in order to explain two phenomena in the investigation of the influential parameters on hole geometry. The first one is the widening of hole diameter under higher process gas pressure. The characterization of the effect of plasma in the drilling process is necessary. The other one phenomenon is the formation of striation on the hole wall near the exit by using nitrogen as process gas. The influence of nitridation as well as the behavior of the molten materials should be further studied by, for example, observing the dynamics using a high speed camera.

As a final remark, the simulation and modeling based on the more complete experiments can be used as a tool to optimize the helical drilling processes. The influence of the process parameters is predictable according to asymptotic modeling. By giving the boundary conditions, the process parameter window can be identified. Even the simulated results with the currently unavailable conditions, such as pulse energy of a second harmonic generation USP laser in tens of millijoules, are possible.

Bibliography

[Ae19] Aerotech Inc.: AGV5D Five-Axis Laser Micromachining Precession Scanner. https://www.aerotech.com/product-catalog/laser-scan-heads/agv5d.aspx.

[AM19] AMPHOS GmbH: Amphos5000 Series: High power ultrafast lasers for scientific applications. https://www.amphos.de/products/amphos5000/.

[An08] Ancona, A. et al.: High speed laser drilling of metals using a high repetition rate, high average power ultrafast fiber CPA system. In Optics express, 2008, 16; pp. 8958–8968.

[An09] Ancona, A. et al.: Femtosecond and picosecond laser drilling of metals at high repetition rates and average powers. In Optics letters, 2009, 34; pp. 3304–3306.

[AR18a] ARGES GmbH: Industry-proven scan heads with between 5 and 8 axes for high-precision drilling and cutting applications. https://www.arges.de/industrial-products/precession/.

[AR18b] ARGES GmbH: Compact scan head for micro drilling and cutting. KOALA.

[As11] Ashkenasi, D. et al.: Laser trepanning for industrial applications. In Physics Procedia, 2011, 12; pp. 323–331.

[Au16] Auerswald, J. et al.: Taper Angle Correction in Cutting of Complex Micro-mechanical Contours with Ultra-Short Pulse Laser. In Journal of Mechanics Engineering and Automation, 2016, 6.

[Ba00] Baeuerle, D.: Laser Processing and Chemistry Springer Verlag. In Heidelberg Berlin, 2000, 13.

[BA05] BARGEL, H.-J.: Werkstoffkunde. Mit 85 Tabellen. Springer, Berlin, 2005.

[Ba15] Bauer, F. et al.: Heat accumulation in ultra-short pulsed scanning laser ablation of metals. In Optics express, 2015, 23; pp. 1035–1043.

[BE03] BERNARDO, A. et al.: High-intensity ultrashort laser-induced ablation of stainless steel foil targets in the presence of ambient gas. In Laser and Particle Beams, 2003, 21; pp. 59–64.

[Be11] Beck, T.: Laser drilling in gas turbine blades: Shaping of holes in ceramic and metallic coatings. In Laser Technik Journal, 2011, 8; pp. 40–43.

[Bh13] Bharatish, A. et al.: Characterization of hole circularity and heat affected zone in pulsed CO2 laser drilling of alumina ceramics. In Optics & Laser Technology, 2013, 53; pp. 22–32.

[Bi03] Binder, A. et al.: High-quality laser microdrilling of metals and ceramics with maximum aspect ratio. In Proceedings of SPIE - The International Society for Optical Engineering, 2003, 4977; pp. 295–305.

[BMB13] BLIEDTNER, J.; MÜLLER, H.; BARZ, A.: Lasermaterialbearbeitung: Grundlagen-Verfahren-Anwendungen-Beispiele. Carl Hanser Verlag GmbH Co KG, 2013.

[Br10] Breitling, D.: Gasphaseneinflüsse beim Abtragen und Bohren mit ultrakurz gepulster Laserstrahlung. Herbert Utz Verlag, München, 2010; p. 139.

[BRD04] Breitling, D.; Ruf, A.; Dausinger, F. Eds.: Fundamental aspects in machining of metals with short and ultrashort laser pulses. International Society for Optics and Photonics, 2004.

[BWE08] Brajdic, M.; Walther, K.; Eppelt, U.: Analysis of laser drilled deep holes in stainless steel by superposed pulsed Nd:YAG laser radiation. In Optics and Lasers in Engineering, 2008, 46; pp. 648–655.

[Ca16] Canon USA, Inc. Optoelectronic Components: 5 Axis Micro Drilling Scanhead. https://www.photonicsonline.com/doc/5-axis-micro-drilling-scanhead-0001.

[Ch09] Cheng, J. et al.: Single-pulse drilling study on Au, Al and Ti alloy by using a picosecond laser. In Applied Physics A, 2009, 95; pp. 739–746.

[Ch96] Chichkov, B. N. et al.: Femtosecond, picosecond and nanosecond laser ablation of solids. In Applied Physics A, 1996, 63; pp. 109–115.

[Da03] Dausinger, F. Ed.: Femtosecond technology for precision manufacturing: Fundamental and technical aspects. International Society for Optics and Photonics, 2003.

[Da17] Davim, J.P. Ed.: Microfabrication and Precision Engineering. Research and Development. Woodhead Publishing, 2017; p. 18.

[Dö13] Döring, S. et al.: Influence of ambient pressure on the hole formation in laser deep drilling. In Applied Physics A, 2013, 112; pp. 623–629.

[Dü08] Dürr, U.: Laser drilling in industrial use. In Laser Technik Journal, 2008, 5; pp. 57–59.

[Du16] Duan, W. et al.: Effect of temporally modulated pulse on reducing recast layer in laser drilling. In The International Journal of Advanced Manufacturing Technology, 2016, 87.

[Ei15] Eifel, S.: Effizienz-und Qualitätssteigerung bei der Lasermikrobearbeitung mit UKP-Lasern durch neue optische Systemtechnik. Apprimus Verlag, Aachen, 2015.

[FD03] Föhl, C.; Dausinger, F. Eds.: High precision deep drilling with ultrashort pulses. International Society for Optics and Photonics, 2003.

[Fi17] Finger, J.-T.: Puls-zu-Puls-Wechselwirkungen beim Ultrakurzpuls-Laserabtrag mit hohen Repetitionsraten. Apprimus Verlag, Aachen, 2017; pp. 70-76.

[Fo07] Forsman, A. C. et al.: SUPERPULSE®: A NANOSECOND PULSE FORMAT FOR IMPROVING LASER DRILLING. San Diego: General Atomics Report GA–A25867, 2007.

[Fö18] Förster, D. J. et al.: Estimation of the depth limit for percussion drilling with picosecond laser pulses. In Optics express, 2018, 26; pp. 11546–11552.

[FR14] Finger, J.; Reininghaus, M.: Effect of pulse to pulse interactions on ultra-short pulse laser drilling of steel with repetition rates up to 10 MHz. In Optics express, 2014, 22; pp. 18790–18799.

[Fr19] Fraunhofer-Gesellschaft: Fraunhofer Cluster of Excellence Advanced Photon Sources CAPS. https://www.fraunhofer.de/en/institutes/institutes-and-research-establishments-in-germany/cluster-of-excellence/advanced-photon-sources.html.

[FRR16] Franco, A.; Rashed, C. A. A.; Romoli, L.: Analysis of energy consumption in micro-drilling processes. In Journal of Cleaner Production, 2016, 137; pp. 1260–1269.

[Fü17] Führa, B. et al. Eds.: High precision drilling with ultra-short laser pulses, 2017.

[GF18] GFH GmbH: GL Trepan. https://gfh-gmbh.de/en/machine-building/configuration/hardware/gl-trepan.

[Gi19] Gillner, A. et al.: High Power Laser Processing with Ultrafast and Multi-Parallel Beams. In Journal of Laser Micro/Nanoengineering, 2019, 14; pp. 129–137.

[Go15] Goya, S. et al.: High-Speed & High-Quality Laser Drilling Technology Using a Prism Rotator,Mitsubishi Heavy Industries Technical Review Vol.52 No.1(2015). In Mitsubishi Heavy Industries Technical Review, 2015, 2015; pp. 106–109.

[GSL16] Gruner, A.; Schille, J.; Loeschner, U.: Experimental Study on Micro Hole Drilling Using Ultrashort Pulse Laser Radiation. In Physics Procedia, 2016, 83; pp. 157–166.

[Ha14] Hartmann, C.: Laserabtrag mit zeitlicher Modulation der Energiedeposition. Apprimus Verlag, Aachen, 2014.

[Ha18a] Hammers-Weber, P.: Flexible microdrilling for test electronics. In microPODUCTION, 2018, 1; pp. 14–18.

[Ha18b] Hambach, N.: Grenzen der Lochdichte beim Perkussionsbohren mit Ultrakurzpulslasern. Apprimus Verlag, Aachen, 2018; p. 112.

[HBG18] He, C.; Bühring, J.; Gillner, A.: Helical drilling of three-dimensional conical converging-diverging nozzle in steel using ultrashort laser pulses. In Procedia CIRP, 2018, 74; pp. 305–309.

[HG09] Hügel, H.; Graf, T.: Laser in der Fertigung. Springer, 2009.

[Ho20] Holo/Or Ltd: Elongated Focus. https://www.holoor.co.il/product/elongated-focus/.

[Ja11] Jaeggi, B. et al.: Influence of the Pulse Duration in the ps-Regime on the Ablation Efficiency of Metals. In Physics Procedia, 2011, 12.

[JKS13] Jui, S. K.; Kamaraj, A. B.; Sundaram, M. M.: High aspect ratio micromachining of glass by electrochemical discharge machining (ECDM). In Journal of Manufacturing Processes, 2013, 15; pp. 460–466.

[Jo08] Joint Committee for Guides in Metrology-JCGM: JCGM 200: 2008. International vocabulary of metrology: basic and general concepts and associated terms (VIM). Working Group 2, France, 2008.

[Ka03] Kamlage, G. et al.: Deep drilling of metals by femtosecond laser pulses. In Applied Physics A, 2003, 77; pp. 307–310.

[Kl14] Klocke, F. et al.: Turbomachinery component manufacture by application of electrochemical, electro-physical and photonic processes. In CIRP Annals-Manufacturing Technology, 2014, 63; pp. 703–726.

[KMG18] Kroschel, A.; Michalkowski, A.; Graf, T.: Model of the final borehole geometry for helical laser drilling. In Advanced Optical Technologies, 2018, 7; pp. 183–188.

[Kn10] Knorz, A. et al. Eds.: High speed laser drilling: parameter evaluation and characterisation, 2010.

[Ko11] Koch, J. et al.: Laserendbearbeitung metallischer Werkstoffe. Zugl.: Ilmenau, Techn. Univ., Diss., 2010. Univ.-Bibliothek; Univ.-Verl. Ilmenau, Ilmenau, 2011; p. 105.

[Ko99] Kononenko, T. V. et al.: Comparative study of the ablation of materials by femtosecond and pico-or nanosecond laser pulses. In Quantum electronics, 1999, 29; p. 724.

[KS99] Kuehnle, G.; Streibl, N.: Optische Vorrichtung zum Bohren mittels Laserstrahls, 1999.

[Ku14] Kuang, Z. et al.: Ultrafast laser parallel microdrilling using multiple annular beams generated by a spatial light modulator. In Journal of Physics D Applied Physics, 2014, 47; p. 115501.

[La16] Lasea: LS-Precess: Precession module. https://www.lasea.eu/en/oem/ls-precess/.

[Li18] Liu, Z. et al.: Manufacturing of hourglass-shaped through holes with varying diameters at different depths by dual-pulse laser drilling and laser-induced plasma-hole interaction. In Manufacturing Letters, 2018, 16; pp. 18–22.

[Lo09] Louwerse, M. C. et al.: Nozzle fabrication for micropropulsion of a microsatellite. In Journal of Micromechanics and Microengineering, 2009, 19; p. 45008.

[Ma99] Marshall, G. F.: Risley prism scan patterns. In (Beiser, L.; Sagan, S. F.; Marshall, G. F. Eds.): Optical Scanning: Design and Application. SPIE, 1999; pp. 74–86.

[MB18] Michel, S.; Biermann, D.: Analysis of the laser drilling process for pilot holes in complex shaped components. In Procedia CIRP, 2018, 74; pp. 398–402.

[Me12] Mezzapesa, F. et al.: Laser ablation dynamics in metals: The thermal regime. In Applied Physics Letters, 2012, 101.

[MFP04] McNally, C. A.; Folkes, J.; Pashby, I. R.: Laser drilling of cooling holes in aeroengines: State of the art and future challenges. In Materials Science and Technology, 2004, 20; pp. 805–813.

[MG14] Michalowski, A.; Graf, T.: Untersuchungen zur Mikrobearbeitung von Stahl mit ultrakurzen Laserpulsen. DoctoralThesis. Herbert Utz Verlag, München, 2014.

[MY15] Mishra, S.; Yadava, V.: Laser Beam MicroMachining (LBMM) - A review. In Optics and Lasers in Engineering, 2015, 73.

[Na18] Nasrollahi, V. et al.: Drilling of micron-scale high aspect ratio holes with ultra-short pulsed lasers: Critical effects of focusing lenses and fluence on the resulting holes' morphology. In Optics and Lasers in Engineering, 2018, 110; pp. 315–322.

[Ne10] Neuenschwander, B. et al.: Processing of metals and dielectric materials with ps-laserpulses: results, strategies, limitations and needs, 2010.

[Ne13] Negel, J.-P. et al.: 1.1 kW average output power from a thin-disk multipass amplifier for ultrashort laser pulses. In Optics letters, 2013, 38; pp. 5442–5445.

[Ne14] Neuenschwander, B. et al.: Surface structuring with ultra-short laser pulses: Basics, limitations and needs for high throughput. In Physics Procedia, 2014, 56; pp. 1047–1058.

[NG10] Nayak, B.; Gupta, M.: Self-organized micro/nano structures in metal surfaces by ultrafast laser irradiation. In Optics and Lasers in Engineering, 2010, 48; pp. 940–949.

[No97] Nolte, S. et al.: Ablation of metals by ultrashort laser pulses. In JOSA B, 1997, 14; pp. 2716–2722.

[No99] Nolte, S. et al.: Polarization effects in ultrashort-pulse laser drilling. In Applied Physics A, 1999, 68; pp. 563–567.

[NSD16] Nolte, S.; Schrempel, F.; Dausinger, F.: Ultrashort Pulse Laser Technology. Springer, Berlin, 2016; pp. 202-203.

[Ok10] Okasha, M. et al.: Laser drilling of nickel alloy: Effect of process gases on drilling time and hole quality. In International Congress on Applications of Lasers & Electro-Optics, 2010; pp. 127–136.

[ON10] Ohmura, E.; Noguchi, S.: Laser Drilling Simulation Considering Multiple Reflection of Laser, Evaporation and Melt Flow. In Advanced Structured Materials, 2010, 3.

[PN10] Park, K.-W.; Na, S.-J.: Theoretical investigations on multiple-reflection and Rayleigh absorption–emission–scattering effects in laser drilling. In Applied Surface Science, 2010, 256; pp. 2392–2399.

[Po05] Poprawe, R.: Lasertechnik für die Fertigung. Grundlagen, Perspektiven und Beispiele für den innovativen Ingenieur. Abtragen und Bohren. Springer, Berlin, 2005.

[Po08] Powell, J. et al.: Laser-oxygen cutting of mild steel: The thermodynamics of the oxidation reaction. In Journal of Physics D: Applied Physics, 2008, 42; p. 15504.

[Po11] Poprawe, R.: Tailored light 2. Laser Application Technology. Springer, Berlin, 2011; p. 521, 62, 349, 522, 388.

[PP18] Pattanayak, S.; Panda, S.: Laser Beam Micro Drilling – a Review. In Lasers in Manufacturing and Materials Processing, 2018, 5; pp. 366–394.

[Ra08] Raciukaitis, G. et al.: Accumulation effects in laser ablation of metals with high-repetition-rate lasers. SPIE, 2008.

[RFR16] Rahmani-Monfard, K.; Fathi, A.; Rabiee, S. M.: Three-dimensional laser drilling of polymethyl methacrylate (PMMA) scaffold used for bone regeneration. In The International Journal of Advanced Manufacturing Technology, 2016, 84; pp. 2649–2657.

[RRF14] Romoli, L.; Rashed, C. A.A.; Fiaschi, M.: Experimental characterization of the inner surface in micro-drilling of spray holes. A comparison between ultrashort pulsed laser and EDM. In Optics & Laser Technology, 2014, 56; pp. 35–42.

[Ru98] Rubenchik, A. M. et al.: Numerical simulation of ultra-short laser pulse energy deposition and bulk transport for material processing. In Applied Surface Science, 1998, 1998; pp. 193–198.

[RV16] Romoli, L.; Vallini, R.: Experimental study on the development of a micro-drilling cycle using ultrashort laser pulses. In Optics and Lasers in Engineering, 2016, 78; pp. 121–131.

[Sc18] Schmidt, M. et al.: Advances in macro-scale laser processing. In CIRP Annals, 2018, 67; pp. 719–742.

[Sm00] Smith, W. J.: Modern Optical Engineering 3rd Ed., Ch. 13. McGraw-Hill, Washington DC, 2000; pp. 106-107.

[SMP10] Sugioka, K.; Meunier, M.; Piqué, A.: Laser Precision Microfabrication. Springer, Berlin, 2010; p. 194, 99.

[SRA13] Schmidt, M.; Roth, S.; Amend, P. Eds.: Erzeugung arbiträrer Bohrungsgeometrien durch ein neuartiges Trepaniermodul, 2013.

[SS12] Saumweber, C.; Schulz, A.: Effect of geometry variations on the cooling performance of fan-shaped cooling holes. In Journal of Turbomachinery, 2012, 134; p. 61008.

[TH06] THYSSENKRUPP MATERIALS EUROPE GMBH: Stahlbezeichnung Nichtrostender Austenitischer Stahl TK 1.4301. http://www.cnc.at/media/pdf/material/Datenblatt_1-4301.pdf.

[Tr04] Trippe, L., Willach, J., Kreutz, E. W., Schulz, W., Petereit, J., Kaierle, S., & Poprawe, R. Ed.: Melt ejection during single-pulse drilling and percussion drilling of micro holes in stainless steel-and nickel-based superalloy by pulsed Nd: YAG laser radiation. International Society for Optics and Photonics, 2004.

[UFK16] Uchtmann, H.; Friedrichs, M.; Kelbassa, I.: Drilling of cooling holes by using high power ultrashort pulsed laser radiation, 2016, 2016.

[VD12] 32540:2012-08:08.2012, Laser beam removing – Thermal removing with laser beam – Terms and definitions, influence factors, procedure.

[Ve07] Verhoeven, J. D.: Steel metallurgy for the non-metallurgist. ASM International, Ohio, 2007; p. 204.

[Wa08] Wawers, W.: Präzisions-Wendelbohren mit Laserstrahlung. Shaker, Düren, 2008.

[Wa15] Watanabe. T. et al.: High speed and quality laser drilling technology by using prism rotating system. In Proceedings of LAMP2015 - the 7th International Congress on Laser Advanced Materials Processing, 2015.

[We08] Weck, A. et al.: Laser drilling of high aspect ratio holes in copper with femtosecond, picosecond and nanosecond pulses. In Applied Physics A, 2008, 90; pp. 537–543.

[We14] Weber, R. et al.: Heat accumulation during pulsed laser materials processing. In Optics express, 2014, 22; pp. 11312–11324.

[WG09] Wawers, W.; Gillner, A.: Device for drilling and for removing material using a laser beam, 2009.

[WRH16] Wlodarczyk, K.; Rumsby, P.; Hand, D.: Picosecond laser cutting and drilling of thin flex glass. In Optics and Lasers in Engineering, 2016, 78; pp. 64–74.

[WZZ11] Wu, Z.; Zhu, X.; Zhang, N.: Time-resolved shadowgraphic study of femtosecond laser ablation of aluminum under different ambient air pressures. In Journal of Applied Physics, 2011, 109; p. 53113.

[Ya12] Yan, Y. et al.: An experimental and numerical study on laser percussion drilling of thick-section alumina. In Journal of Materials Processing Technology, 2012, 212; pp. 1257–1270.

[Zi15] Zibner, F. et al.: 1µm adjustment-tolerance for high-precision helical laser drilling. In Proc. SPIE, 2015, 9582; 95820C-1-11.

[ZLK06] Zeng, D.; Latham, W. P.; Kar, A.: Shaping of annular laser intensity profiles and their thermal effects for optical trepanning. In Optical Engineering, 2006, 45; p. 14301.

Appendix

Matlab code for calculation of the superposed laser intensity in classic helical drilling:

```
%Superposed Laser Intensity distribution in helical drilling with
fixed helical radius
clc
clear all
%Laser parameters
lambda=0.515e-3;          %Laser wavelength, Unit: mm
tp=7e-12;                 %Laser pulse duration, Unit: seconds
m_sqr=1.2;                %M square of laser beam
lf_m=400000;              %Max. laser output frequency, Unit: Hz
E_p=150e-6;               %Max. laser pulse energy, Unit: Joules
w0=10e-3;                 %Effective laser focal spot radius (f=60
mm),Unit: mm
P_a=60;                   %Max. averange laser power, Unit: Watts
zr=pi*w0^2/(lambda*m_sqr);       %Reighley length of laser beam,
Unit: mm

%Applied laser parameters
P_percent=0.8;          %Applied percentage of output laser single
pulse energy
divider=10;               %Divider of laser output pulse
lf=lf_m/divider;          %Applied laser frequency, Unit: Hz
E_ap=E_p*P_percent;       %Applied laser pulse energy, Unit: Joules
lp=P_a*P_percent*(lf/lf_m);%Applied laser power, Unit: Watts
P_peak=P_percent*(E_p/tp);%Output laser peek power, Unit: Watts
tb=0.1;                    %Drilling time, Unit: seconds
z=0;                      %z position
wz=w0*sqrt(1+(z/zr).^2); %Spot diameter in z position, Unit: mm
Iz=P_peak/(pi*(wz/10)^2);%Intensity of laser beam at z position,
Unit: Watts/cm^2
rh0=0.096;                %Helical radius at wedge prism 0 degree
rho=0.15;                %size of x-y axis
n_motor=60;               %Mechanical rotation speed of motor, Unit:
round per second
nr=2*n_motor;             %Optical rotation speed, Unit: round per
second
ni=nr*tb;                     %Number of revolutions at a certain
helical radius,optical rotation speed by drilling time
```

```
thi=2*pi*nr/lf;          % Angle interval of two laser spots in a
round
overl=1-((2*pi*rh0*nr/lf)./(2*wz+2*pi*rh0*tp));%Overlapping rate in a
circle at rh1

x=linspace(-rho,rho,401);%Scale of x
y=linspace(-rho,rho,401);%Scale of y
[px,py]=meshgrid(x,y);%meshgrid

%Superpose of Inteisity rh0
Ibeam=0;
for ti=0:1/lf:tb;
x0=rh0.*cos(2*pi*nr.*ti);
y0=rh0.*sin(2*pi*nr.*ti);
Ibeam0_1=Iz*(w0/wz).^2*exp(-2*((px-x0).^2)./(wz.^2)).*exp(-2*((py-
y0).^2)./(wz.^2));
Ibeam=Ibeam+Ibeam0_1;
end

surf(px,py,Ibeam);
shading interp;
xlabel('x /mm','fontsize',16);
ylabel('y /mm','fontsize',16);
zlabel('Laser Intensity/W/cm^{2}','fontsize',16);
title('Superposed Laser Intensity in Classic Helical
drilling','fontsize',20);
colorbar
colormap('jet');
set(gcf, 'renderer', 'zbuffer')
opengl software;
box off;
grid on;
```

Matlab code for calculation of the superposed laser intensity in dynamic helical drilling:

```
%Sperposed Laser Intensity Distribution in helical trpanning with
varied rotating speed of wedge prism
clc
clear all
% General laser parameters
lambda=0.515e-3;          %Laser wavelength, Unit: mm
tp=1e-12;                 %Laser pulse duration, Unit: seconds
m_sqr=1.2;                %M square of laser beam
lf_m=600000;              %Max. laser output frequency, Unit: Hz
E_p=125e-6;               %Max. laser pulse energy, Unit: Joules
w0=10e-3;                 %Effective laser focal spot radius (f=60
mm),Unit: mm
P_a=75;                   %Max. averange laser power, Unit: Watts
zr=pi*w0^2/(lambda*m_sqr);       %Reighley length of laser beam,
Unit: mm

%Parameters of helical trepanning
%Applied laser parameters
P_percent_t=0.1;          %Applied percentage of output laser single
pulse energy in helical trepanning
divider_t=15;             %Divider of laser output pulse
lf_t=lf_m/divider_t;        %Applied laser frequency, Unit: Hz
E_ap_t=E_p*P_percent_t;     %Applied laser pulse energy, Unit:
Joules
lp=P_a*P_percent_t/divider_t;%Applied laser power, Unit: Watts
P_peak_t=P_percent_t*(E_p/tp);%Output laser peek power, Unit: Watts
z_t=0;                    %z position
wz_t=w0*sqrt(1+(z_t/zr).^2); %Spot diameter in z position, Unit: mm
Iz_t=P_peak_t/(pi*(wz_t/10)^2);%Intensity of laser beam at z
position, Unit: Watts/cm^2

% Mechanical parameters setting
n_motor=60;          %Mechanical rotation speed of motor, Unit: round
per second
nr=2*n_motor;        %Optical rotation speed, Unit: round per second
v_wedge_1=1;              %Rotation speed of wedge prism (step
motor), Unit: degree/second
te_1=8/v_wedge_1;           %Duration of trepanning
t0=0; %Time point at rh0 (at beginning), Unit: second
t0_d=1; %Drilling duration at rh0 (at beginning), Unit: second
rh0=0.007; %Helical radius at beginning - polynomial fitted
te=0; %Drilling duration at rhe (at end), Unit: second
rhe=0.0956; %Helical radius at end - polynomial fitted

x=linspace(-0.12,0.12,201);%Scale of x
```

```
y=0;%Scale of y
% y=linspace(-0.12,0.12,201);%Scale of y
[px,py]=meshgrid(x,y);%meshgrid


% Superpose of Inteisity in first circular revolution
%Intensity of helical drilling: rh0=0.007
Ibeam0=0;
for ti=0:1/lf_t:t0_d;
x0=rh0.*sin(2*pi*nr.*ti);
y0=rh0.*cos(2*pi*nr.*ti);
Ibeam0_1=Iz_t*(w0/wz_t).^2.*exp(-2*((px-x0).^2)./(wz_t.^2)).*exp(-
2*((py-y0).^2)./(wz_t.^2));
Ibeam0=Ibeam0+Ibeam0_1;
end

% Superpose of Inteisity in last circular revolution at rhe=0.0956
Ibeame=0;
for ti=0:1/lf_t:te;
x0=rhe.*sin(2*pi*nr.*ti);
y0=rhe.*cos(2*pi*nr.*ti);
Ibeame_1=Iz_t*(w0/wz_t).^2.*exp(-2*((px-x0).^2)./(wz_t.^2)).*exp(-
2*((py-y0).^2)./(wz_t.^2));
Ibeame=Ibeame+Ibeame_1;
end

% Superpose of Inteisity in spiral revolution
%Intensity of helical trepanning v_wedge=0.5 degree/s
Ibeam1=0;
for ti=0:1/lf_t:te_1;
rh_1=(7+6.11*v_wedge_1*ti+0.62*(v_wedge_1^2)*(ti.^2))/1000; %Helical
radius and time - polynomial fitted
x0=rh_1.*sin(2*pi*nr.*ti);
y0=rh_1.*cos(2*pi*nr.*ti);
Ibeam1_1=Iz_t*(w0/wz_t).^2.*exp(-2*((px-x0).^2)./(wz_t.^2)).*exp(-
2*((py-y0).^2)./(wz_t.^2));
Ibeam1=Ibeam1+Ibeam1_1;
end
Ibeam_t1=Ibeam0+Ibeam1+Ibeame;

% Plot of v_wedge
h=plot(x,Ibeam_t1);
set(h,'LineWidth',1.5);
set(gca,'FontSize',14);
hleg=legend('V{\_}wedge=1°/s');
set(hleg,'FontSize',14);
```

```
axis([-0.125 0.125 0 8e16]);
xlabel('x /mm','fontsize',15);
ylabel('Superposed laser intensity / W/cm^{2}','fontsize',15);
title('3D superposed laser intensity distribution in helical
cutting','fontsize',20);
set(gcf, 'renderer', 'zbuffer')
opengl software;
box on;
grid on;
```